DEVELOPMENT OF A LONG-RANGE ULTRASONIC IMAGING SYSTEM IN AIR USING AN ARRAY TRANSMITTER

SAHDEV KUMAR

A Thesis for the Degree of

'Doctor of Engineering'

DEVELOPMENT OF A LONG-RANGE ULTRASONIC IMAGING SYSTEM IN AIR USING AN ARRAY TRANSMITTER

Graduate School of Engineering

ELECTRICITY AND MATERIALS ENGINEERING COURSE
AICHI INSTITUTE OF TECHNOLOGY

MARCH 2017

SAHDEV KUMAR

Contents

Chapter 1: Introduction

1.1 What is ultrasonic sound? ---------- 1
1.2 Applications of ultrasonic sound ---------- 2
1.3 Techniques available for 3D measurement ---------- 4
1.3.1 Stereo camera ---------- 4
1.3.2 Laser scanner ---------- 5
1.3.3 Pattern projection ---------- 6
1.4 Overview of ultrasonic imaging sensor system ---------- 6
1.4.1 Phased array system ---------- 7
1.4.2 Principle of ultrasonic imaging sensor system ---------- 7
1.4.3 Types of imaging sensor system ---------- 8
1.4.4 Issues concern ultrasonic imaging sensor system ---------- 10
1.4.5 Signal processing for resolution ---------- 12
1.5 Sound field divergence of single transmitter ---------- 14
1.5.1 Concept of array transmitter ---------- 16
1.6 Purpose of this work ---------- 16
1.7 Composition of thesis ---------- 17
References ---------- 19

Chapter 2: High Power Ultrasonic Transmitter Array for 3-D Range Imaging.

2.1 Introduction ---------- 23
2.2 Theory ---------- 23
2.2.1 Continuous wave ---------- 23
2.2.2 Pulse modulation ---------- 29
2.2.3 Measurable range ---------- 34
2.3 Transmitter array structure ---------- 35

2.4 Experimental set-up ---------- 37
2.5 Experimental method ---------- 38
2.6 Experimental results ---------- 39
2.6.1 Characteristics of array transmitter ---------- 39
2.6.2 Pulse modulation and sound pressure level ---------- 42
2.6.3 Pulse modulated directivities ---------- 43
2.7 Conclusion ---------- 45
References ---------- 45

Chapter 3: Long-Range Measurement System Using Ultrasonic Transmitter Array and Range Sensor in Air

3.1 Introduction ---------- 48
3.2 Ultrasonic transmitter array ---------- 49
3.3 Ultrasonic receiver array ---------- 49
3.4 Principle of object detection ---------- 57
3.5 Experimental set-up ---------- 58
3.6 Experimental results ---------- 59
3.6.1 Measurable range ---------- 59
3.6.2 Image detection ---------- 61
3.7 Conclusion ---------- 65
Reference ---------- 66

Chapter 4: Isotropic Divergence Controllable Ultrasonic Transmitter Array for 3-D Range Imaging

4.1 Introduction ---------- 68
4.2 Theory ---------- 69
4.3 Structure of divergence controllable transmitting system ---------- 76
4.4 Experimental results ---------- 78
4.4.1 SPL at different divergence ---------- 78
4.4.2 Directivities at different divergence ---------- 79
4.4.3 Measurable range ---------- 81
4.4.4 Image detection ---------- 82

4.4.5 Object detection view angle ---------- 87
4.5 Conclusion ---------- 88
References ---------- 89

Chapter 5: Anisotropic Divergence Controllable Ultrasonic Transmitter Array for 3-D Range Imaging

5.1 Introduction ---------- 91
5.2 Theory ---------- 92
5.3 Structure of divergence controllable transmitting system ---------- 99
5.4 Experimental results ---------- 100
5.4.1 SPL of array transmitter with anisotropic divergence -------- 100
5.4.2 Directivities with anisotropic divergence ---------- 101
5.4.3 Measurable range using anisotropic divergence ---------- 103
5.4.4 Detection of range image ---------- 104
5.5 Conclusion ---------- 107
References ---------- 108

Chapter 6: Summary ---------- 109

Scope of the future work ---------- 111

List of papers ---------- 113

Acknowledgement ---------- 117

Chapter 1

Introduction

1.1 What is ultrasonic sound?

Ultrasonic sound wave investigations involve the study of sound waves propagating at frequencies beyond the human audible range from 20 to 20,000 Hz. Very high frequency sound waves above the limit of human hearing were generated by English scientist Francis Galton in 1876, through his invention, the Galton whistle.

Even though piezoelectric and magnetostrictive effects were known but they were not utilized in any useful ultrasonic instruments due to lack of progress in electrical technology and hence Galton's work showed negligible curiosity for over three decades on ultrasonic instrument application. However, the experiences of world war during 1914-1918, attracted interest in the subject when French physicist Paul Langevin and Russian scientist Chilowsky, developed a powerful high frequency ultrasonic echo-sounding device, called 'hydrophone' in France. The hydrophone was further improved in classified research activities and deployed extensively in the surveillance to detect the submarines as well as under water communication in 1916.

It was felt that rapid growth in the field of electronics after world war-I was the need of time. In 1925, Pierce used quartz and nickel transducers for generating and detecting ultrasonic sound frequencies extending up to MHz range. By the time, Debye and Sears as well as Lucas and Biquard, independently discovered the ultrasonic diffraction grating to boost the steady progress in the use of ultrasonic sound to study the acoustical properties of liquids and gases. And by the 1930s, ultrasonic investigations

into the properties of solids were being done. A Soviet scientist Sokolov, is considered as the father of ultrasonic testing and published details of the experimental design of quartz generators, methods of coupling the generators to the test piece in order to achieve maximum energy transfer, and also various methods of detecting the ultrasonic energy after transmission through the test piece in 1935. Moreover, the scope of ultrasonic sound has been enhanced considerably by adopting pulse methods derived from Radio Detection and Ranging (RADAR) techniques, and, it has been widely applied in, e. g., the non-destructive testing of materials, medical diagnosis, and instrumentation and control applications. Other potential uses of high intensity ultrasound including cleaning, emulsification, drilling, sub-micro and micro material processing methods could also be realized.

New materials and techniques were discovered in 1960s and with the developments of microwave propagation, it could possible to generate ultrasonic waves at frequencies up to 100 GHz for its further applications in fundamental research in physics, electronic communications and computer technology.

The ultrasonic use is preferred to audible sound in various applications owing to the following reasons:

1. Ultrasonic sound has directional properties, with greater directivity at higher frequencies and is suitable for flaw detection and underwater signalling.

2. Higher frequencies means “shorter wavelengths”, i.e., less than or equal to the samples of the material for propagation, is important for small thickness measurement and high resolution flaw detection.

3. Ultrasonic sound is silence and hence makes it advantageous in high intensity applications. Such applications are possible with higher efficiency at audible frequencies, but resulting noise may be intolerable and possibly injurious.

Ultrasonic applications are classified based on either low or high intensity.

Low intensity ultrasonic waves are normally used either for investigating the properties of material samples which do not change its structural and chemical properties or control methods. Most low intensity ultrasonic wave applications involve very high frequencies, typically in MHz range, with the acoustic power involved might be from a few microwatts (μW) to several tens of milliwatts (mW). On the other hand, high intensity ultrasound is used for changing the properties of material through which it is passed. Often high intensity ultrasonic wave frequencies are just above the audible limit, with the acoustic power involved from a few mW to kW. Ultrasound with its frequency range is used for various functions. A categorization of ultrasound with its functions is shown in Fig. 1.1.

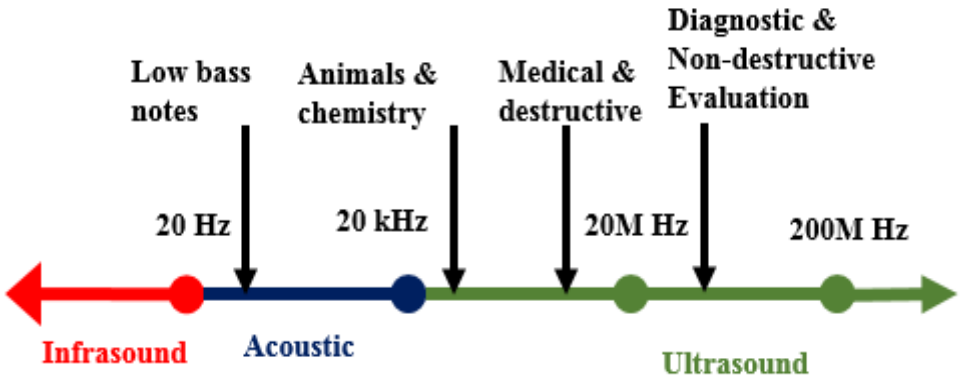

Fig. 1.1: Ultrasound applications as per frequency range

1.2 Applications of ultrasonic sound

The most common use of ultrasound is in ultrasonic imaging and at present most widely used for bio-medical applications. Ultrasound also has a number of other industrial applications such as image processing, inspection modalities, three-dimensional (3D) imaging etc. Their use in creating images is based on the reflection and transmission of the ultrasonic pulsed wave at a boundary. When an ultrasound wave travels inside an object that is made up of different materials (such as the human body), each time it encounters a boundary (e.g., muscle and bone or muscle and fat); a part of the ultrasonic wave is reflected while as other part gets transmitted. The reflected ultrasonic pulsed waves are detected and used to construct an object image.

Ultrasound is also used in RADAR and Sound Navigation and Ranging (SONAR) technologies; both of which work on the same principle in which the ultrasound pulses is transmitted in the form of short burst with the fixed interval, which gets partially reflected back from the target and received back by the receiver. Some creatures such as Bats and Dolphins also use ultrasound to find out their prey based on the principle of finding an object distance using an ultrasonic sound wave reflection, called "echo". If the speed of sound in the medium is known, then object distance can be obtained. The time required for an echo to return, is calculated and converted into distance for the known speed of sound in that medium.

1.3 Techniques available for 3D measurement

There are some other techniques also used for 3D measurements of any object, namely

1. Stereo Camera
2. Laser Scanner
3. Pattern Projections

1.3.1 Stereo camera

Some latest models of Stereo Camera are available in the market and their working principle is shown in Fig. 1.2, in which two cameras with parallel optical axes placed at the distance *d* between them and line connecting the camera lens centres is considered as baseline. This baseline is perpendicular to the line of sight of both the cameras. X axis of the 3D coordinate system is parallel to the baseline. The origin O lies in mid-way between the lens centre and with the coordinate geometry, image of point P is obtained.

Limitations of the stereo camera

Stereo camera can measure accurately for short range only. The disparity and corresponding point's image matching are the main drawback of this system.

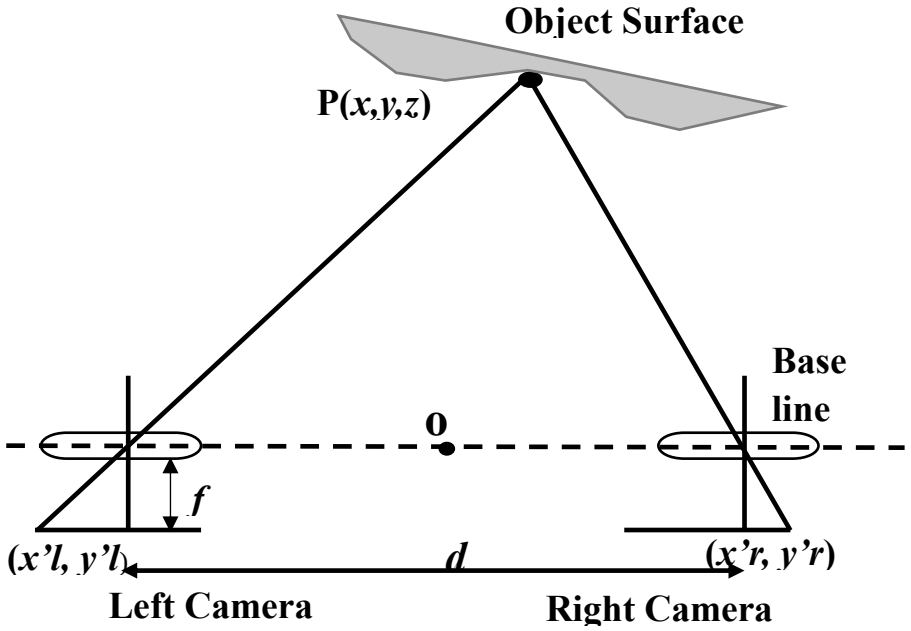

Fig. 1.2: Working principle of stereo cameras.

1.3.2 Laser scanner

Another technique used for 3D measurement is light amplification by stimulated emission of radiation (LASER) scanner. There are many devices that can be called 3D scanners. Any device that measures the physical world using lasers, lights or x-rays and generate dense point clouds or polygon meshes can be considered as a 3D scanner. They are also known as 3D digitizers, laser scanners, white light scanners, industrial computed tomography (CT), light detection and ranging or laser imaging detection and ranging (LIDAR) etc. The common uniting factor of all these devices is that they capture the geometry of physical objects with hundreds of thousands or millions of measurements. Fig 1.3 shows the measurement method of scanner.

Limitations of scanner

Scanners are suitable for medium range only and long range measurement is not possible. The experimental results of this technique are not reliable due

to higher noise and slow data acquisition.

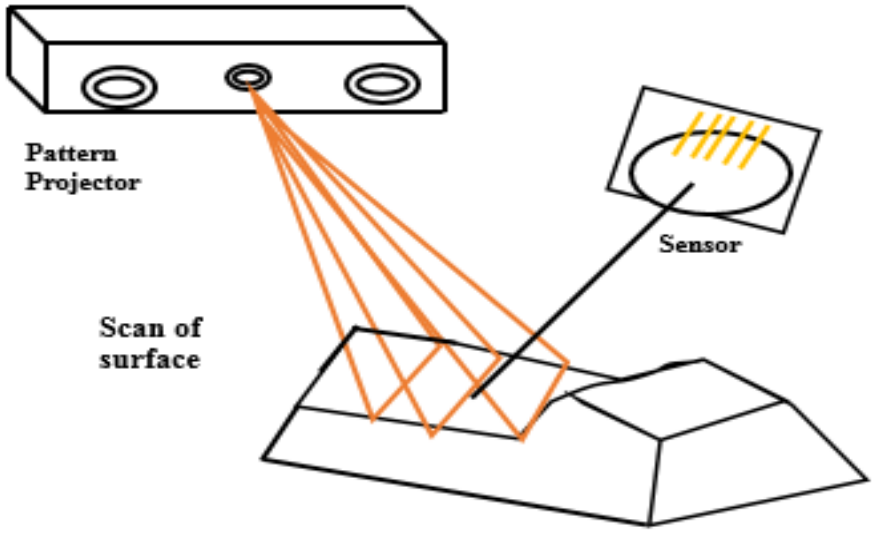

Fig. 1.3: Measurement method of scanner.

1.3.3 Pattern projection

Pattern projection is also used for 3D measurement of an object in air. In this technique structured light generates a full pattern to cover the object so that the surface can be captured as whole field recording. The encoding of structured pattern becomes important because it determines the local feature of the recorded images that to be identified in spatial recognition and height evaluation.

Limitations of pattern projection

Pattern projections are fast and long range measurement is possible if both resolution and robustness are high.

1.4 Overview of ultrasonic imaging sensor system

An ultrasonic imaging sensor system has the following merits over other conventional techniques. First of all its constructions is simple, second it is one of the fastest measurement technique, third it maintains the privacy while

monitoring human daily activities and last this technique is useful in adverse atmospheric conditions such as rain, fog, smoke, darkness etc.

1.4.1 Phased array system

Conventional ultrasonic transducers for Non-Destructive Testing (NDT) commonly consisting of either a single active element that both generates and receives high frequency sound waves, or two paired elements, one for transmitting and one for receiving. Phased array probes, on the other hand, typically consists a number of transducer and each one of them can generate pulses separately. The elements may be arranged in a strip (linear array), a ring (annular array), a circular matrix (circular array), or any other more complex patterns. In range sensing system low frequencies is used. A phased array system will also include a sophisticated computer-based instrument that is capable of driving the multi-element probe, receiving and digitizing the returning echoes, and plotting that echo information in various standard formats. Unlike conventional flaw detectors, phased array systems can sweep a sound beam through a range of refracted angles or along a linear path, or dynamically focus at a number of different depths, thus increasing both flexibility and capability in inspection setups.

1.4.2 Principle of ultrasonic imaging sensor system

In ultrasonic range imaging sensor system an electric signal of known frequency above the human audible limit > 20 kHz is generated in the form of modulated pulse and received back by an ultrasonic receiver after reflection from an object. The electrically generated ultrasonic signal is converted to analogue signal from its digital form through digital to analogue converter (DAC) before its transmission in air. The ultrasonic analogue signal is again converted into the digital form by an Analogue to Digital Converter (ADC) after its detection by the receiver for signal processing such as the auto correlation function.

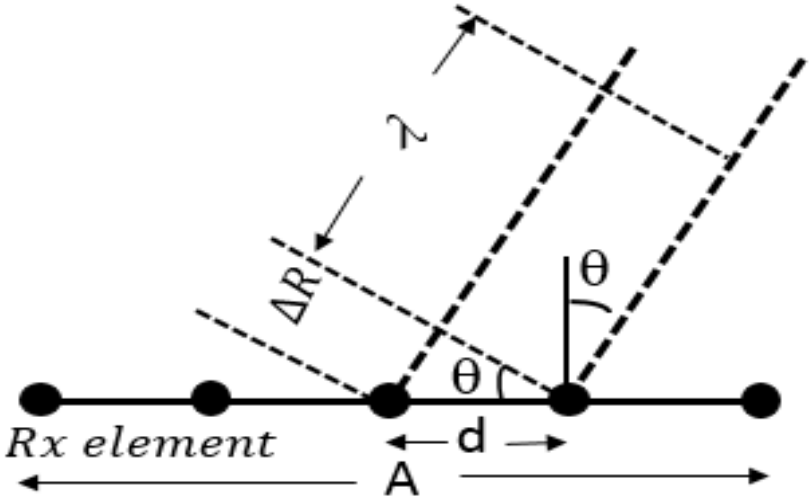

Fig. 1.4: Linear array receiver for measuring the angle θ of the target based on the difference in arrival time $\Delta T = \frac{\Delta R}{c}$ between adjacent elements.

In order to find the direction of the target object from the transceiver, an angle measurement system is needed. A linear array of receivers is used to receive a plane wave reflected from the object as depicts in Fig. 1.4. An incident angle θ creates a difference in the Time-of-flight between neighbouring elements with the following relationship as given by Eq. (1.1) [6-7]

$$\Delta T = \frac{d}{c}\sin(\theta) \tag{1.1}$$

Here, d and c denote the inter element space and sound wave velocity respectively. That corresponds to a phase shift $\emptyset = \frac{2\pi d}{\lambda}$ sin (θ), λ is the wavelength. In the same way, to transmit a pulse with the angle θ from normal, the phase of the transmit signal should be shifted by ϕ between each element.

1.4.3 Types of imaging sensor system

Generally, imaging sensor system can be classified in two types

(i) Scanning method

Scanning method is widely used in medical and underwater imaging and not good for long range measurement. Therefore, for long range measurement non-scanning method is useful. They have the merit of fast measurement but low resolution and measurable range. Scanning method has the opposite characteristics being slower but having high resolution and long measurable range [1-3].

(ii) Non-scanning method

This non-scanning method can be further divided in two types

(a) Holographic

Holography is a branch of optics used for recording and displaying an image. The two concepts, interference and diffraction are commonly used in optics and their combined form make a single branch called holography and optical data processing. Interference and diffraction in communication terminology are known as modulation and demodulation. It became possible that information stored in an interference pattern (modulation) can be recorded as a result of diffraction of light by the recorded interference pattern (de-modulation) [4, 5].

(b) Beam forming of receiver

(i) Delay-and-sum Beamforming

The delay-and-sum beamforming is the simplest techniques for realizing directional array systems and also knows as classical beamforming. Initially delay-and-sum arrays were used in narrowband operation to focus arrays in a particular direction. Narrowband beamforming is generally implemented with the phase shifts and is referred as phased-array beamforming. The

delay-and-sum beamforming uses delays between each array element that compensate for differences in the propagation delay of the desired signal direction across the array. The signals generating from a desired direction are summed in phase and others becomes null due to destructive interference. The shape of the beam and side lobes along with the position of the nulls of the array can be controlled by adjusting the weights of the delay-sum beam former.

(ii) Delay-and-multiplication Beamforming

Delay-and-multiplication operations are used to increase the sharpness of main lobe.

1.4.4 Issues concern ultrasonic imaging sensor system

Although, ultrasonic range imaging system has several advantages over other conventional methods but it has some drawbacks also such as bigger size, ghost image, low resolution and low measurement range etc. These drawbacks are being eliminated as discussed below

(a) Size

The one of the major drawback of imaging sensor system is the bigger size of the array receiver. This drawback has been resolved with the recent development of Micro Electro Mechanical System (MEMS) through which it became possible several tens and/or several thousand receivers can be adjusted in a very small area. The real through of imaging sensor system is the development of MEMS technology that significantly reduces the size. An integrated circuit has been developed that consist of single transmitter and array receiver in a single chip [6, 7]. Further, an array receiver has been constructed using PZT thin film [8, 9].

(b) Ghost image

Another drawback of the imaging sensor system is obtaining ghost images. It is due to the large inter-element space of the array receiver than that of the

wave length of the ultrasonic sound. The ghost images appear due to the strong reflected signal from other objects located in different direction. The grating lobes and side lobes cause ghost image. This drawback is resolved reducing the inter-element space of microphones using the MEMS technology. An array receiver that composed of total eight small area and each small area consists of four receivers. After delay-and-sum operations, delay-and-multiply operations are applied on the received signal. Such receiver decreases the grating lobes and side lobes thus eliminating the ghost image. [10-11]. Further attempt has been made by increasing the number of element in the receiver array and arranging them in different patterns [12].

The pitch of the side lobe is calculated by Eq. (1.2) as follows [4]

$$\sin\theta_{side} = \frac{m\lambda}{(n-1)d} \tag{1.2}$$

Where, *d* is the pitch of the elements, *n* is the number of elements, and *m* is the order of the side lobes. Since elements are placed at 10 mm intervals, the number of elements is 12, and the wavelength of the ultrasonic wave is 8.6 mm, side lobes with a pitch of 4.5°, or 0.078 radians [= 8.6 mm/10 mm × (12-1)], appear at lower angles. Grating lobes appear at an angle using Eq. (1.3) as follows

$$\sin\theta_{grating} = \frac{m\prime\lambda}{d} \tag{1.3}$$

Where, *m*' is the order of the grating lobes. The pitch becomes $\sin^{-1}\left(\frac{8.6\ \text{mm}}{10\ \text{mm}}\right) = 1.0\ \text{rad.} = 60\ \text{deg.}$

(c) Resolution

Resolution is another drawback of the imaging sensor system due to the large number of array receivers used in the system. This drawback has been resolved using the dispersed ultrasonic array receiver and applying the delay-and-multiply operations (H. Furuhashi et al.) [13]. The camera image has been taken into consideration to improve the resolution along with the array receiver. [14, 15].

(d) Measurable range

Ultrasonic sound is absorbed by the air, therefore measurable range is limited to a few meters only. Some efforts have been made to improve the measurable range such as

(i) Increasing the number of transmitting elements

Measurable have been improved up to 15 m by increasing the number of transmitting element and developing the high power transmitter array. With this system measurable range improved significantly and the directivity of transmitter array becomes very narrow [16-18].

(ii) Using electric spark discharge

Another attempt to increase the measurable range is development of electrical spark discharge. Measurable has been improved over 5 m with this method and object detection view angle also present up to a few degrees. With this system high power sound is generated by short circuit. This method is dangerous and someone may get injured. Further, one can loss his eyesight due to sparking [19, 20].

(iii) Spread spectrum pulse compression technique

Using the spread spectrum pulse compression technique, we have successfully increased the S/N ratio, therefore, measurable range improved up to 8 m. Object detection view angle up to a few degree is also obtained [21-23].

(iv) Acoustic lens

Using acoustic lens, measurable range up to 6 m has been reported and object detection view angle is present to a few degrees [24].

1.4.5 Signal processing for resolution

Before the discussion of aperture synthesis or super resolution, it is equally important to address the need to make proper use of acoustic aperture for high resolution. Let us consider a one-dimensional aperture containing '*n*'

equally spaced liner detectors or *'n'* equally spaced sampling points, then there are '*2n'* of input information, phase and amplitude for each frequency band. If this is processed to form an image using, i.e. Fast Fourier Transform (FFT), it ends up with '*2n'* output words of information including phase and amplitude and no loss of information is expected. Although, most imaging systems only display intensity and thus *'n'* of information is the final output and half of the information get lost. By Rayleigh criteria, it may be readily seen that there should be twice as many points in the intensity display, spaced half as far as in a phase display. It ends up with the required '*2n'* output and the full resolution capability of the acoustic aperture which is being used.

It is observed that the two sources cannot be resolved in the 20 x 20 pixel intensity display, even they are in out of phase and their separation is also greater than Rayleigh distance. After interpolation to obtain the display in 40 x 40 pixels, the two sources are clearly resolved. There are two methods for processing the interpolation (a) Synthetic-aperture processing (b) Super resolution processing [30-34].

(a) **Synthetic-aperture processing**: This processing is possible by two ways

(i) The receiver aperture is synthesized by motion of either the object, or the receiver, or the transmitter, or any two of these.
(ii) The receiver aperture is synthesized by multiplexing transmitters, so that no motion is involved.

(b) Super resolution processing

A method has been proposed by Gerchberg [29] is designed to be more robust against noisy environments. This approach, is called the error-energy reduction method, is an extension of Harris method [27, 28]. In this method, the input (far-field holographic) data are first Fourier transformed to yield the conventional image. The image is then modified by setting all of the image points outside the known extent of the true object to zero. The image thus modified is Fourier transformed to form a far-field hologram over a larger aperture than originally available, with the original hologram data being substituted only where it was available (i.e., over the original aperture)

and the new data being used outside this region.

These steps are repeated until a criterion based on the estimated object energy outside the known extent of the true object is satisfied and known as converge. The range image resolution depends on the signal bandwidth. The shorter pulse width modulation has larger bandwidth and gives better range image resolution. The bandwidth limitations are imposed by the bandwidth of the transmitters or receivers as they are resonant devices. The range image resolution could be improved using pulse compression technique [35-37].

When a short modulated pulse incidents on the receiver array at an angle, it does not reach all the elements of the array receiver at the same time. Therefore, time-delay beam-forming is used, as a result some of the outer elements are completely missing the pulse, reducing the resolution for off-axis objects. This effect has been analysed and does not have serious effect [38-41].

1.5 Sound field divergence of single transmitter

It is necessary to understand the sound field radiation by a single element transmitter before designing a phased array transmitter. Single element transmitter`s sound field characteristics are calculated with the following considerations; (i) The size and shape of the transmitting element (ii) The transmitted pulse properties and (iii) The characteristics of the medium of propagation.

The rate at which the energy in this region diverges is a function of the source diameter (D), the radiated wavelength (λ) and (γ) is the absorption coefficient. The highest amplitude signal occurs on the axis of the transducer and amplitude decreases on the angular displacement from the axis as shown in Fig. 1.6. Although the signal is radiated into the entire half space, most of the energy is included in this conical far field region. The lateral limits of this cone is defined as the angle at which the signal amplitude is reduced by 6 dB relative to the axial amplitude and angle at which the signal amplitude is reduced by 6 dB and calculated by the Eq. (1.4)

$$\gamma = \sin^{-1}(0.7 \times \frac{\lambda}{D}) \tag{1.4}$$

It can be observed that when λ (wavelength) is large in comparison to D (diameter), the divergence is large. It makes the object positioning of the reflector more difficult due to the larger sound field. Therefore, during inspection of the quality of the material, ultrasound transmitters having small divergence angle are preferred, so that the reflector can be located more precisely. This divergence angle can be reduced by reducing the ratio of λ/D in the Eq. (1.3). There are two methods to reduce the divergence angle; (i) producing the higher frequency or increasing the diameter of the transmitter and (ii) Focusing the ultrasound source itself but it is not possible using single transmitter.

In some of the applications we required small divergence angle such as inspection of quality of material and detection of fault in a product. On the other hand in some applications wide divergence angle is required such as 3D range imaging. Ultrasound source cannot be focused using single transmitter, therefore concept of array transmitter has been proposed [25, 26].

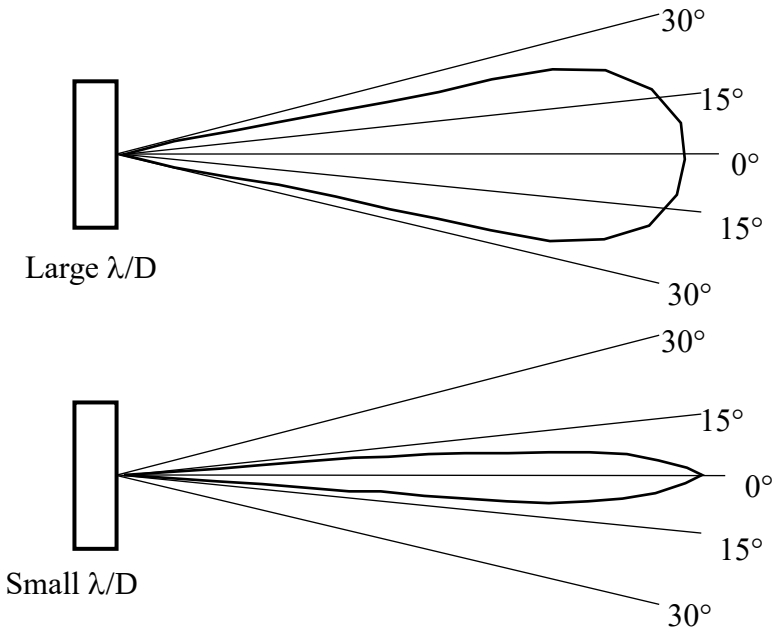

Fig. 1.6: Directivity pattern of single transmitter.

1.5.1 Concept of array transmitter

The measurable range using conventional ultrasonic method is limited due to the fundamental characteristics of ultrasonic waves. Thus high power array transmitters could be used in non-destructive evaluations and inspection modalities. Also, measurable range of the 3D image sensor may be improved using such type of array transmitter owing to their high sound pressure level. With this consideration, a high power ultrasonic transmitter array (UTA) has been developed.

With increased use of ultrasonic testing and measurements in past several years, such as scanning techniques for both contact and immersion method during production and in-service inspection programs to determine the quality of the product. Due to a variety of component configurations and potential flaw geometries it is often necessary to perform several inspections each with a different probe configuration to assure the defect findings, if any. A purposely designed phased array probe can perform various inspections without changing hardware to sufficiently reduce the inspection time.
Using array structure following functions can be performed

- Ultrasonic sound source can be focused
- Isotropic divergence control is possible on ultrasonic sound source
- Anisotropic divergence control is possible on ultrasonic sound source

1.6 Purpose of this work

Due to the fundamental properties of ultrasonic sound, the conventional ultrasonic range imaging system is restricted to measure 3D position of an object only up to a few meters. Therefore, main focus remained to improve the measurable range. The measurable range could be improved up to 8 m by spread spectrum pulse compression method when a steel plate (10 cm width x 12 cm length) has been used as an object and detected accurately [22].

A high power sound source also has been developed by spark discharge [20] and measurement range has been improved over 5 m. This method is dangerous for the safety point of view and one can suffer for permanent

hearing loss or visibility.

Keeping in mind the above factor, a safe and convenient method was the primary requirement for the development of high power sound source. Therefore, a high power ultrasonic transmitter array has been constructed. With the development of high power sound source, measurable range is expected to be improved. With this idea, that high ultrasonic power can be maintained for long distance, an ultrasonic transmitter array has been developed.

This work has undertaken owing to the fact that in last few decades the applications of ultrasound has been increased to a great extent. A high power UTA for 3D range imaging system would improve the scope of ultrasonic sound applications not only in the advanced fields of control engineering, security, alignment, flaw detection, robotics, amusement, sub-micro and micro material processing industrial utilities etc. but also in bio-medical science and engineering.

The ultrasonic imaging sensor system is a simple and cost effective technique for 3D position and shape recognition of an object. Additional advantage of this system is that it is useful in adverse atmospheric conditions. Before developing such system, minutely all the point must be borne in mind to optimise the performance of the system. With the concept of transmitter array, it could be possible to focus the sound source. The main focus of this work are as follows

- Improvement in measurable range over 15 m.
- Improvement in the object detection view angle over 15^{o}.

1.7 Composition of thesis

In order to improve the measurable range, a 2D transmitter array has been proposed that can generate high power. Therefore, a high power ultrasonic transmitter array has been constructed. In this dissertation, a long range imaging sensor system using high power array transmitter is being reported and explained in chapter wise. This thesis composed of 6 chapters as follows.

In **Chapter-1**, background of the field of range imaging sensor is described and make comparisons with other conventional techniques for 3D measurement of an object with the range imaging sensor system using ultrasonic sound. The motivation and purpose of this study is also described.

Chapter-2 describes about the principles and configurations of the array transmitter. The characteristics of the transmitter on the number of elements, modulated pulse width etc. is investigated theoretically. Experimental investigation is also performed and compared with the theoretical results. The performance of the transmitter on range imaging system is also discussed theoretically.

Chapter-3 presents principle and configuration of the long-range measurement system using UTA and URA. The experimental studies were conducted on the measurable range using (i) single ultrasonic transmitter (SUT) with single ultrasonic receiver (SUR) (ii) SUT with ultrasonic receiver array (URA) (iii) UTA with SUR (iv) UTA with URA and compared their performances.

Chapter-4 describes the improved 3D measurement field of an object by controlling the sound divergence of the UTA to improve the object detection view angle of the system. The coordinate system of the divergence control of UTA and the configuration of the system have been explained. The characteristics of the transmitter is investigated theoretically and compared with experimental results. A range imaging system using this transmitter and ultrasonic receiver array is constructed. The performance of the system is investigated and compared with the system using the ultrasonic array transmitter without the sound divergence control.

Chapter-5 discussed the range imaging system using UTA with anisotropic divergence control. In some particular cases a wide horizontal field and narrow vertical field is required for measurement. With anisotropic divergence control system, independent control on horizontal and vertical divergence is possible. The principle and the configuration both are described in detail. The characteristics are investigated theoretically and

compared with the experimental results. The performance of the range image sensor system using UTA, has been discussed and compared with the system using UTA without sound divergence control and that with the isotropic divergence control.

Chapter-6 summarizes this dissertation. Further, scope for the future research work is also given.

References

[1] L. Azar, Y. Shi and S.C. Wooh, Beam focusing behavior of linear phased arrays, NDT & E International, 33, (2000), pp. 189-198

[2] Y. Lu, H.Y. Tang, S.Fung, B.E. Boser and D.A. Horsley, Pulse-echo ultrasound imaging using an A1N piezoelectric micromachined ultrasonic transducer array with transmit beam-forming, J. Microelectromechanical systems, 25 (1) (2016), pp.179-187.

[3] E. Konetzke, M. Rutsch, M. Hoffmann, A. Unger, R. Golinske, D. Killat, S.N. Ramadas, S. Dixon and M. Kupnik, Phased array transducer for emitting 40-kHz air-coupled ultrasound without grating lobes, Proc. IEEE Ultrasonics Symposium, 2015, IEEE Xplore, DOI: 10.1109/ULTSYM.2015.0019 (2015).

[4] A. Korpel, Acoustic imaging and holography, IEEE Spectrum, 52 (1968), pp.45-52.

[5] Dunn F. et al., Springer handbook of acoustics, Ed. Thomas Rossing. Springer (2015).

[6] R. J. Przybyla, H. Y. Tang, A. Guedes, S. E. Shelton, D. A. Horsley and B. E. Boser, Digital ultrasonic rangefinder on a chip, IEEE Journal of Solid-State Circuits, 50 (1) (2015), pp.320-334.

[7] R. J. Przybyla, S. E. Shelton, A. Guedes, R. Krigel, D. A. Horsley and B. E. Boser, In-air ultrasonic range finding and angle estimation using an array of ALN Micromachined transducers, IEEE Sensors, J. 11 (11) (2011), pp.2690-2697.

[8] K. Yamashita, L. Chansomphou, H. Murakami and M. Okuyama, Ultrasonic micro-array sensors using piezoelectric thin films and resonant frequency tuning, Sensors and Actuators A 114 (2004), pp. 147-153.

[9] K. Yamashita, H. Katata, M. Okuyama, H. Miyoshi, G. Kato, S. Aoyagi and Y. Suzuki, Arrayed ultrasonic microsensors with high directivity for in-air use using PZT thin film on silicon diagrams, Sensors and Actuators Acous. Physical 97-98 (2002), pp. 302-307.

[10] H. Furuhashi, Y. Uchida and M. Shimizu, Imaging sensor system using rectified delay-and-multiply operations with an ultrasonic array, Industrial Electronics 2008, IECON 2008 (2008), pp. 1891-1895.

[11] H. Furuhashi, Y. Uchida and M. Shimizu, Imaging sensor system using a composite ultrasonic array, IEEE Sensors 2009, IEEE Xplore (2009), pp.1467-1472.

[12] S. Harput and A. Bozkurt, Ultrasonic phased array device for acoustic imaging in air, IEEE Sensors Journal 8 (11) (2008), pp.1755-1762.

[13] H. Furuhashi, J.Valle, Y.Uchida and M. Shimizu, Imaging sensor system using dispersed ultrasonic array, Proc. of ICCAS 2007 (2007), FEP-35, pp. 2385-2388.

[14] H. Furuhashi, Y. Kuzuya, Y. Uchida and M. Shimizu, Three-dimensional imaging sensor system using an ultrasonic array sensor and a camera. IEEE Sensors 2010, IEEE Xplore A2P-P4 (2010), pp.713-718.

[15] H. Furuhashi, Y. Kuzuya, Chen Gal, and M. Shimizu, Three-dimensional imaging of a human body using an array of ultrasonic sensors and a camera, 2nd International conf. on Advances in intelligent and soft computing camera. 145 (2012), pp. 325-330.

[16] J. Majchrzak, K. Michalski and G. Wiczynski, Distance estimation with a long range ultrasonic sensor system, IEEE Sensors Journal, 9 (7) (2009), pp.767-773.

[17] Datashseet, 6500 series sensor ranging module, sens Corp, Inc. 2004, Dec.18 2007. [Online]. Available:www.senscomp.com /6500smtmod.htm.

[18] Datasheet, Technical specification for 600 series instrument grade electrostatic transducer, Polaroid 6/95, Sep. 8 2008. [Online]. Available: www.engr.udayton.edu/faculty/jloomis/ece445/topics/sonar/6500.pdf.

[19] J. M. M Aberu, R. Ceres, C. Leopoldo, M.A. Jime'nez and P. Gonza'lez-de-Santos, Measuring the 3D-position of a walking vehicle using ultrasonic and electromagnetic waves, Elsevier Science S.A. Sensors and Actuators, 178 (1999), pp.131-138.

[20] T. Tanaka, S. Lee, M. Uno, K. Inoue, S. Aoyagi, K. Yamashita and M. Okuyama, Improvement of ultrasonic micro array sensor using the amorphous fluorocarbon polymer film, the transactions of the institute of electrical engineers of Japan. A publication of sensors and micromachines society 127 (1) (2007), pp.7-13.
[21] Y. Zhenjing, H. Li, C. Lina, Improvement of measurement distance in multi-channel ultrasonic ranging systems thorough adaptive chaotic pulse position width modulation excitation sequences, Insight-Non-Destructive testing and condition monitoring 58 (7) (2016), pp. 324-330.
[22] H. Furuhashi, S. Kumar and M. Shimizu, Signal processing of a 3D ultrasonic imaging sensor that uses the spread spectrum pulse compression technique, Lecture notes in information technology, Proc. 2012 Int. Conf. on Future Information Technology and Management Science & Engineering FITMSE 2012, 14 (2012), pp.145-150.
[23] H. Inubushi, N. Takahashi, H. Zhu and K. Taniguchi, Ultrasonic 3D image sensor employing PN Code and Beam-forming Technologies, IEICE Trans. Acous. J90-A (6) (2007), pp.517-523.
[24] Sai Hou, Buren Mandula, Wei Quan, Sahdev Kumar and Hideo Furuhashi, Imaging of a wave reflected by an object using an acoustic lens in air, IMEKO XXI World Congress, in USB 5 pages. (2015).
[25] B.W. Drinkwater and P.D. Wilcox, Ultrasonic arrays for non-destructive evaluation: A review, NDT and E International, 39 (7) (2006), pp.525-541, DOI: 10.1016/J. ndteint. 2006.03.006.
[26] A.J. Fenn, D.H. Temme, W.P. Delaney and W.E. Courtney, The development of phased-array radar technology, Lincoln Lab. Journal, Vol. 12, No. 2, (2000), pp. 321-340.
[27] F.J. Harris, Diffraction and resolving power, JOSA, Vol. 54, No.7 (1964), pp. 931-933.
[28] F.J. Harris, On the use of windows for harmonic analysis with the discrete Fourier-transform, Proc. IEEE, Vol. 66 (1978), pp. 51-83.
[29] R.W. Gerchberg, Super-resolution through error energy reduction. Journal of Modern Optics, Vo. 21 No. 9 (1974), pp. 709-720.
[30] R.W. Schafer and L.R. Rabiner, A digital signal processing approach to interpolation, Proc. IEEE, Vol. 61, (1973), pp.692-702.
[31] G.J. Grevera and J.K. Udapa, An objective comparison of 3-D image interpolation method, IEEE Trans. Med. Imag., Vol. 17 No.4 (1998), pp.

642-652.
[32] R.K. Mueller, Advances in holography, vol.1, N. H. Farhat, Ed. New York; Marcel Dekker, (1975), p.45.
[33] R.F. Koppelmann and P.N. Keating, Three dimensional acoustic imaging, presented at the Eighth Int. Symp. On Acoustical Imaging, May30-Jun, Key Biscayne, Florida, (1978).
[34] H.P. Brucker, Cross-sensor beamforming with a sparse line array, J. Acoust. Soc. Amer., vol.61, (1977), pp.494-498.
[35] H. Kolsky, stress waves in solids, Dover Publications, New York, (1963).
[36] W.C. Elmore and M.A. Heald, Physics of waves, Dover publications, New York, (1985).
[37] D. Royer and E. Dieulesaint, Elastic waves in solids I and II Springer Verlag, Berlin, (2000).
[38] L.M. Brekhovskikh, Waves in layered media 2nd Edition, Academic press, New York, (1980).
[39] J.D. Achenbach, Wave propagation in elastic solids, Elsevier science publisher, Amsterdam, (1990).
[40] B.A. Auld, Acoustic fields and waves in solids 2nd Edition Vol.1&2, Krieger publishing, Florida, (1990).
[41] K. Preston, Use of pattern recognition for signal processing in ultrasonic histopathology, NBS Special publication 453, Proc. Seminar on Ultrason. Tissue Characterization, May (1975).

Chapter 2

High Power Ultrasonic Transmitter Array for 3-D Range Imaging[1, 2]

2.1 Introduction

Recently, 3D shape and size measurement of an object is one of the thrust areas and efforts are being made to improve the measurement range and resolution [7, 11]. There are several techniques available for 3D position and shape recognition such as stereo camera, laser scanners, pattern projections etc. have been discussed in the previous chapter with their merits and limitations. Ultrasonic imaging sensor system is also one such technique and works on pulse echo method. In spite of low resolution, this technique has several advantages over them. This technique can be used in adverse atmospheric conditions [3-10].

In this chapter, configuration of the ultrasonic transmitter array (UTA), its coordinate system and simulation directivity with different pattern of transmitter array and pulse modulation have been discussed. Experimental study has been conducted at room temperature considering the ultrasonic wave speed 345 m/s and compared with the theoretical calculations.

2.2 Theory

2.2.1 Continuous wave

First of all, ultrasonic sound from the array transmitter for continuous-wave transmission is discussed. The directivity of a circular ultrasonic transmitter is described by Eq. (2.1) [1, 2]

$$D(\theta) = \frac{2J_1(ka\sin\theta)}{ka\sin\theta} \tag{2.1}$$

Here, θ is the direction of the sound wave, k is the wave number, a is the radius of an element, and J_1 is the Bessel function of the first kind. The radius of an element is 4.3 mm, an ultrasonic frequency of 40 kHz, and the wave velocity is 345 m/s. If there are many transmitting elements at position P_i (x_i, y_i, 0) in the plane z = 0 directed toward the z axis as shown in Fig. 2.1, the total sound pressure from all the elements will be given by Eq. (2.2)

$$p(x,y,z) = \sum_i \; D(\theta_i)A_i \frac{e^{-2\pi i\frac{r_i}{\lambda}}}{r_i} \tag{2.2}$$

Here, r_i is the distance between position P_i of the element and the observation point P(x, y, z), θ_i is the angle between the z axis and the vector $\overrightarrow{P_iP}$, and A_i is the amplitude. If point P is sufficiently far from the origin compared with the size of the array, Eq. (2.2) can be approximated as Eq. (2.3)

$$P(x,y,z) = \sum_{i=1}^{n} D(\theta_i)A_i \frac{e^{-2\pi i\frac{\sqrt{(x-x_i)^2+(y-y_i)^2+z^2}}{\lambda}}}{\sqrt{(x-x_i)^2+(y-y_i)^2+z^2}}$$

$$\approx D(\theta)A\frac{1}{r}\sum_{i=1}^{n}\exp(-2\pi i\frac{r - x_i\frac{x}{r} - y_i\frac{x}{r}}{\lambda})$$

$$= D(\theta)A\frac{1}{r}e^{-2\pi i\frac{r}{\lambda}}\sum_{i=1}^{n}\exp(2\pi i\frac{x_i sin\theta_x + y_i sin\theta_y}{\lambda})$$

$$|P(x,y,z)| =$$

$$A\frac{1}{r}D(\theta)|\sum_{i=1}^{n}\exp\left(2\pi i\frac{x_i sin\theta_x + y_i sin\theta_y}{\lambda}\right)| \qquad (2.3)$$

Here, r is the distance between the origin (i.e., the center of the array) and the observation point P(x, y, z), θ is the angle between z axis and $\overrightarrow{\text{OP}}$. The θ_x and θ_y are the angles between the $\overrightarrow{\text{OP}}$ and the yz & xz planes respectively. It is assumed that all the elements have the same sound pressure amplitude.

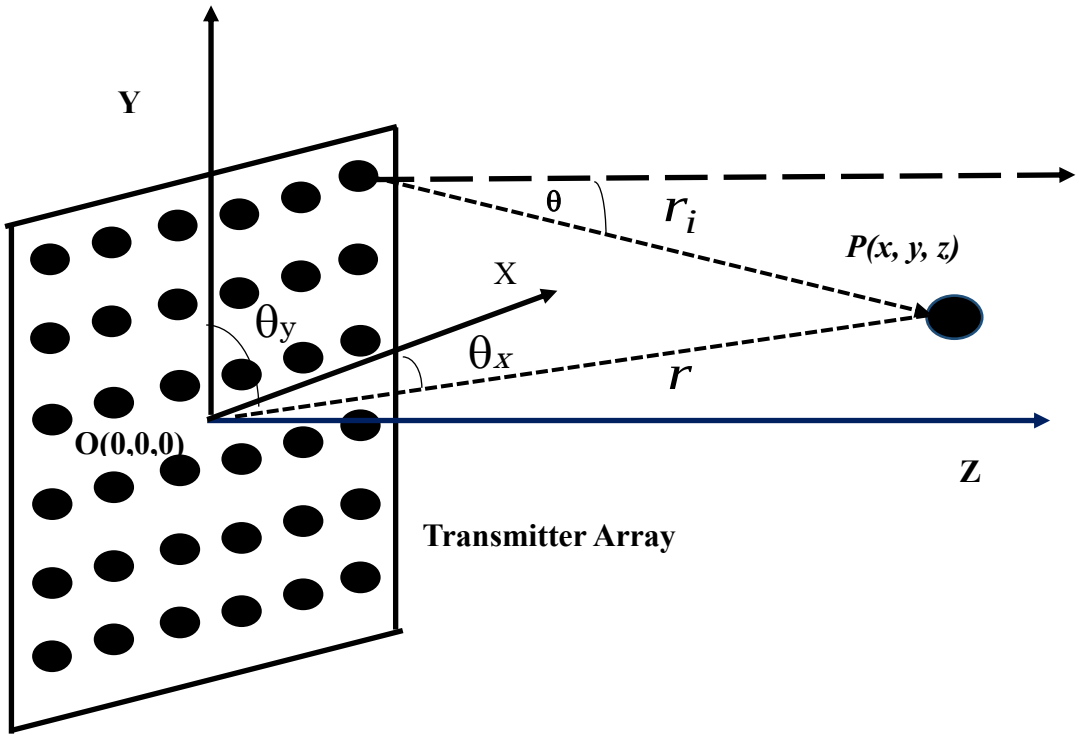

Fig. 2.1: The coordinate geometry for sound pressure calculations.

Fig. 2.2 shows the directivity of single element having a radius of 4.3 mm according to Eq. (2.1).

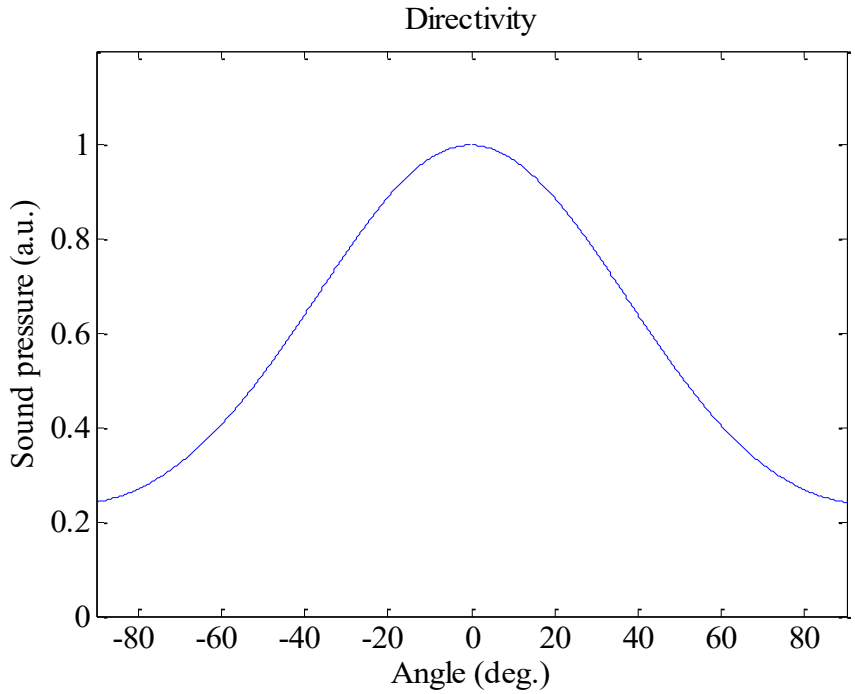

Fig. 2.2: Directivity of single transmitter.

Fig. 2.3 shows the directivities calculated using Eq. (2.3). The elements having radius of 4.3 mm and $n \times n$ transmitting elements are located in square matrix with inter element space of 10 mm in the x and y directions. Here, we assume $\theta_x = \theta;\ \theta_y = 0$, then. The sound pressure is normalized by A/r, here A is the signal amplitude and r is the distance between center of array to the observation point . The sound pressure at the center ($\theta = 0^o$) is directly proportional to the number of elements. The directivity increases with an increase in number of elements. Grating lobes appear at $\theta = 50 - 70°$ because the distance between each element (10 mm) is greater than the wavelength of the ultrasonic wave (8.6 mm). The simulation directivities with different pattern of transmitter array such as (2×2), (5×5), (10×10), (12×12) and (20×20) are shown in Figs. 2.3 (a)-(e). The directivity is about 5° (half width) for an array of (12×12) elements as shown in Fig. 2.4. The sound pressure 144 times higher than the single transmitter is obtained by this array transmitter.

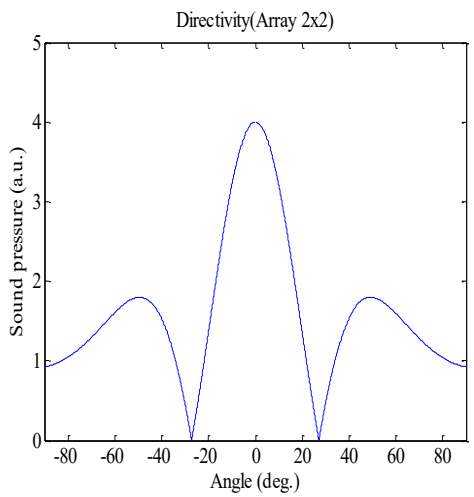

(a) (2×2)

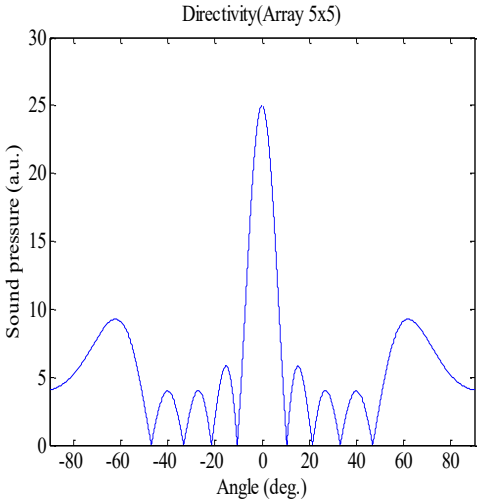

(b) (5× 5)

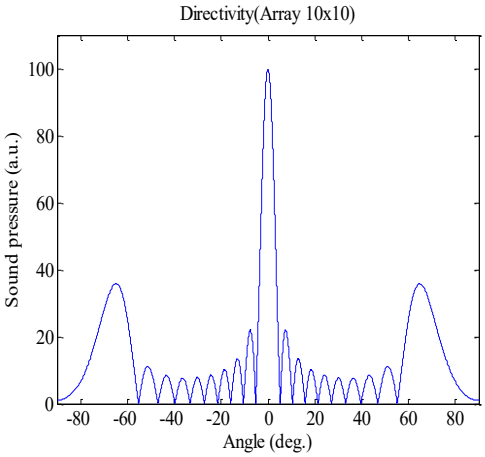

(c) (10× 10)

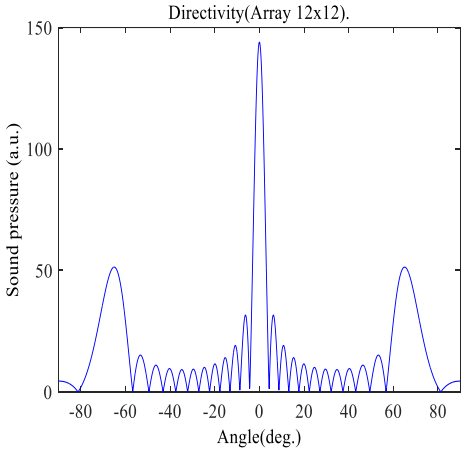

(d) (12× 12)

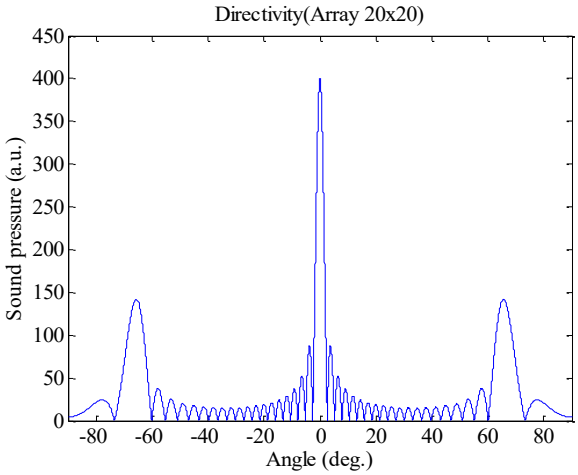

(e) (20 ×20)

Fig. 2.3: Directivities with different pattern of Transmitter arrays.

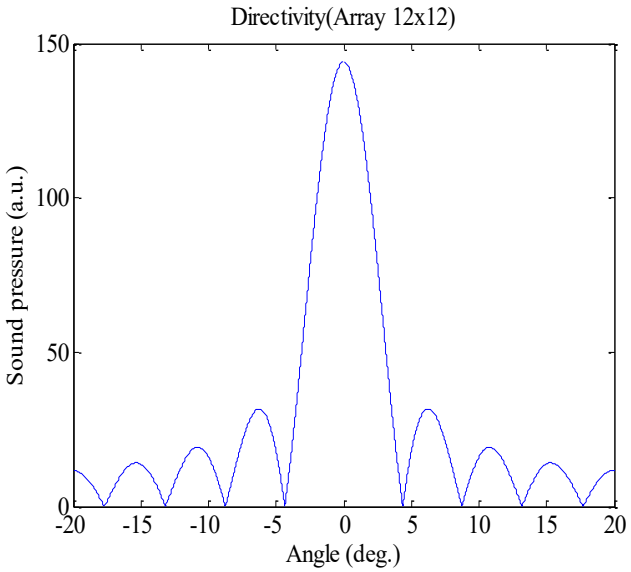

Fig. 2.4: Directivity of ultrasonic array transmitter with (12×12) elements. The sound pressure is normalized by A/r.

Fig. 2.5 shows a two-dimensional color map of the sound pressure for the directions θ_x and θ_y. There are many side lobes along the θ_x and θ_y directions. The side lobes are small in other areas. Fig. 2.6 shows the directivity of (12×12) array transmitter in the direction $\theta_x = \theta_y$. In this case

$$\tan\theta = \sqrt{(\tan\theta_x)^2 + \left(\tan\theta_y\right)^2} \quad = \sqrt{2}\tan\theta_x \tag{2.4}$$

The side lobes become small and the directivity becomes slightly large due to the short average distance of the elements in this direction.

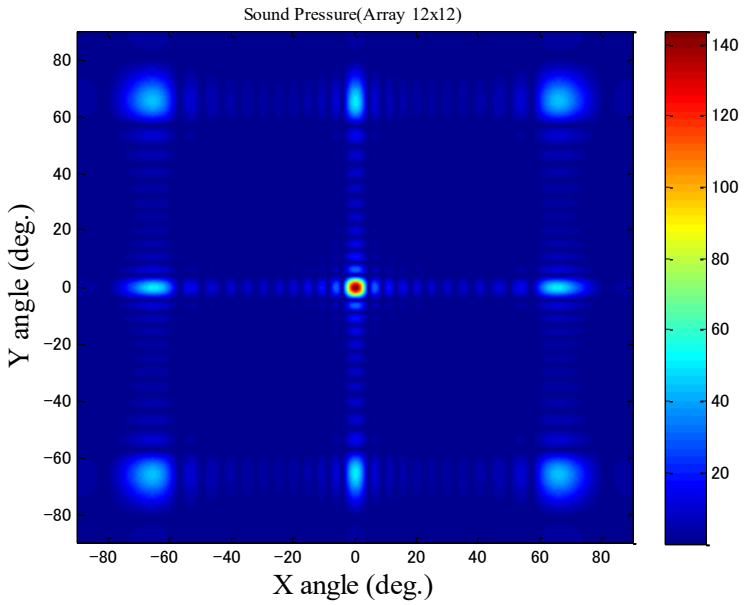

Fig. 2.5: Two-dimensional image of sound pressure. Ultrasonic array transmitter has (12×12) elements. The sound pressure is normalized by A/r.

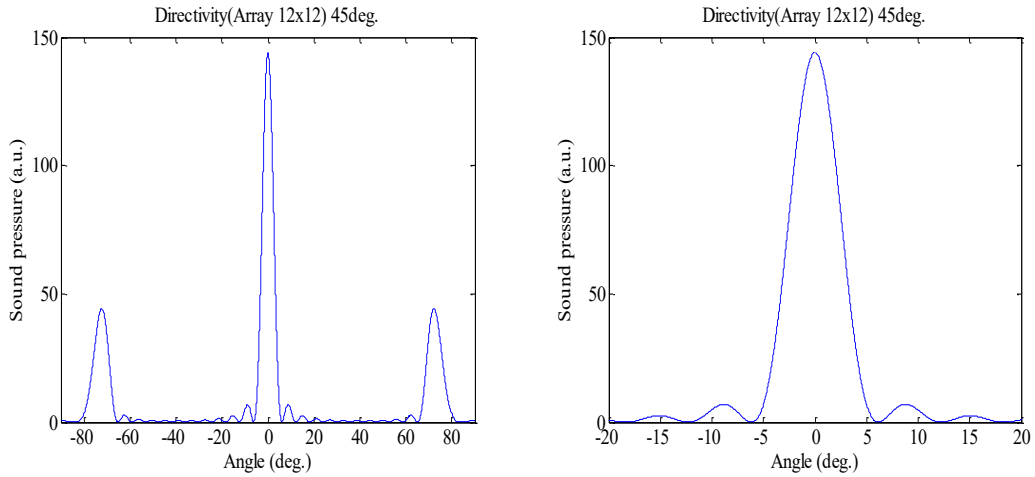

(a) -90° to 90° (b) -20° to 20°

Fig. 2.6: Directivity of ultrasonic array transmitter with (12×12) elements. The sound pressure is normalized by A/r.

2.2.2 Pulse modulation

The range sensors, employ pulse-modulated wave and detect the distance of the object by the pulse echo method using time-of-flight (ToF). This section

discusses the influence of modulation on the transmitter array. It is assumed that the sound amplitude is pulse modulated as given by Eq. (2.5). [1, 2]

$$A = A_0 e^{-\frac{1}{\sqrt{2}}(2t/\tau)^2} \tag{2.5}$$

Here, τ is the pulse width (half) and A_0 is the initial sound pressure. The sound pressure at point P(x, y, z) is calculated using the Eq. (2.6) as follows

$$P(x,y,z)=\sum_{i=1}^{n} D(\theta_i) A_0 e^{-\frac{1}{\sqrt{2}}\{\frac{2(t-r_i/c)}{\tau}\}^2} \frac{e^{-2\pi i \frac{r_i}{\lambda}}}{r_i} \tag{2.6}$$

Here, c is the wave velocity and λ is the wave length. If point P is sufficiently far from the center of the UTA then Eq. (2.6) can be expressed as Eq. (2.7) and (2.8) as follows

$$P(x,y,z) = D(\theta) A_0 \frac{e^{-2\pi i \frac{r}{\lambda}}}{r} \times \sum_{i=1}^{n} \exp(-2\pi i \frac{x_i \sin\theta_x + y_i \sin\theta_y}{\lambda}) \times \exp\left[-\frac{1}{\sqrt{2}} \left\{ \frac{2(t - \frac{r}{c} + \frac{x_i \sin\theta_x + y_i \sin\theta_y}{c})}{\tau} \right\}^2 \right] \tag{2.7}$$

The sound pressure becomes as follows

$$
\begin{aligned}
|P(x,y,z)| &= D(\theta)A_0 \\
&\times \left| \sum_{i=1}^{n} \exp\left(-2\pi i \frac{x_i \sin\theta_x + y_i \sin\theta_y}{\lambda}\right) \right. \\
&\left. \times \exp\left[-\frac{1}{\sqrt{2}} \left\{ \frac{2\left(t - \frac{r}{c} + \frac{x_i \sin\theta_x + y_i \sin\theta_y}{c}\right)}{\tau} \right\}^2 \right] \right|
\end{aligned}
\tag{2.8}
$$

Here, r is the distance between center of the array O (0, 0, 0) and observation point P(x, y, z). The θ_x and θ_y are the angles of vector OP along with X axis and Y axis, respectively. The wave velocity, wave length and pulse width are denoted by c, λ and, τ respectively.

Fig. 2.7 shows the directivity using 1 ms, 0.5 ms and 0.1 ms according to Eq. (2.8) for time $t = r/c$. The directivity does not change when the pulse width is 0.5 ms, whereas it changes significantly when the pulse width is 0.1 ms. This is because different elements have different arrival times due to their different distances r_i. Since the transmitter on the edge of the array is located 55 mm from the center, the maximum difference in the arrival times of different elements is given by Eq. (2.9)

$$
\Delta t = \frac{(n-1)d\sin\theta}{2c} \tag{2.9}
$$

Here, d the inter element space, c the wave velocity and n the number of arrays. The maximum value is obtained 0.16 ms. If the pulse width is shorter than the maximum obtained value by Eq. (2.9), pulse modulation will greatly affect the directivity. However, the main lobe does not change even when the

pulse width is 0.1 ms. It is because on the z axis $\theta_x = \theta,\ \theta_y = 0$ and therefore $\sin\theta_x\, x_i + \sin\theta_y\, y_i = 0$.

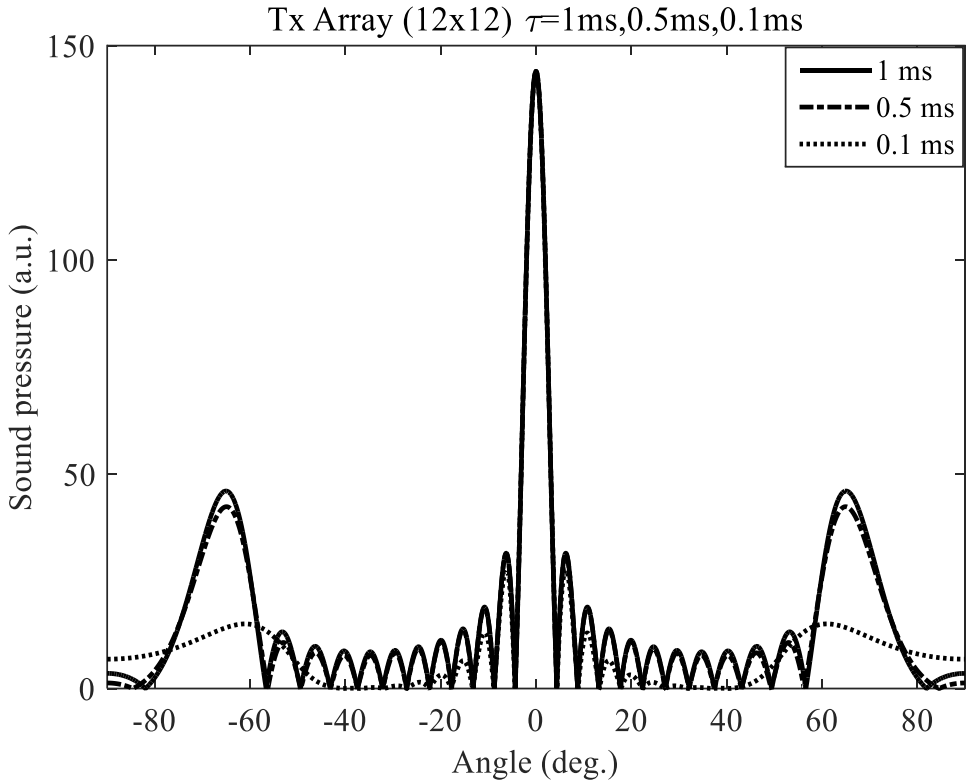

Fig. 2.7: Simulation directivity of ultrasonic transmitter array by modulated pulses 1, 0.5, and 0.1 ms. The sound pressure is normalized by A_0/r.

Fig. 2.8 shows waveforms of modulated signals for various directions. The time of origin $t = r/c$. The sound pressures are normalized by those obtained using Eq. (2.3) for the continuous wave. The pulse waveform does not change significantly when the pulse width is 1 ms. However, the waveform is significantly affected by the pulse width 0.1 ms but it does not change in the θ=0° direction. In time domain, the waveform separates into two peaks increasing the angular direction. It is due to the center of the waveform risen and two pulses eventually merge into a single pulse. The width of the waveform increases with an increase in angular direction.

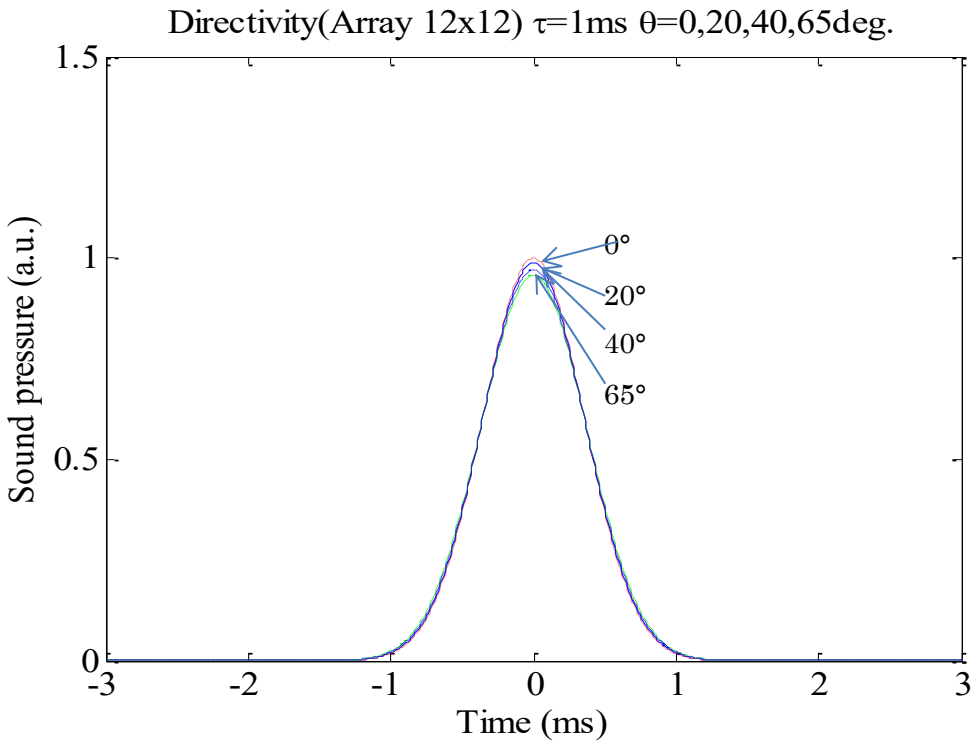

(a) Pulse width: 1 ms

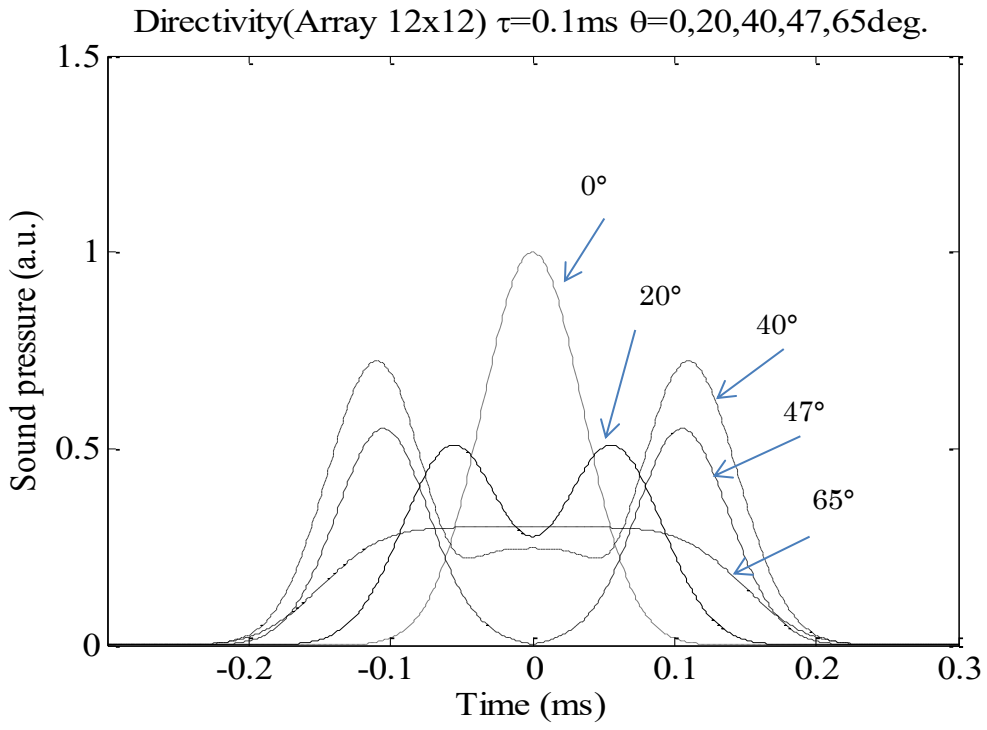

(b) Pulse width: 0.1 ms

Fig. 2.8: Waveforms of modulated signal. The origin of time is $t = r/c$. The sound pressure is normalized by Eq. 2.3 for a continuous wave.

2.2.3 Measurable range

Fig. 2.9 shows the dependence of measurable range of transmitter array with respect to single transmitter. The ratio of the sound pressure of array transmitter to that of single transmitter is denoted by *K* and is 40. Simulation measurable range is calculated with this value and varying the value of absorption coefficient such as 1 m^{-1}, 0.1 m^{-1}, 0.01 m^{-1}, and 0 m^{-1} respectively. The measurable range of single transmitter is considered 3 m. It is observed that measurable increases as the absorption coefficient value decreases and maximum measurable range is obtained when there is no absorption.

The transmitter sends a pulse, and waves reflected from an object are detected by the receivers. The received signal amplitude *A* is proportional to the following quantity given by Eq. (2.10) [1, 2, 7, 11]

$$\mathrm{A} \propto \frac{e^{-2\gamma r}}{r^2} \tag{2.10}$$

Here, r is the distance and γ is the absorption coefficient. Denoting the measurable ranges $r`$ and $r``$, when using single transmitter and array transmitter, respectively. Then a relationship may be given by Eq. (2.11) as follows

$$\frac{e^{-2\gamma r`}}{r`^2} = K\frac{e^{-2\gamma r``}}{(r``)^2} \tag{2.11}$$

Here, *K* is the ratio of the transmission sound pressures of the array transmitter to that of single transmitter. The measurable range increases with the increase in sound pressure.

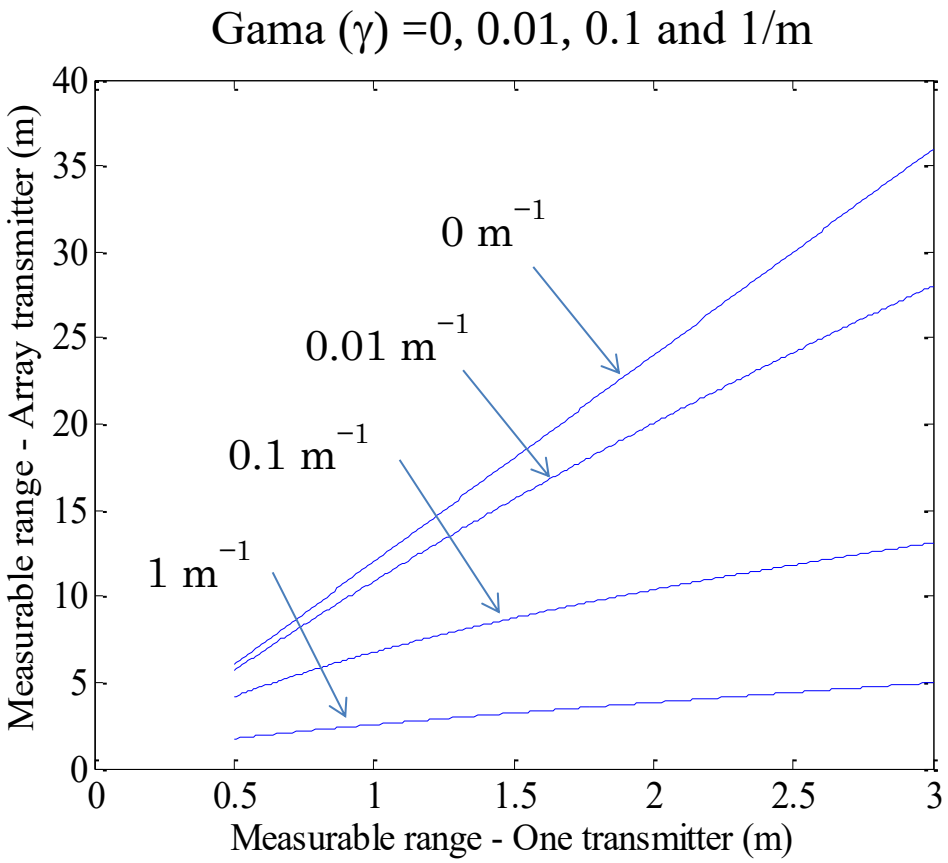

Fig. 2.9: Dependences of measurable ranges of array transmitter system as a function of single-transmitter system. The ratio (K) of transmitting sound pressure is 144.

2.3 Transmitter array structure

Fig. 2.10 is the photograph of the developed high power ultrasonic transmitter array. The developed UTA has been designed by (12×12) array pattern with the inter element spacing of 10 mm. The device TA4010B (radius of 4.3mm) has been used as transmitter and placed in the x-y plane. This device has the directivity of 100° (-6 dB) [8-10].

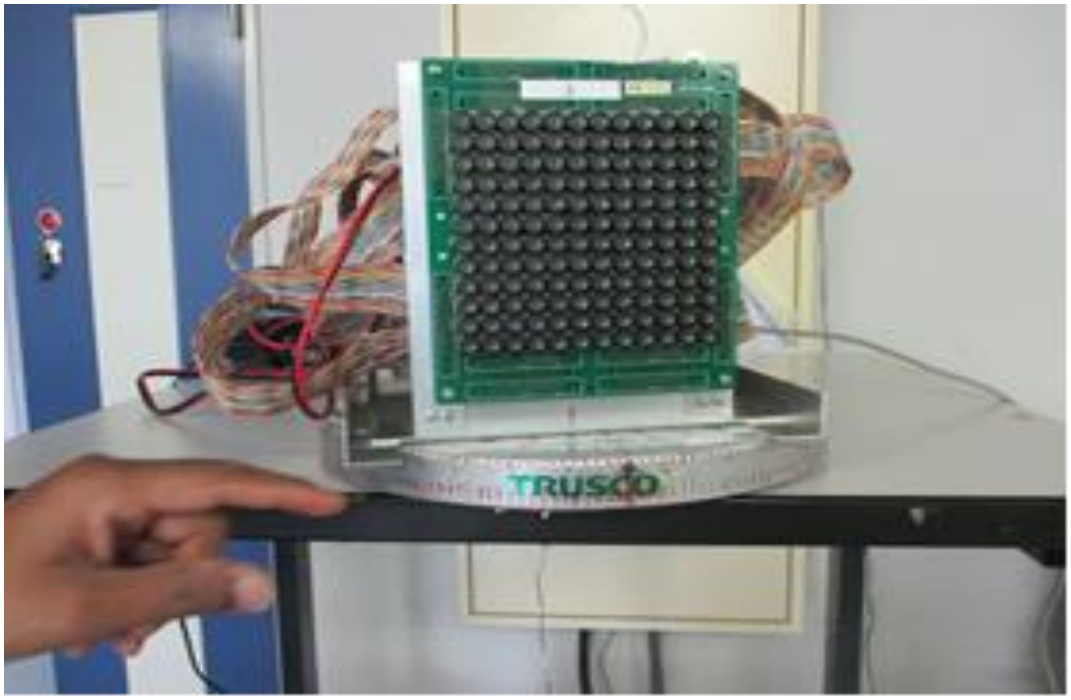

Fig. 2.10: A photograph of the developed ultrasonic transmitter array

Fig. 2.11 shows a block diagram of transmission system. A 40 kHz signal is generated by field programmable gate array (FPGA) in the form of 2 ms pulse width with pulse repetition period 100 ms. There are 144 transmitting elements which are controlled by the four FPGA's. Therefore, each FPGA controls the 36 transmitting elements. One of them acts as the mother board and feed the amplified signal to other three called the slave boards. Both, pulse width and pulse repetition period are controlled by personal computer (PC). The generated digital signals are converted to analogue form by D/A convertors and amplified. Each convertor controls each transmitter independently and equally amplified signal sent to the transmitter before transmission. It gives the equal experimental conditions for each time. The device DAC (AD5415) is being used as a convertor at a sampling rate of 1μs. The converter consists of 2 channels each with 12 bits resolution. The transmitting elements are operated with a maximum voltage of 30 V_{pp}.

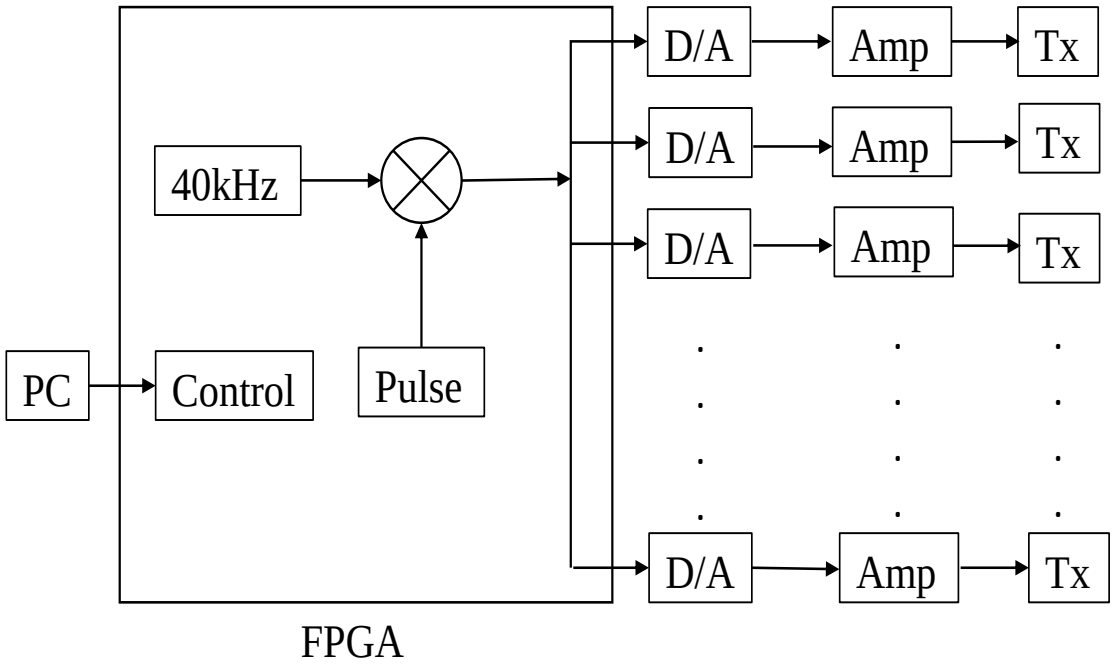

Fig. 2.11: A block diagram of the transmission system

2.4 Experimental set-up

Experimental set-up is shown in Fig. 2.12. Transmitter and receiver (sensor) are 5 m apart from each other and 1.5 m above the ground. A 40 kHz signal is generated by field programmable gate array (FPGA) in the form of 2 ms pulse width with pulse repetition period 100 ms. The analogue signal is received by the receiver and amplified using operational amplifier LM324N up to 30 V_{pp}.

Receiver was calibrated with the transmitted frequency/amplitude using a microphone of free-field response with the diameter approximately 6 mm (46BE; frequency range 4Hz-80kHz, dynamic range 36dB-157dB, G.R.A.S Sound and Vibration A/S), a data acquisition module (USB-4431;24-Bit Analog I/O, sampling rate of 102.4kS/s, and National Instrument Corp.). The whole transmission system is controlled by the PC [1, 2, 8, 9, 10, 11].

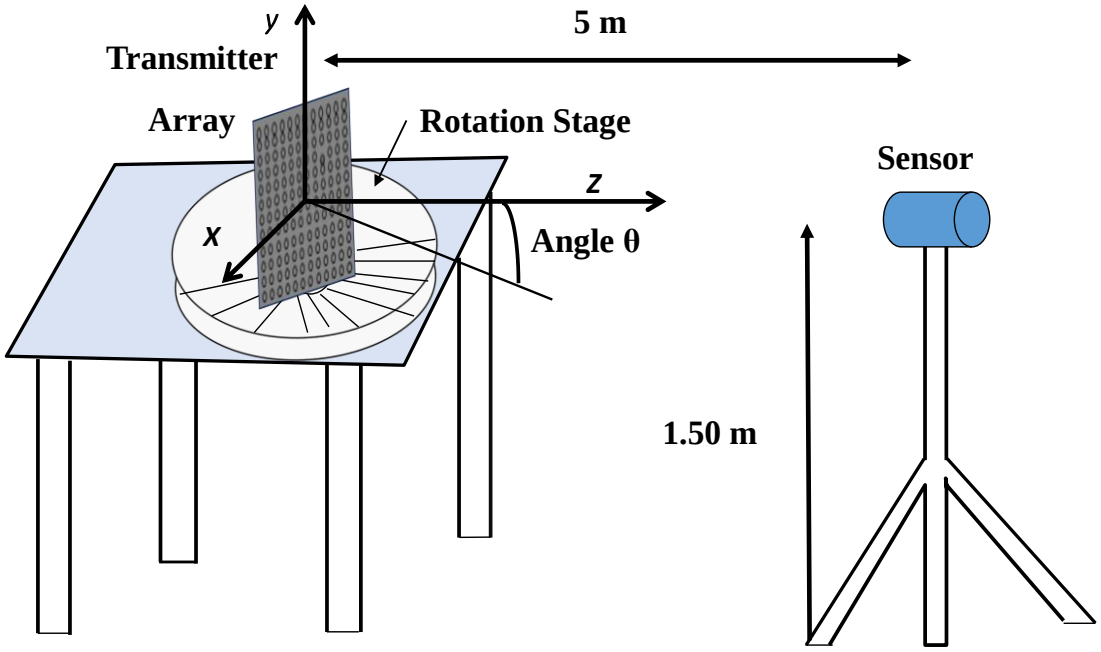

Fig. 2.12: Experimental set-up.

2.5 Experimental method

The device being used as receiver is MA40S4R (Murata Co. Ltd) and its directivity is 80° (-6dB). In this experiment the output of the receiver is amplified about 50 times from its input. To avoid the saturation of the signal due to the amplification capacity of the operational amplifier, input signal of the receiver has been controlled manually. For the experimental uniformity, we allowed only limited signal, to reach to the sensor so that the maximum amplification should not exceed > 6 volt.

Method of reception of transmitted signal is shown in Fig. 2.13. The receiver was 5 m away from the transmitter and speed of the sound is considered 345 m/s at room temperature (23° C). The time taken to travel 5 m distance by the signal is 14.5 ms. Therefore, input pulse is directly received after 14.5 ms. The Peak to peak voltage of the received signal is measured rotating the transmitter on azimuthal angle from 0°~ 90° at 2° steps.

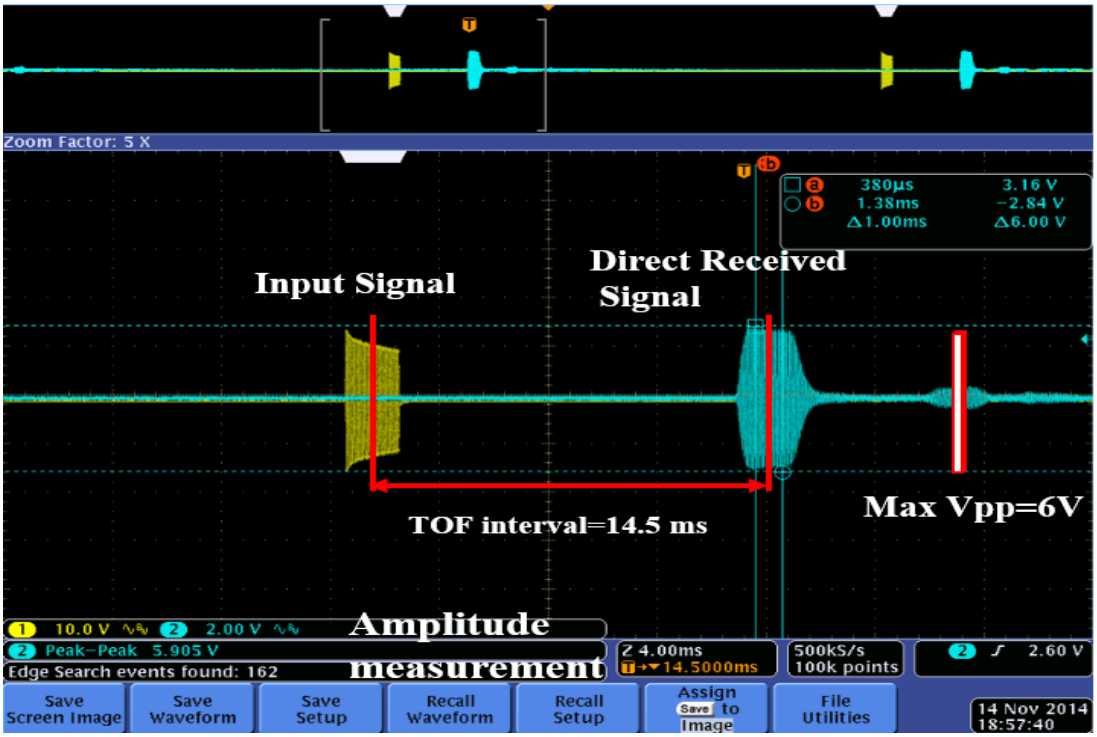

Fig. 2.13: Experimental measurement method.

There was no need to control the input signal of the receiver for (1×1), (2×2) and (5×5), because, the peak to peak voltage of the direct received signal with amplification was < 6 volt. The input signal of receiver for UTAs (10×10) and (12×12) need to be controlled.

2.6 Experimental results

2.6.1 Characteristics of array transmitter

The fundamental characteristics of the array transmitter is investigated in this section. A prototype transmitter is shown in Figs. 2.14 (a) - 2.18 (a). Figs. 2.14 (b) - 2.18 (b) show the theoretical and experimental directivities of different pattern of transmitters; (1×1), (2×2), (5×5) (10×10) and (12×12), respectively. As number of transmitting element increases the sound pressure also increases. The experimental results are in good agreement with the simulation results. According to simulation result, the object detection view angle becomes narrow on increasing the number of transmitting elements.

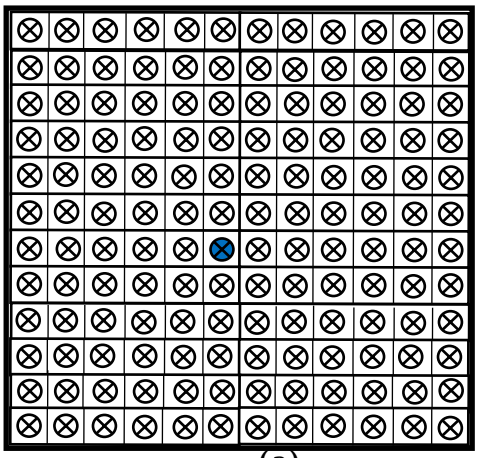

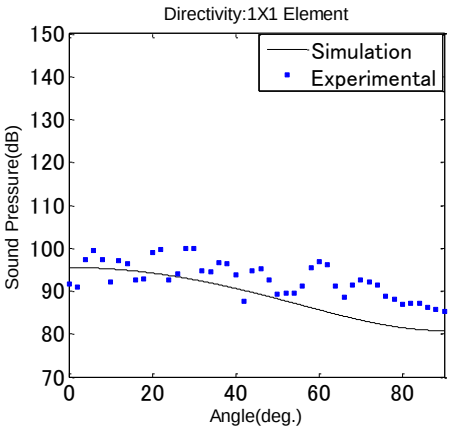

(a) (b)

Fig. 2.14(a): Single Transmitting element (b): Theoretical and experimental directivity.

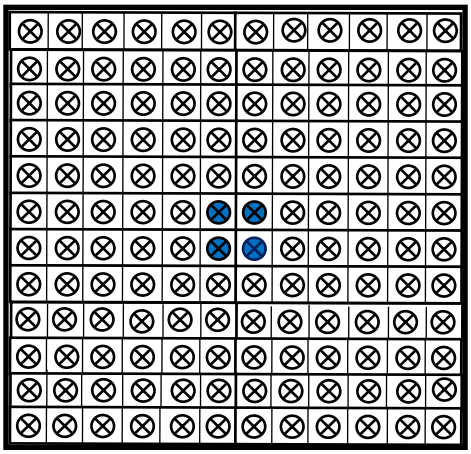

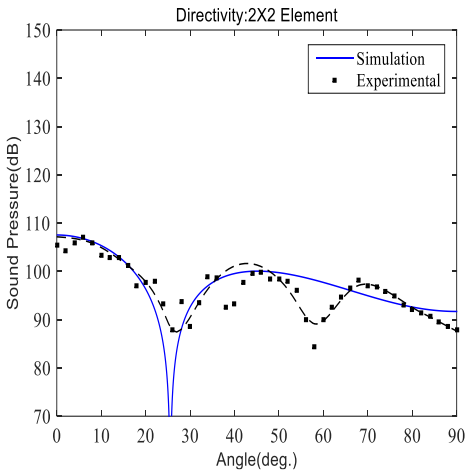

(a) (b)

Fig. 2.15 (a): (2×2) array pattern; (b): Theoretical and experimental directivity.

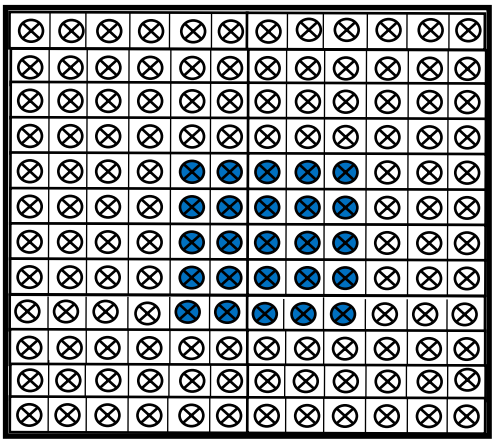

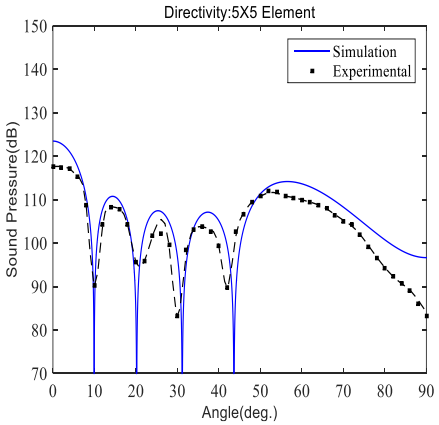

(a) (b)

Fig. 2.16 (a): (5×5) array pattern; (b): Theoretical and experimental directivity.

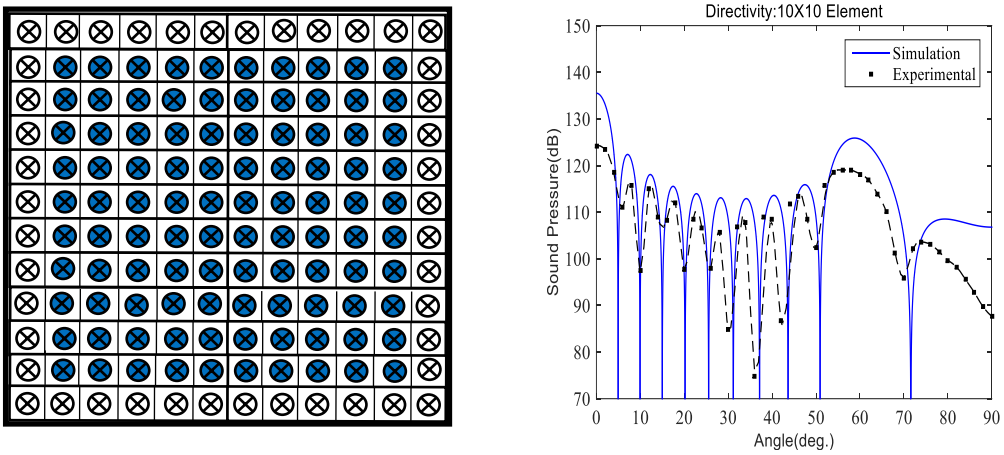

(a) (b)

Fig. 2.17 (a): (10×10) array pattern; (b): Theoretical and experimental directivity.

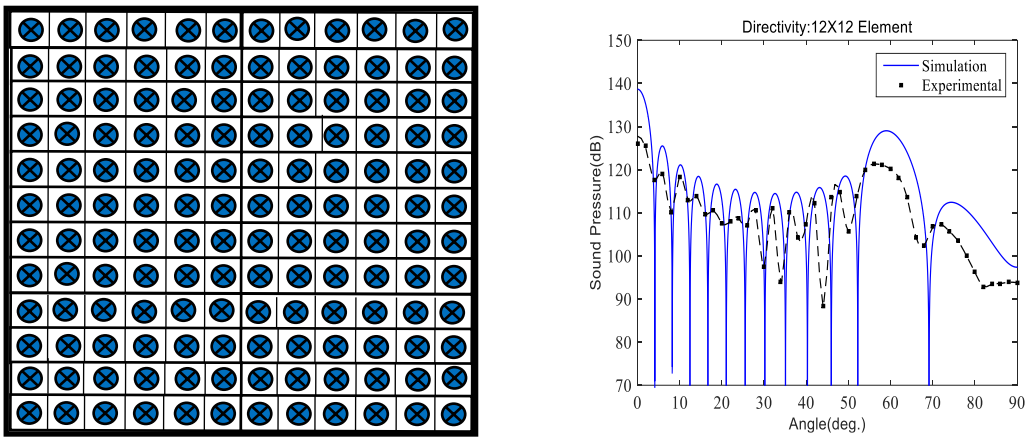

(a) (b)

Fig. 2.18 (a): (12×12) array pattern; (b): Theoretical and experimental directivity.

The sound pressue levels with respect to number of transmitting element (theoretical vs experimental results) are shown in Fig. 2.19. Our theoretical results shows that the directivity increases linearly as we increase the number of transmitting elements. However, experimental results show, that sound pressure level does not increase linearly, it is because of air turbulance and individual characteristics of each transmitting element.

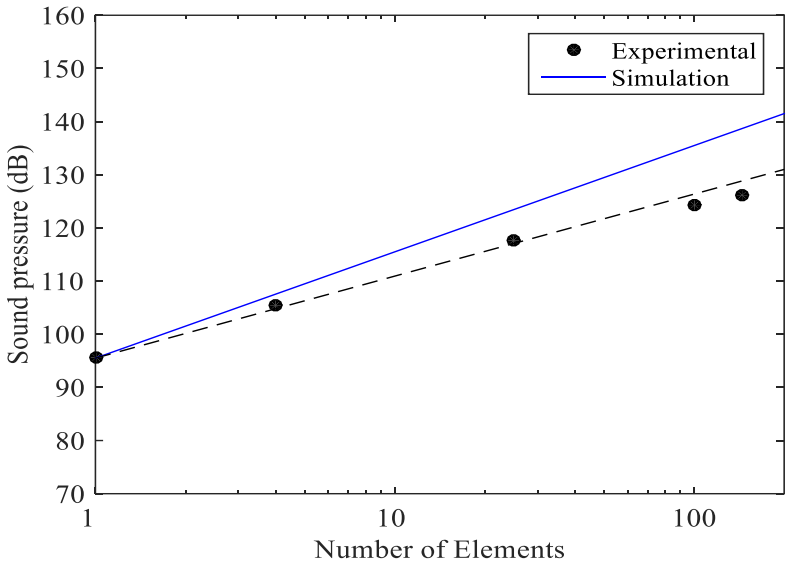

Fig. 2.19: Dependence of SPL with respect to number of transmitting elements.

2.6.2 Pulse modulation and sound pressure level

The characteristics of array transmitter on the pulse modulation is investigated. Input pulse widths applied to the UTA and received output pulse widths are shown in Fig. 2.20. Pulse modulation of the transmitted signal has been confirmed by receiving the directly applied pulse widths such as 2 ms, 1 ms and 0.5 ms.

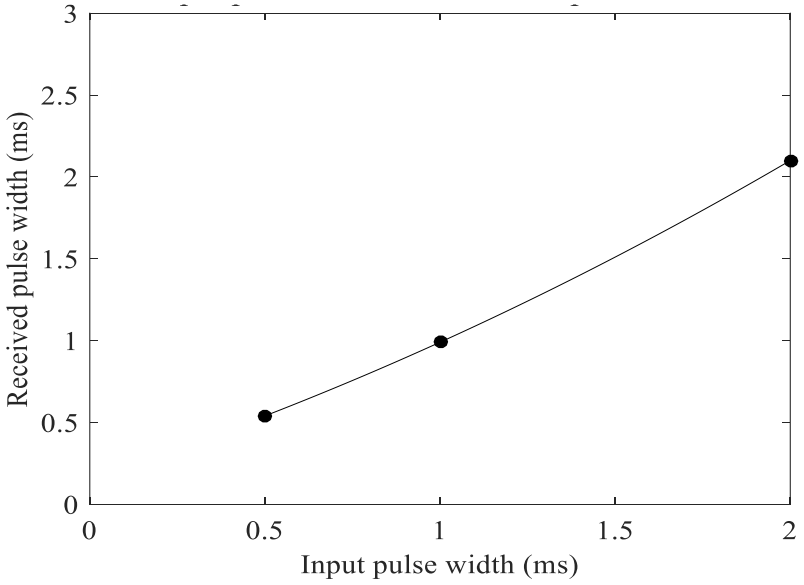

Fig. 2.20: Received pulse width as a function of input pulse width.

Fig. 2.21 shows the sound pressure level of UTA and single transmitter. Both transmitters show similar trend, therefore array structure has no influence of the pulse modulation. The SPLs using UTA at 0^o with 2 ms, 1 ms and 0.5 ms pulse width and pulse repetition period 100 ms were 123.8, 125.9 and 126 dB and using single transmitter were 92.52, 93.14 and 94 dB, respectively. A small difference in the sound pressure is obtained using different pulse width, it is due to the frequency response of each element.

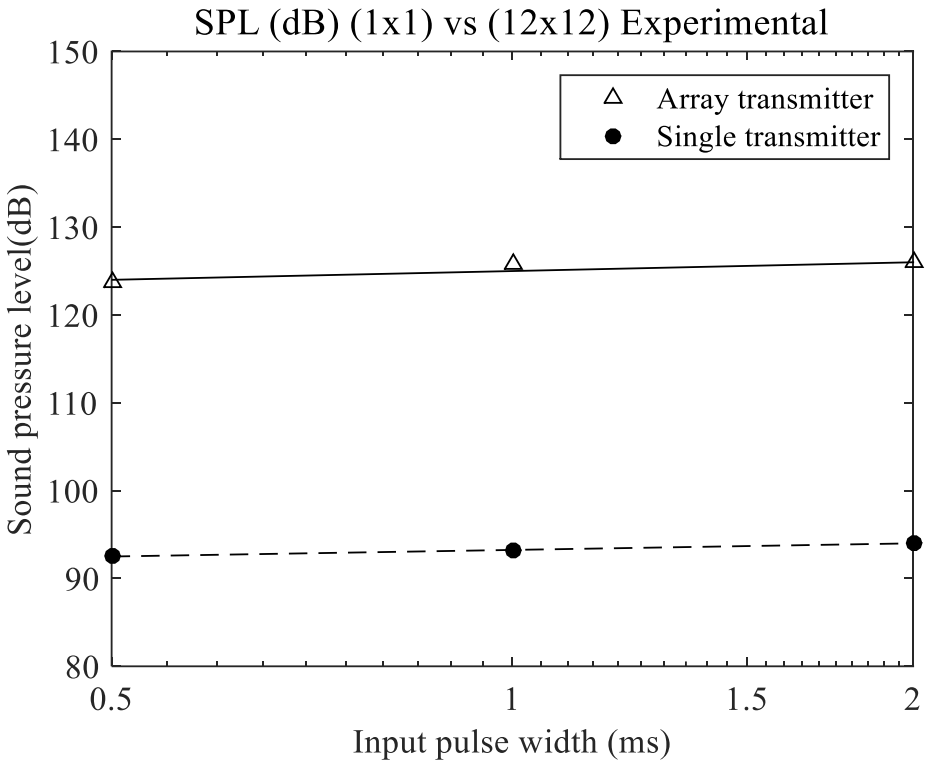

Fig. 2.21: Dependence of SPL with respect to pulse width (UTA and single transmitter).

2.6.3 Pulse modulated directivities

Figs. 2.22 (a)-(c) show the simulation and experimental directivity of UTA with 2 ms, 1 ms and 0.5 ms pulse widths respectively using Eq.(2.8) considering time $t=r/c$. The smooth line shows the simulation results and dots are the experimental results.

According to experimental conditions; d=10 mm, n=12, c=345 m/s and maximum value of $Sin\theta$ is taken, then maximum arrival time is 0.16 ms. If the pulse width is less than this value, the directivity is greatly affected. Further,

main lobe does not change with the shorter pulse (0.1 ms) also due to the resonance frequency as shown in Fig. 2.7. The experimental results are in good agreement with the theoretical results. With this high power (12×12) transmitter array, 32 dB higher sound pressure level is obtained than that of single transmitter.

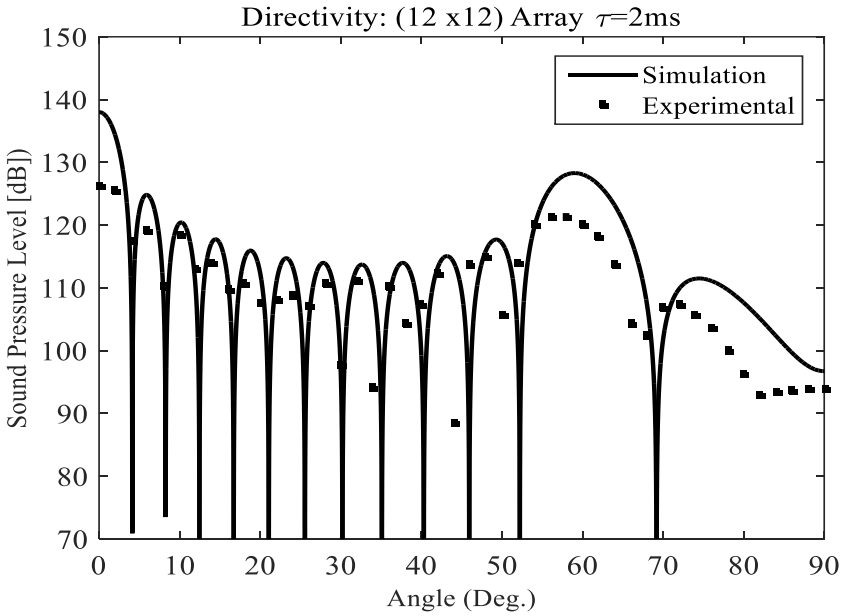

(a) τ=2 ms

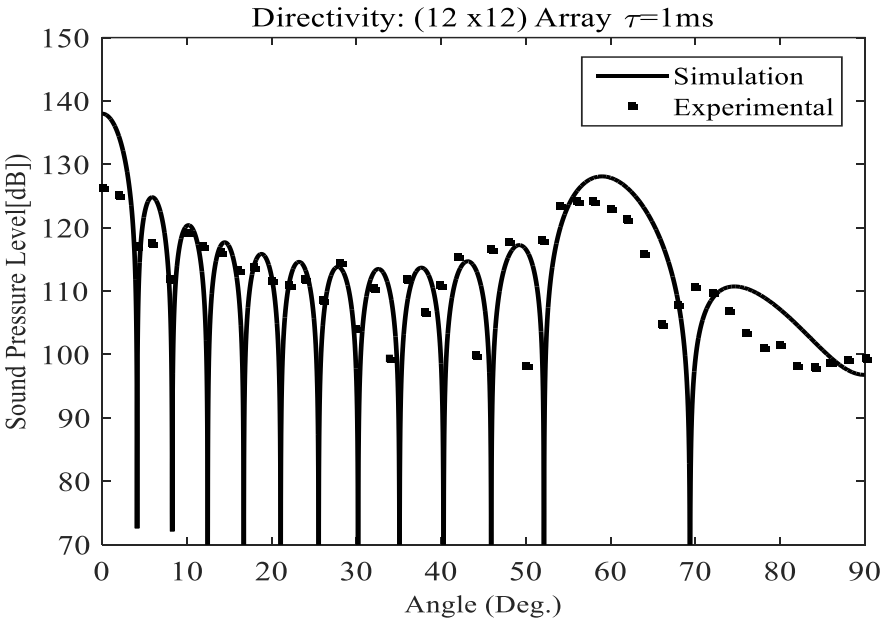

(b) τ=1 ms

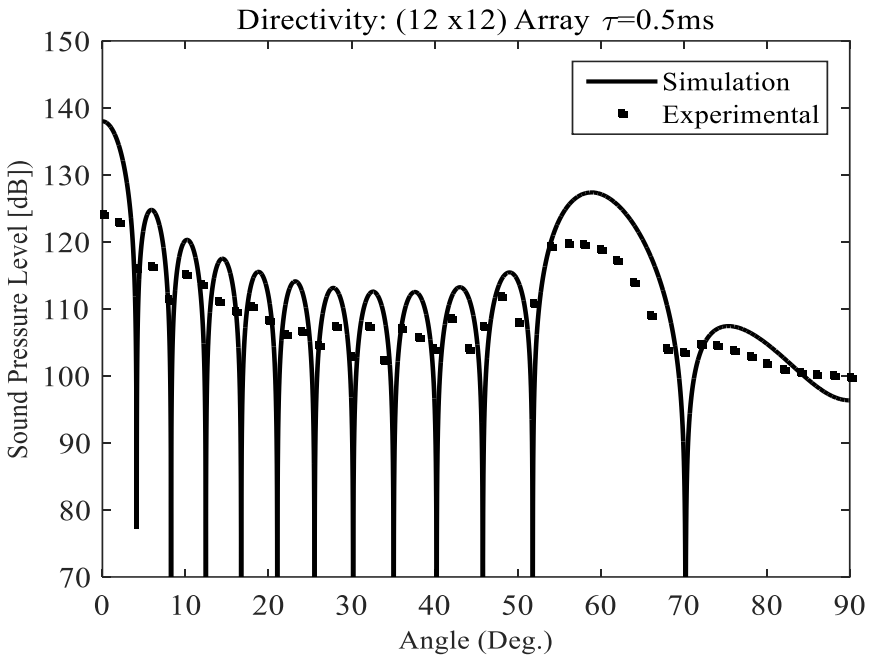

(c) τ=0.5 ms

Fig. 2.22: UTA directivities with short pulse modulation.

2.7 Conclusion

An ultransonic transmitting system has been developed using (12×12) array pattern of transmitting elements. Charactrization of the system are performed with the following considerations; (i) Different pattern of Transmitter array (ii) Pulse modulation. The developed system worked satisfactory on both factors. Sound pressure increases as number of transmitting element increases. Theoretically, sound pressure increases linearly but not experimentally. It is due to various factors such as air turbulance, humidity, temperature, individual characteristics of each element etc. In comparison of conventional method >30 dB higher sound pressure level has been obtained with this system. Secondly, array transmitter and single transmitter both show the same trend when pulse modulation applied to the system. It means array structure has no influence of the modulated pulse. A very small difference in sound perssure level is found due to the frequency response of each element. Experimental results are in good agreement with the theoretical calculations.

References

[1] S. Kumar, K. Ichi and H. Furuhashi, Theoretical investigation of high-power ultrasonic array transmitter for a range sensor in air, Proc. IEEE, Int. Conf. on Industrial Technology ICIT 2013, IEEE Xplore (2013), pp.1190-1195, DOI:10.1109/ICIT.2013.

[2] S. Kumar, Q. Wei and H. Furuhashi, Characteristics of high power ultrasonic array transmitter in the air, Proc. IEEE 2015, Int. Conf. on Recent Developments in Control, Automation and Power Engineering, RDCAPE-2015, (2015) pp.209-213, DOI:10.1109 /RDCAPE.2015.7281397.

[3] R. Hickling and S.P. Marin, The use of ultrasonics for gauging and proximity sensing in air, J. Acoust. soc. Am. 79(4) (1986), pp.1151-1160, DOI:10.1121/1.393387.

[4] D. H. Turnbull and F.S. Foster, Beam Steering with Pulsed Two-Dimensional Transducer Arrays, IEEE Transactions on Ultrasonics, Ferroelectrics and Frequency control, 38 (4) (1991).

[5] P.N. Keating, T. Sawatari and G. Zilinskas, Signal processing in acoustic imaging, Proc. IEEE 67(4) (1979), pp.496-510, DOI: 10.1109/ PROC.1979.11279.

[6] L.J. Griffiths and K.M. Buckley, Quiescent pattern control in linearly-constrained adaptive arrays, IEEE transactions on acoustic, speech and signal processing, ASSP-35 (1987), pp.917-926.

[7] T. Tanaka, S. Lee, M. Uno, K. Inoue, S. Aoyagi, K. Yamashita and M. Okuyama, Improvement of ultrasonic micro array sensor using the amorphous fluorocarbon polymer film, the transactions of the institute of electrical engineers of Japan. A publication of sensors and micromachines society 127 (1) (2007), pp.7-13.

[8] H. Furuhashi, J. Valle, Y. Uchida and M. Shimizu, Imaging sensor system using dispersed ultrasonic array. Proc. of Int. conf. on control, automation and system (ICCAS 2007), FEP-35, (2007), pp.2385-2388.

[9] H. Furuhashi, Y. Uchida and M. Shimizu, Imaging sensor system using rectified delay-and-multiply operations with an ultrasonic array, Proc. IEEE, IECON 2008, IEEE Xplore (2008), pp.1891-1895.

[10] H. Furuhashi, Y. Uchida and M. Shimizu, Imaging sensor system using composite ultrasonic array, Sensors 2009, IEEE Xplore (2009), pp. 1467-1472.

[11] H. Furuhashi, S. Kumar and M. Shimizu, Signal processing of a 3D ultrasonic imaging sensor that uses the spread spectrum pulse compression technique, Lecture notes in information technology, Proc. 2012 Int. Conf. on Future Information Technology and Management Science & Engineering FITMSE 2012, 14 (2012), pp.145-150.

Chapter 3

Long-Range Measurement System Using Ultrasonic Transmitter Array and Range Sensor in Air[1-3]

3.1 Introduction

Ultrasonic wave applications in robotics, amusement, security, and industrial use have amazing benefits of this technology. Ultrasonic transmitter arrays (UTAs) have been used for beam forming [4-8]. In general, they are used for directional scanning and obtaining range images. Moreover, ultrasonic range sensors without beam scanning have been investigated. They use single transmitter in combination with receiver arrays. The distance of object is calculated using the time of flight measurement method, and the direction is calculated by delay-and-sum (DAS) operations [9–12]. Such an ultrasonic imaging sensor system has several advantages over others due to its simple construction and maintaining privacy while monitoring human activities. The measurable range of such system is limited up to a few meters in air due to the absorption of ultrasonic waves. Therefore, we focused our work for improvement in the measureable range.

Following efforts have been made to improve the measurable range; spread spectrum pulse compression techniques [12], and developing a high-power transmitter via spark discharge, [13, 14] etc. The measurable range > 6 m using first method and >10 m by the second method has been reported. We propose and construct a high power ultrasonic transmitter array for further improvement in measurable range. The characteristics of the UTA were investigated via computer simulations and experimentally [9-11].

3.2 Ultrasonic transmitter array (UTA)

The same UTA has been used as shown in Fig. 2.11 in Chapter-2 that consists of (12 ×12) arrays of transmitting elements; the device T4010B4 (Nippon Ceramic Co. Ltd). The sound pressure level 126 dB has been obtained with this UTA [1, 2].

3.3 Ultrasonic receiver array (URA)

Fig. 3.1 shows ultrasonic receiver array (URA) that has been developed for range sensing. It consists of 32 receivers (Knowledge Acoustics, SP0103NC3-3; 6.15 mm × 3.76 mm) [3].

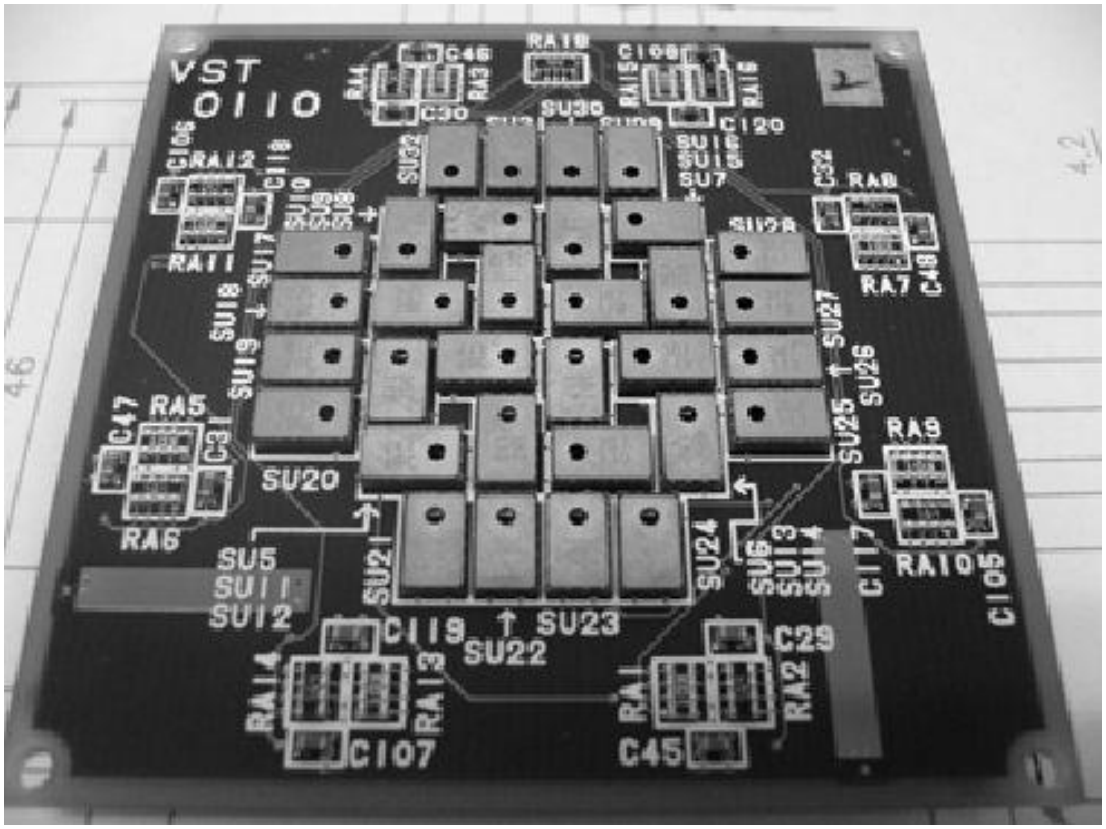

Fig. 3.1: The developed ultrasonic receiver array (URA).

Fig. 3.2 is the block diagram of ultrasonic receiving system. The transmitted ultrasonic sound is received by the receivers after reflection from the object. Then received signal is converted to digital by an A/D converter system using a device TSM-372012 (Interface Corporation). Signal conversion from analog to digital takes place after every 2.5 μs with a resolution of 12 bits. The DAS operations were performed on all direction to determine the 3D positions of target objects using MATLAB and Simulink. The whole system (transmitting and receiving) is controlled by a PC. Noise is reduced to its threshold level and range images are obtained by time-of-flight measurement method. Positions of the URA elements are shown in Table-3.1.

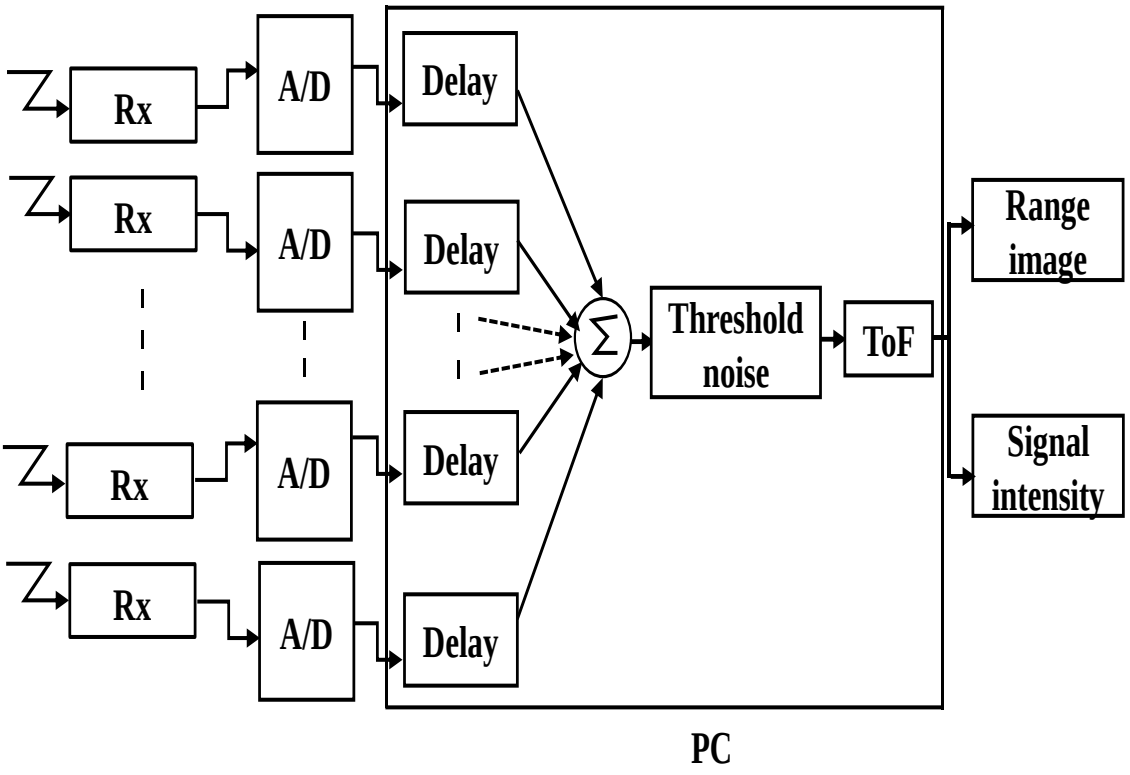

Fig. 3.2: A block diagram of ultrasonic receiving control system.

Table-3.1: Position of receiving elements (mm)

Ele. No.	X axis	Y axis	Ele. No.	X axis	Y axis
1	0	0	17	-11.1	4.2
2	0	-4.2	18	-11.1	0
3	4.2	-4.2	19	-11.1	-4.2
4	4.2	0	20	-11.1	-8.4
5	-4.2	0	21	-4.2	-15.3
6	0	-8.4	22	0	-15.3
7	8.4	-4.2	23	4.2	-15.3
8	4.2	4.2	24	8.4	-15.3
9	0	6.9	25	15.3	-8.4
10	-6.9	4.2	26	15.3	-4.2
11	-6.9	4.2	27	15.3	0
12	-4.2	-11.1	28	15.3	4.2
13	4.2	-11.1	29	8.4	11.1
14	11.1	-8.4	30	4.2	11.1
15	11.1	0	31	0	11.1
16	8.4	6.9	32	-4.2	11.1

Delay-and-sum operations are used on the reflected signal received by the sensor array. Let us consider a one dimensional array consisting of *n* receiving elements with the inter element space *d*. If the angle of the reflected signal from an object is θ and time delay is applied by Eq. (3.1) as shown in Fig. 3.3.

$$(n-1)\frac{d\ \ Sin\theta_0}{\lambda} \tag{3.1}$$

Here, *n* is the number of receiving element, λ is the wavelength of the ultrasonic sound, *d* is the inter element space and θ_o is the angle of deviation. The phase difference is given by Eq. (3.2) as follows

$$(n-1)\frac{d\ \ (Sin\theta - Sin\theta_0)}{\lambda} \tag{3.2}$$

If the duration of the pulsed ultrasonic sound is > (*n*-1) *d/c* the received sound pressure in that direction is calculated by Eq. (3.3) as follows

$$P(\theta) = \sum_{n=1}^{N} D(\theta) \exp\{i2\pi \frac{(n-1)d\ \ (Sin\theta - Sin\theta_0)}{\lambda}\}$$

$$= D(\theta) \frac{1 - \exp\{i2\pi \frac{Nd\ \ (Sin\theta - Sin\theta_0)}{\lambda}\}}{1 - \exp\{i2\pi \frac{d\ \ (Sin\theta - Sin\theta_0)}{\lambda}\}}$$

$$= D(\theta) \frac{\mathrm{Sin}\{\pi \frac{Nd\ \ (Sin\theta - Sin\theta_0)}{\lambda}\}}{\mathrm{Sin}\{\pi \frac{d\ \ (Sin\theta - Sin\theta_0)}{\lambda}\}} \exp\{i\pi \frac{(N-1)d(Sin\theta - Sin\theta_0)}{\lambda}\} \tag{3.3}$$

Dividing the Eq. (3.3) by N, a normalized Eq. (3.4) is obtained as follows

$$P_w(\theta) = D(\theta) \frac{\mathrm{Sin}\{\pi \frac{Nd\ \ (Sin\theta - Sin\theta_0)}{\lambda}\}}{\mathrm{N}\ \ \mathrm{Sin}\{\pi \frac{d\ \ (Sin\theta - Sin\theta_0)}{\lambda}\}} \exp\{i\pi \frac{(N-1)d(Sin\theta - Sin\theta_0\}}{\lambda}\} \tag{3.4}$$

If Omni-directional microphones are used, then sound pressure becomes as Eq. (3.5)

$$|P_w(\theta)| = |\frac{\mathrm{Sin}\{\pi \frac{Nd\ \ (Sin\theta - Sin\theta_0)}{\lambda}\}}{\mathrm{N}\ \ \mathrm{Sin}\{\pi \frac{d\ \ (Sin\theta - Sin\theta_0)}{\lambda}\}}| \tag{3.5}$$

Theoretical investigations have been made using receiver array according to Eq. (3.5) considering inter element space d=5 mm, wave velocity is 345 m/s and ultrasound frequency 40 kHz.

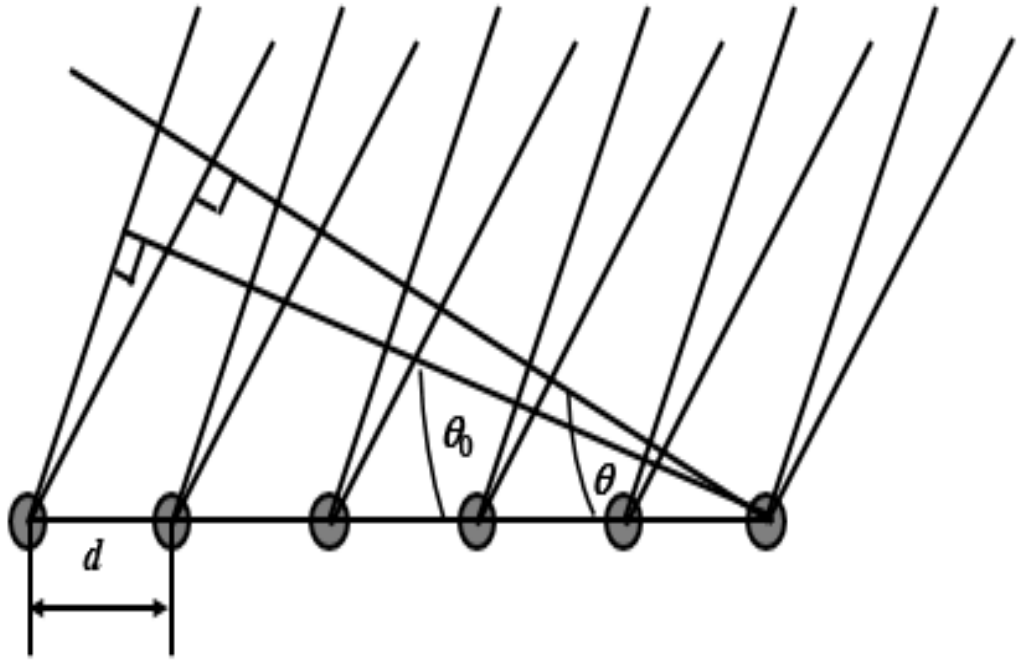

Fig. 3.3: One dimensional receiver array.

Fig. 3.4 shows the directivities of the array receiver when the angle of deviation θ_0 is 0°, 20° and 40°. The width (FWHM) is about 10° when the angle of deviation is 0°. If the threshold level is 90% of the peak, the resolution is a few degrees. The width slightly increases with the increase in the angle of the deviation. There are many side lobes and may cause ghost images, if strong sound is received from the direction of side lobes. A grating lobe also appears for the angle of deviation in 40°.

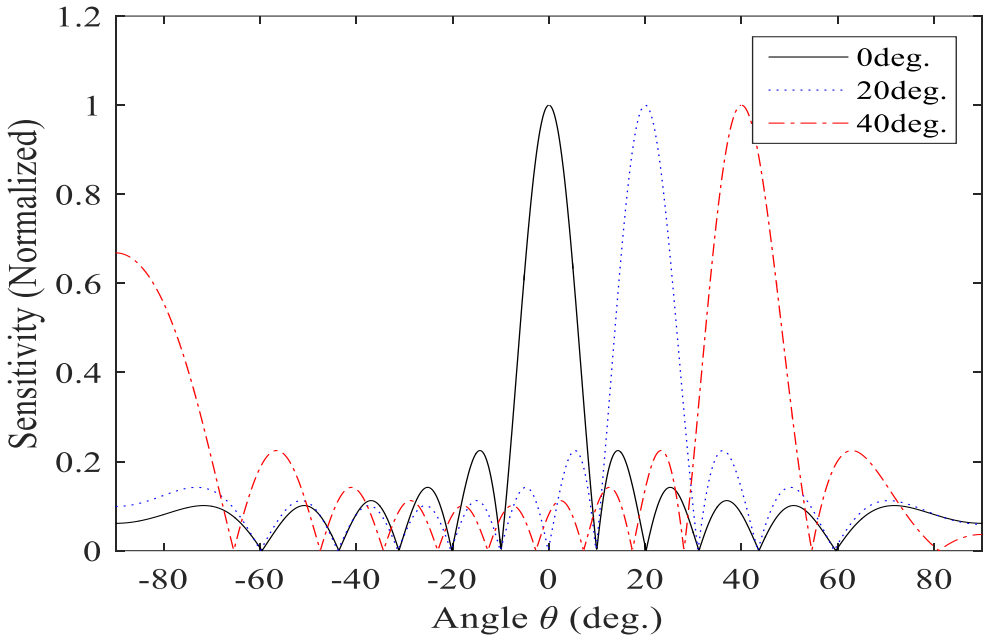

Fig. 3.4: Directivities of the array receiver at the angle of deviation θ_0 =0º, 20º and 40º.

Fig. 3.5 shows the directivity of the sensitivities for the number of elements 3, 10 and 20. The angle of the deviation is 0º. The width decreases with the increase in the number of elements.

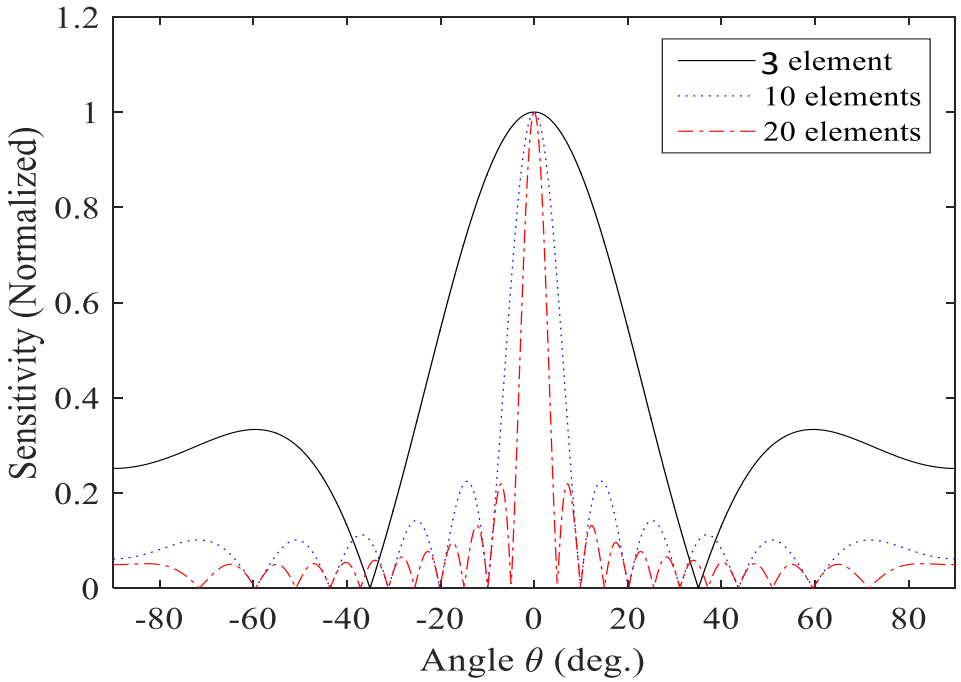

Fig. 3.5: Directivity of the array receiver for the number of elements 3, 10 and 20.

The width (FWHM) is approximately calculated by

$$\frac{\sin\left(N\frac{\pi d}{\lambda}\frac{\Delta\theta}{2}\right)}{N\sin\left(\frac{\pi d}{\lambda}\frac{\Delta\theta}{2}\right)} \approx \frac{1}{2}$$

$$N\frac{\pi d}{\lambda}\frac{\Delta\theta}{2} \approx \frac{2}{3}\pi$$

$$\Delta\theta \approx \frac{4\lambda}{3Nd} \qquad (3.6).$$

Fig. 3.6 shows the dependence of the width of the directivity on the number of elements.

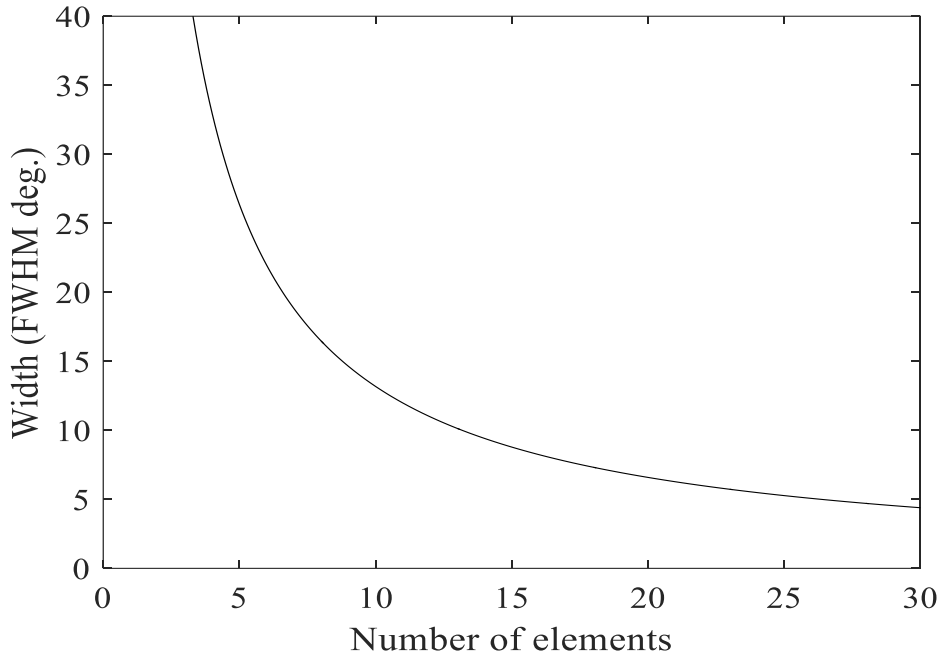

Fig. 3.6: Dependence of the width of the directivity for the array receiver on the number of elements.

The m th order side lobes appear at the angle given by Eq. (3.7)

$$\pi\frac{Nd(\sin\theta-\sin\theta_0)}{\lambda} = \pi\left(m+\frac{1}{2}\right) \qquad (3.7)$$

$$\theta = \sin^{-1}\left(\frac{\lambda}{Nd}\left(m+\frac{1}{2}\right)+\sin\theta_0\right)$$

The normalized sound pressure is calculated using Eq. (3.8) as follows

$$|P_m| \approx \left|\frac{1}{N\sin\left\{\pi\frac{(m+1/2)}{N}\right\}}\right| \tag{3.8}$$

Fig. 3.7 shows the dependence of the side lobes sensitivities normalized by the main lobe. The side lobe decreases with the increase in the number of elements. However, it does not become to 0. The value of the 1st order side lobe becomes to $\frac{2}{3\pi} \approx 0.2$ for the large number of elements.

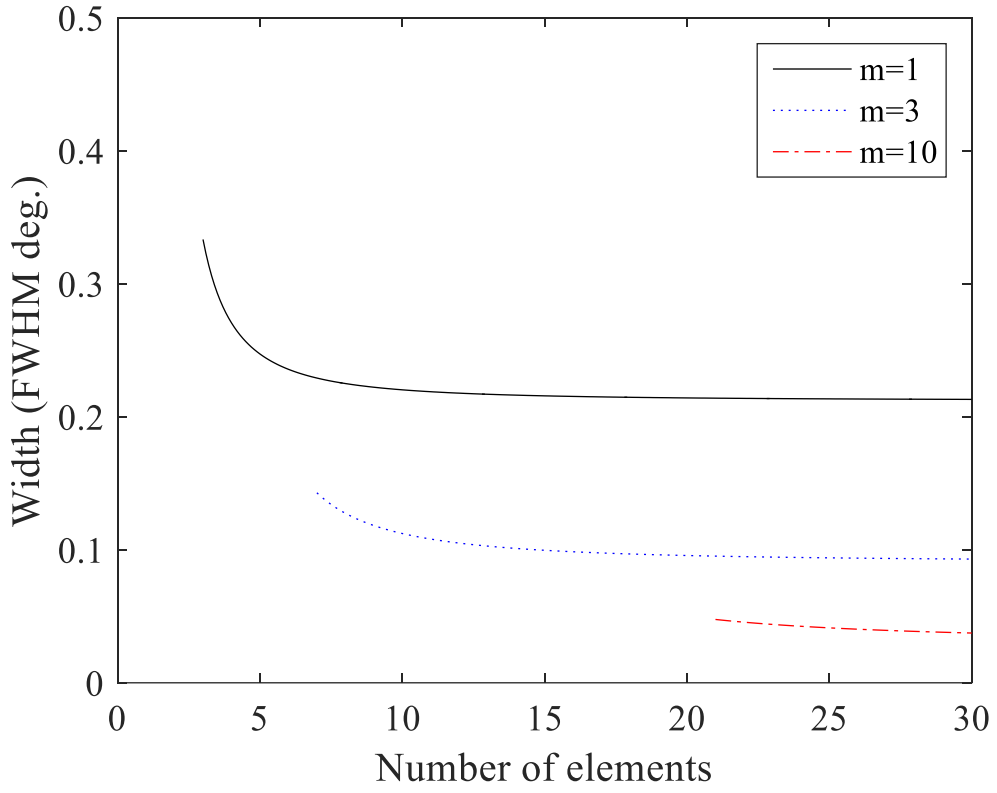

Fig. 3.7: Dependence of the width of the directivity for array receiver on the number of elements for the side lobe orders 1, 3 and 10.

3.4 Principle of object detection

In our ultrasonic imaging system, transmission and reception part are controlled by a personal computer (PC). Noise is reduced to its threshold level and range images are obtained by time-of-flight (TOF) measurement method. The Delay-and-sum (DAS) operations are performed on all directions to determine the 3D position of target object using MATLAB and Simulink.

Measurable range is detected using short pulse width and pulse repetition period was kept in such a way that previously transmitted pulse is completely received back after reflecting from an object, before the transmission of next pulse. Ultrasonic waves are emitted by UTA, reflected back from an object and received by the URA. The DAS operations are performed to process the reflected signals detected by the URA. The distribution of the maximum signal intensity in the 3D image of the range data are calculated at the time when the correlated signal reaches to its maximum value.

The images are displayed in a standard set of pixels and determined by MATLAB and Simulink program. The total angular field of view of ultrasonic receiver array is also fixed. For example an object placed at particular distance in $\theta = 0°$ direction from transmitter array, its range image is expected to be located at the center position of the standard set pixels in the x-y plane is given by Eqs. (3.9) and (3.10) as follows

$$0^o \times \frac{pixels\ \ in\ \ column}{view\ \ angle} + \frac{pixels\ \ in\ \ column}{2} \quad (3.9)$$

$$0^o \times \frac{pixels\ \ in\ \ row}{view\ \ angle} + \frac{pixels\ \ in\ \ row}{2} \quad (3.10)$$

The obtained pixel point is considered as center. The image of the object is obtained at the center when located in $\theta = 0°$ from UTA and distance of an object is measured by matching image color with the color bar on the z-axis. The true position of the object is (θ_x (deg.), θ_y (deg.), distance (m)) = (0^o, 0^o, distance (m)) and measured position (θ_x (pixels), θ_y (pixels), distance (m)) =

(0 pixel, 0 pixel, distance (m) by color match on z axis). It gives the position of the object = (0 pixel × deg./pixel, 0 pixel × deg./pixel, distance (m) by the color match on z axis) i.e., (0^o, 0^o, distance (m) by the color match).

Similarly, when same object is placed an angle in θ direction with respect to the z axis (Fig. 2.1) its range image is expected to be some pixels shifted from the center of the standard set of pixels in x-y plane is given by Eqs. (3.11) and (3.12) as follows

$$\text{angle of object in horizontal direction} \times \frac{pixels\ in\ column}{view\ angle} + \frac{\text{pixels in column}}{2} \quad (3.11)$$

$$\text{angle of object in vertical direction} \times \frac{pixels\ in\ row}{view\ angle} + \frac{\text{pixels in row}}{2} \quad (3.12)$$

The obtained pixel point is compared with center and position of the object is measured as (number of pixels horizontally shifted from center × deg./pixel, number of pixels vertically shifted from center × deg./pixel, distance (m) by color match on z axis) i.e., (angle of object in horizontally (deg.), angle of object in vertically (deg.), distance (m) by the color match).

The resolution of the range detection depends on the transmitted pulse width, wave speed, object distance and size. Resolution may be estimated by Eq. (3.13) as follows

$$\Delta z = \left(\frac{Pulse\ \ width\ \ (sec) \times Wave\ \ velocity(m/s)}{2}\right) + range\ \ error\ \ (m) \quad (3.13)$$

3.5 Experimental set up

Experimental set up for range measurement is shown in Fig. 3.8. Transmitter and receiver were placed adjacent at the distance of 30 cm and facing in the same direction. A reflector (hard board) (30 cm width x 80 cm height) was placed in front of transceiver. Measurable range is considered until a

reflected signal is clearly distinguishable from the noise [3].

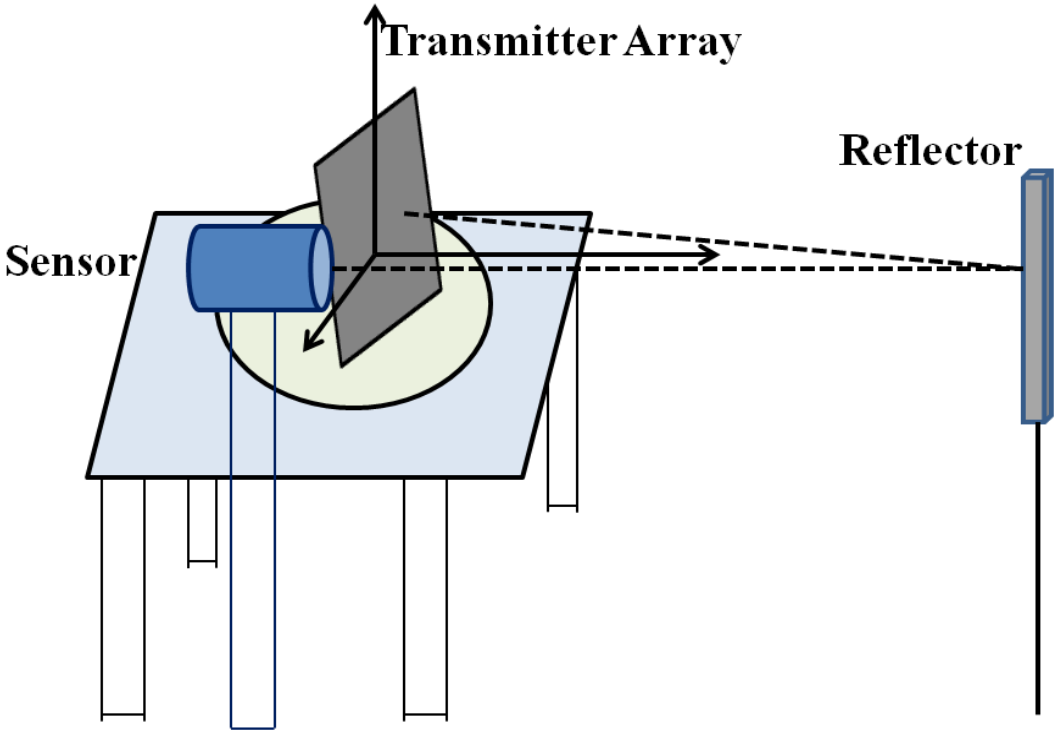

Fig. 3.8: Experimental set-up for measurable range.

3.6 Results

3.6.1 Measurable range

First of all, measurable range using single receiver and single transmitter has been confirmed. Measurable range using single transmitter with single receiver, 7 m ± 0.5 m and array transmitter with single receiver, 16 m ± 0.5 m has been obtained, respectively.

The measurable range is affected by the absorption of the ultrasonic sound in air and discussed in the previous chapters. The absorption coefficient is measured in the present experimental conditions, locating the receiver in front of single transmitter and measuring the sound pressure at the interval of 1 m. Figure 3.9 shows the dependence of the sound pressure on the distance between transmitter and the receiver. The sound pressure have the dependences on the distance expressed by the Eq. (3.14) as follows

$$\text{Sound presure} \propto \frac{1}{r} exp(-\gamma r) \tag{3.14}$$

Where, r is the distance and γ is absorption coefficient. Eq. (3.14) can be rewritten as Eq. (3.15) as follows

$$\ln(sound\ \ pressure \times r) = A_0 - (\gamma r) \tag{3.15}$$

Where, A_0 is a constant value.

The solid line in the figure shows the curve-fitting result with the following equation. $\ln(sound\ \ pressure \times r) = A_0 - (\gamma r)$ using MATLAB program. Absorption coefficient γ is calculated as 0.12 ± 0.02 /m. When measurable ranges for a single transmitter and UTA are denoted by *r'* and *r*" respectively and γ is the absorption coefficient, we can formulate a relation as shown Eq. (3.16) [1, 2]

$$\frac{e^{-2\gamma r'}}{r'^2} = K \frac{e^{-2\gamma r''}}{r''^2} \tag{3.16}$$

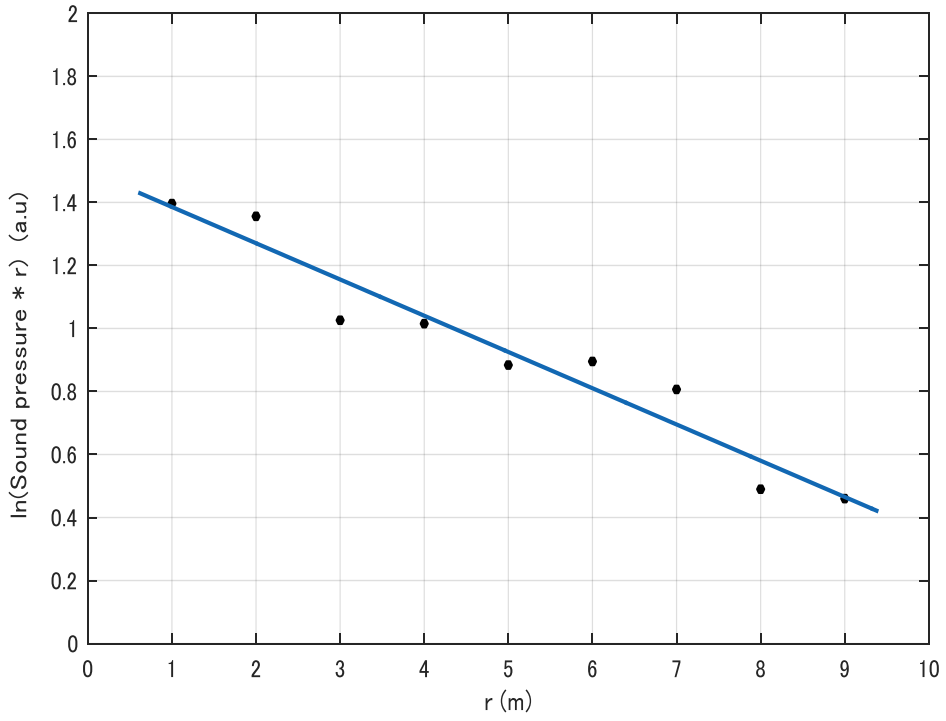

Fig. 3.9: Dependence of sound pressure on the distance of the receiver located in front of the single transmitter; Curve-fitting:$\ln(sound\ \ pressure \times r) = A_0 - (\gamma r)$

Where, K is the ratio of transmitted sound pressure of UTA to that of the single transmitter and is approximately 40 ± 10. Therefore, theoretical measurable range of the UTA is 15.6 m ± 2.2 m according to Eq. (3.16). The experimental result is in good agreement with this theoretical result.

The measurable range calculated using Eq. (3.16) for $\gamma = 0.12$/m and $K = 40$, as shown in Fig. 3.10. The experimental results for a single receiver are also plotted (the results for array transmitter are discussed in the next section). The effect of the high-power transmitter is large on the object for which the measurable range with a single transmitter is short. The effect was reduced because of the large absorption of sound in air with the increase in the range.

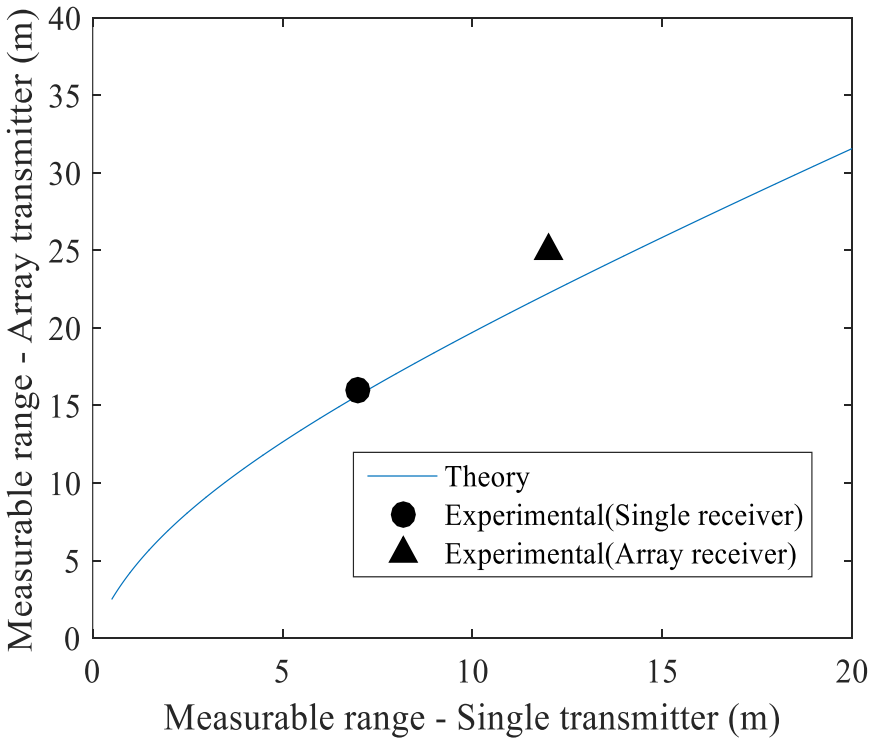

Fig. 3.10: Measurable range for $\gamma = 0.12/\text{m}\ \ and\ \ k = 40$; Single receiver: Black Circle, Receiver array: Black Triangle, Theory: Solid line

3.6.2 Image detection

The performance of range imaging system using the array transmitter and the array receiver also investigated. Measurable ranges were detected using 2 ms pulse width at the pulse repetition period 400 ms. Ultrasonic waves are emitted by UTA, reflected back from reflector and received by the URA. The DAS operations are performed to process the reflected signals detected by URA. Figure 3.11 (a) shows the maximum signal intensity distribution when a reflector was placed in front of the transmitter array. The distribution of the maximum signal intensity in the 3D image of the range data are calculated at the time when the correlated signal reaches to its maximum value. The range images are displayed in 21×21 pixels constructed using MATLAB and Simulink program. The total angular field of view of ultrasonic receiver array is $105^{o} \times 105^{o}$ (full angle). The reflector placed at 16 m in $\theta_x = \theta_y = 0°$ directions (position (0^{o}, 0^{o}, 16 m)) from transmitter array, its range image is expected to be located at the center position of 21×21 pixels in the x-y plane. The pixel point (11, 11) is the center and now defined as (0, 0). The image of the reflector is successfully obtained at the center, and distance of the reflector is estimated on the z axis, as shown in Fig. 3.11 (a) as 15.8 m. The position of the reflector can be written as (0^{o}, 0^{o}, 16 m) and range image is detected at (0 pixel, 0 pixel, 15.8 m), it represents the measured position as (0^{o}, 0^{o}, 15.8 m) on the z axis as shown in Fig 3.12 (a).

When reflector is placed in $\theta x = 15°$ and $\theta y = 0°$ directions at the distance of 16 m, the signal intensity and range image are shown in Fig. 3.11 (b) and 3.12 (b). The position of the reflector is (15^{o}, 0^{o}, 16 m). The range image is detected at (3 pixel, 0 pixel, 15.6 m), it represents the measured position as (15^{o}, 0^{o}, 15.6 m).

Here, ultrasonic pulse width is 2 ms, ultrasonic wave speed is 345 m/s and object positioning error is 20 cm, which gives the measurement error of ± 0.55 m. This value is in agreement with the measured experimental error of ± 0.5 m. The resolution of the range detection depends on the transmitted pulse width, reflector distance and size and calculated according to Eq. (3.13)

$$\Delta z = \left(\frac{Pulse\ \ width\ \ (s) \times Wave\ \ velocity(m/s)}{2}\right) + range\ \ error\ \ (m)$$

$$\frac{0.002 \times 345}{2} + 0.20\ m = 0.55\ m$$

Measurable range of the UTA with URA was approximately 25 m ± 1 m, and for single transmitter with URA was approximately 12 m ± 0.5 m. The signal intensity reduces with an increase in deviation angle. Signal intensity reduced to one third at θ = 15° direction in comparison to θ = 0°. Image of the reflector is obtained at the center of the pixel (11, 11) and pixel (14, 11) accordingly. Measurement results are in correlation with the image detection. Hence, system performance on the range image detection has high degree of accuracy in front direction as well as in diagonal directions.

When, reflector is placed at 25 m in $\theta_x=\theta_y$ = 0° directions. The position of the reflector is (0°, 0°, 25 m) and its range image is detected at (0 pixel, 0 pixel, 24.5 m), that represents the measured position (0°, 0°, 24.5 m) as shown in Fig. 3.13 (a) and (b) respectively. In case reflector is placed at 12 m in $\theta_x=\theta_y$ = 0° directions. The position of the reflector is (0°, 0°, 12 m) and its range image is detected at (0 pixel, 0 pixel, 11.6 m), that represents the measured position (0°, 0°, 11.6 m) as shown in Fig. 3.14 (a) and (b) respectively. Measurable range using array receiver is also plotted in Fig. 3.6. Experimental results are in good agreement with the theoretical calculations using Eq. (3.11).

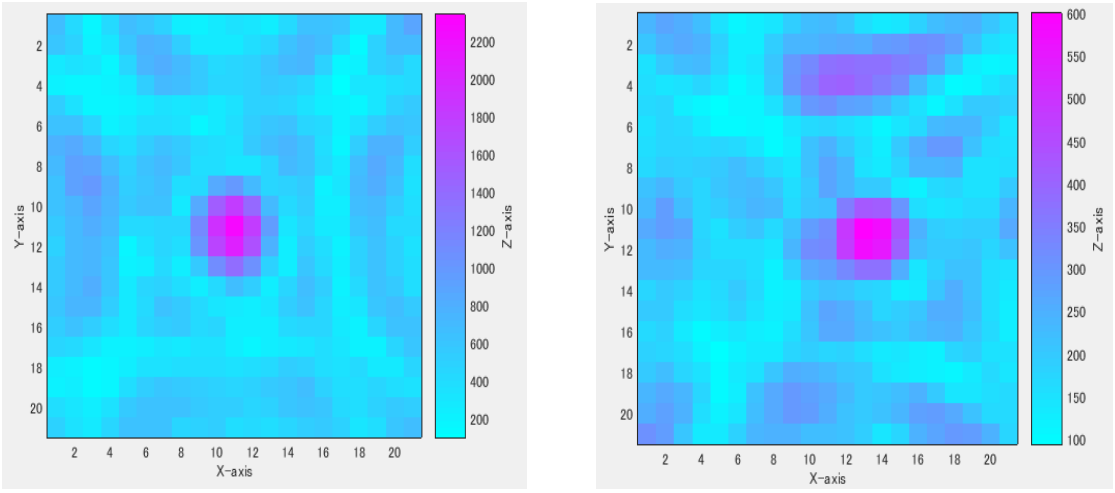

(a) θ = 0° (b) θ = 15°

Fig. 3.11: Signal intensities (a.u.) after delay-and-sum operations: Reflector at 16 m in different directions. X and Y axis are 5°/div.

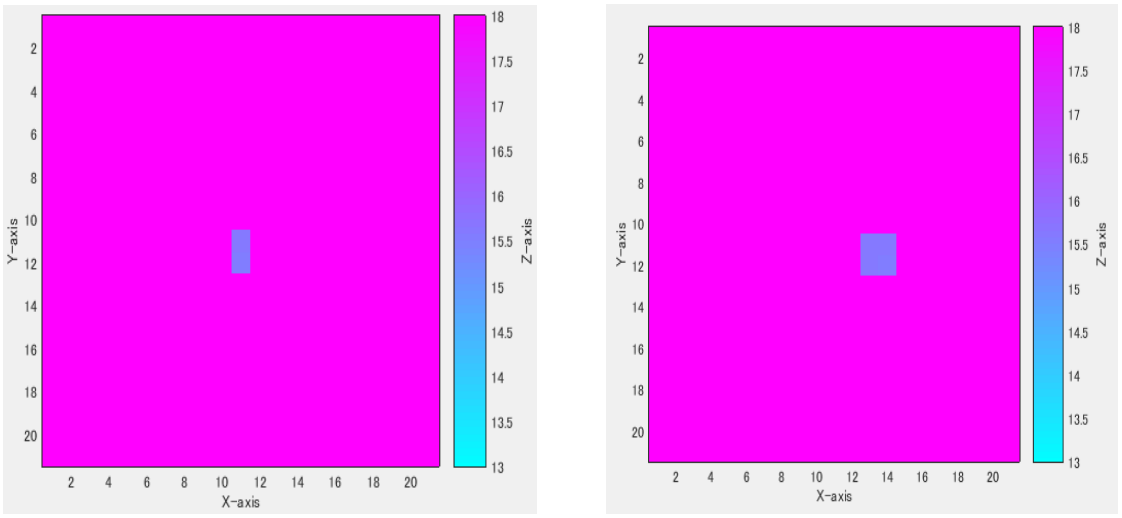

(a) θ =0º (b) θ = 15º

Fig. 3.12: Range images (m) on z axis: Reflector at 16 m in different directions. X and Y axis are 5º/div.

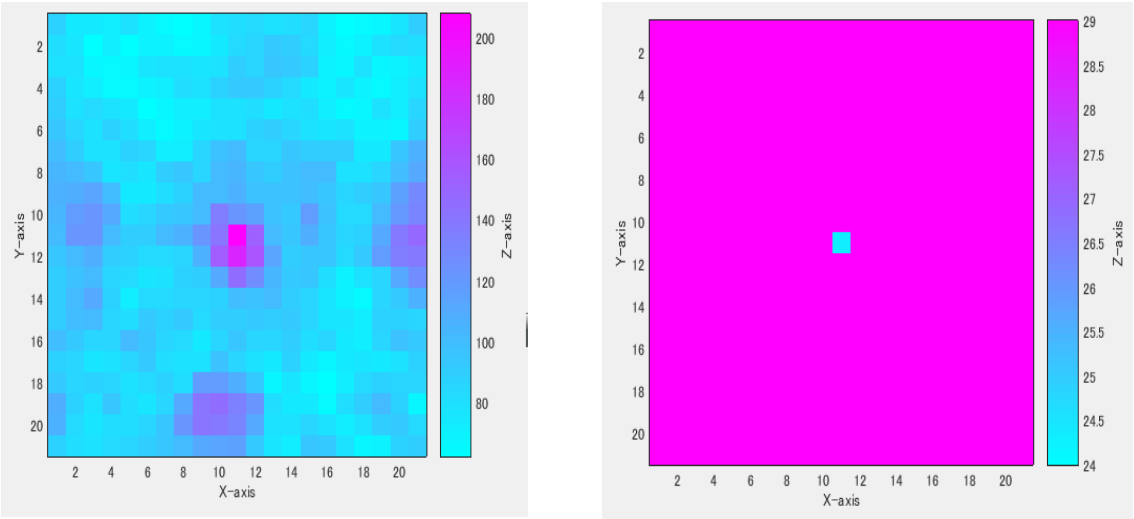

(a) Signal intensity (a.u.) on z axis. (b) Range image (m) on z axis.

Fig. 3.13: Signal intensity after delay-and-sum operations and range image: Reflector at 25 m in θ = 0º direction. X and Y axis are 5º/div.

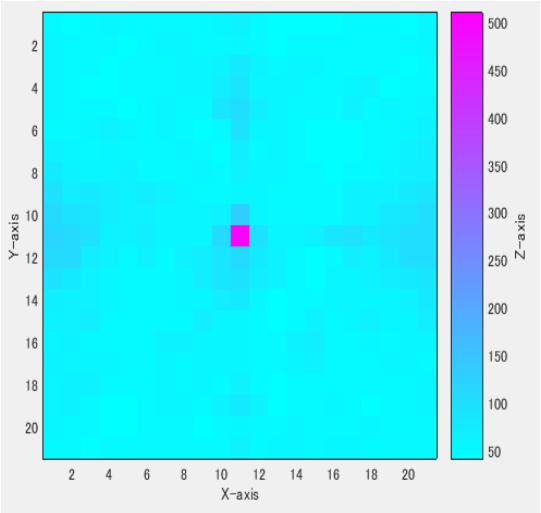

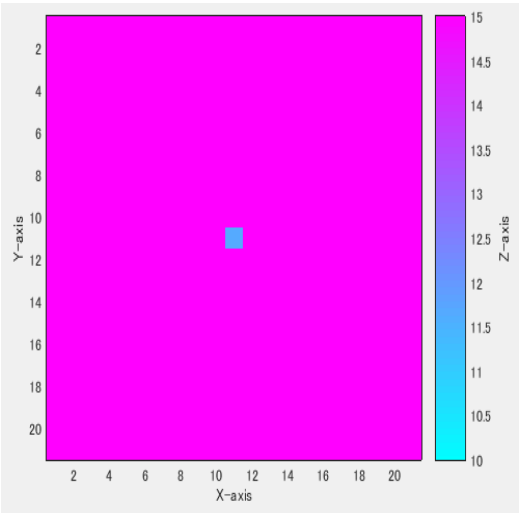

(a) Signal intensity (a.u.) on z axis. (b) Range image (m) on z axis.

Fig. 3.14: Signal intensity after delay-and-sum operations and range image: Reflector at 12 m in $\theta = 0^{o}$ direction, X and Y axis are 5^{o}/div.

3.7 Conclusion

An imaging sensor system has been constructed using array transmitter and array receiver. The UTA consisting of 144 transmitter elements exhibit 40 times higher sound pressure than the SUT. Developed ultrasonic receiver array consists of 32 receivers. A reflector is clearly detected in the direction it was positioned. With this system measurement is possible up to 25 m in the air. The experimental results are in good agreement with the theoretical calculations. Using our novel UTA system we have successfully demonstrated the range imaging of a reflector placing at different positions. These results are useful to expand further applications of ultrasonic range sensor.

System worked satisfactorily and measurable range 25 m has obtained successfully. Measurable range has been confirmed by placing a reflector and detecting its range image accuretaly in the same direction within the experimental error.

With the developed long range measurement system, measurable range has been improved significantly, but the directivity of the array transmitter is very narrow. Therefore, to improve the directivity a divergence controllable

array transmitter has been proposed. The principles are discussed in detail in the next chapter [15].

References

[1] S. Kumar, K. Ichi and H. Furuhashi, Theoretical investigation of high-power ultrasonic array transmitter for a range sensor in air, Proc. IEEE, Int. Conf. on Industrial Technology ICIT 2013, IEEE Xplore (2013), pp.1190-1195.

[2]S. Kumar, Q. Wei and H. Furuhashi, Characteristics of high power ultrasonic array transmitter in the air, Proc. IEEE 2015, Int. Conf. on Recent Developments in Control, Automation and Power Engineering, RDCAPE-2015 (2015), pp.209-213, DOI:10.1109/ RDCAPE .2015.7281397.

[3] S. Kumar and H. Furuhashi, Long-range measurement system using ultrasonic range sensor with high-power transmitter array in air, Ultrasonics 74 (2017), pp.186-195, DOI:10.1016/j.ultras.2016.10.012.

[4] B.W. Drinkwater and P.D. Wilcox, Ultrasonic arrays for non-destructive evaluation: a review, 39 (7) (2006), pp.525-541, DOI:10.1016/J.ndteint.2006.03.006.

[5] R. Hickling and S.P. Marin, The use of ultrasonics for gauging and proximity sensing in air, J. Acoust. Soc. Am. 79(4) (1986), pp.1151-1160, DOI: 10.1121/1.393387.

[6] R. Stoessel, N. Krohn, K. Pfleiderer and G. Busse, Air-coupled ultrasound inspection of various materials, Ultrasonics 40 (1-8) (2002), pp.159-163, DOI: 10.1016/S0041-624X (02) 0013-0.

[7] P.N. Keating, T. Sawatari and G. Zilinskas, Signal processing in acoustic imaging, Proc. IEEE 67(4) (1979), pp.496-510, DOI: 10.1109/ PROC.1979.11279.

[8] L.J. Griffiths and K.M. Buckley, Quiescent pattern control in linearly-constrained adaptive arrays, IEEE transactions on acoustic, speech and signal processing, ASSP-35 (1987), pp.917-926.

[9] H. Furuhashi, Y. Kuzuya, Y. Uchida and M. Shimizu, Three dimensional imaging sensor system using an ultrasonic array sensor and a camera. Sensors 2010, IEEE Xplore, (2010), pp.713-718.

[10] H. Furuhashi, Y. Kuzuya, C. Gal and M. Shimizu, Three-dimensional

imaging of a human body using an array of ultrasonic sensors and a camera, Proc. IEEE, CACS 2011, Int. Congress on Computer Application and Computational Science, 145 (2011), pp.325-330.
[11] H. Inubushi, N. Takahashi, H. Zhu and K. Taniguchi, Ultrasonic 3D image sensor employing PN code and beam-forming technologies, IEICE Trans. J90 (6) (2007), pp.517-523.
[12] H. Furuhashi, S. Kumar and M. Shimizu, Signal processing of a 3D ultrasonic imaging sensor that uses the spread spectrum pulse compression technique, Lecture notes in information technology, Proc. 2012 Int. Conf. on Future Information Technology and Management Science & Engineering FITMSE 2012, 14 (2012), pp.145-150.
[13] T. Tanaka, S. Lee, M. Uno, K. Inoue, S. Aoyagi, K. Yamashita and M. Okuyama, Improvement of ultrasonic micro array sensor using the amorphous fluorocarbon polymer film, the transactions of the institute of electrical engineers of Japan. A publication of sensors and micromachines society 127 (1) (2007), pp.7-13.
[14] K. Yamashita, H. Murakami and M. Okuyama, Ultrasonic phased –array sensor using PZT thin film and three-dimensional object detection using BBD. Journal of the Korean Physical Society, (Vol.42) April 2003, (2003), pp.S1108-S1112.
[15] S. Kumar, K. Ichi and H. Furuhashi, Theoretical investigation of divergence control of directivity of an ultrasonic transmitter array, SICE annual Conf. 2013, Abstract SuCT2.1 (2013), pp.803-807.

Chapter 4

Isotropic Divergence Controllable Ultrasonic Transmitter Array for 3-D Range Imaging[1-5]

4.1 Introduction

In this chapter the behavior of the ultrasonic transmitter array (UTA) system at different divergence angles has been discussed. A long-range measurement system has been developed that consists of a high power UTA and ultrasonic receiver array (URA). Measurable range has been improved over 25 m with this system [3]. The sound pressure level increases with an increase in the number of transmitting elements but the image detection view angle decreases to several degrees in comparison of conventional method [1, 2, 5, 6-8]. The reflector could not detected when it was positioned in the direction $\theta = 15°$ at the distance of 25 m. The measurable range for this direction is about 16 m. The signal intensity reduced to one third in this direction in comparison to $\theta = 0°$ as a result reduction in measurable range in that direction [2].

In order to improve the measurable range in $\theta = 15°$ direction, a new method using phased array transmitter has been proposed that can control the phase of each element [4, 9-12]. Such a transmitter generally used for beam scanning. However, we used it to spread the sound divergence and a wider view angle is also expected. In this chapter, principle of the divergence control using phased array has been described and constructed the transmitter following the its principle. The characteristics of the transmitter is investigated theoretically and experimentally. Furthermore, a range sensor system using the transmitter array and array sensor system has been developed and evaluated the effectiveness of the system [13, 14].

4.2 Theory

Fig. 4.1 shows the coordinate system used in divergence control calculations. Considering a sound source located on line L behind the array then divergence ϕ is calculated by Eq. (4.1) as follows [4]

$$\tan\phi=\frac{w}{2L} \tag{4.1}$$

Where w is the size of the window.
Let us assume that sound having a specific divergence is generated by a point sound source and a window.

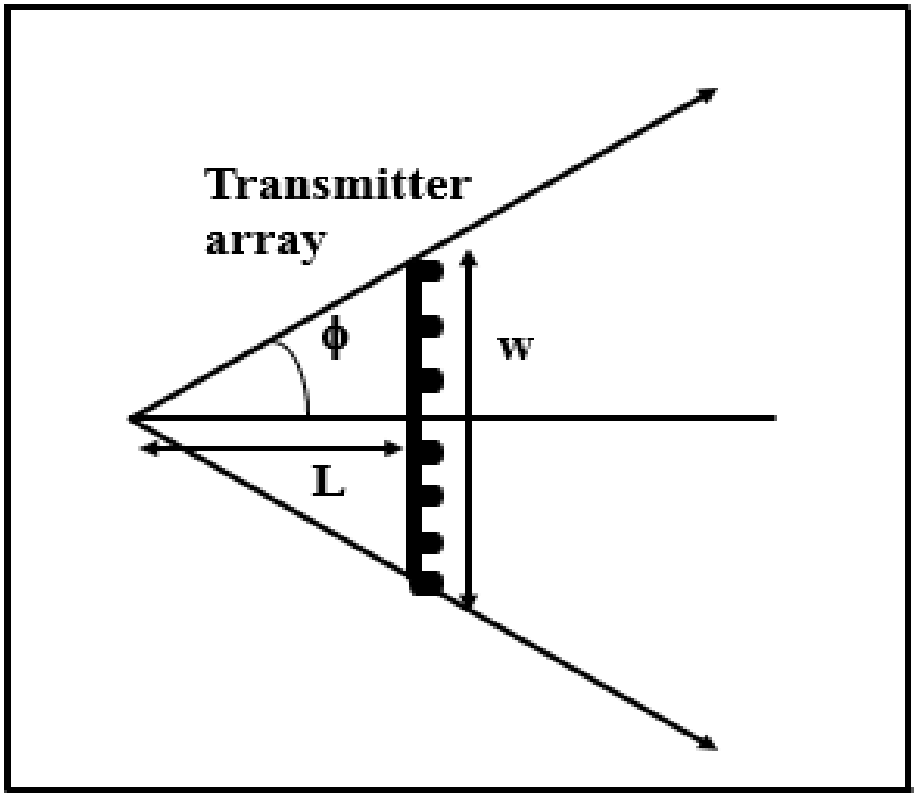

Fig. 4.1: Divergence control of calculation in x direction.

If the observation point is far from the sound source, then divergence of the directivity as in the above situation is obtained by generating the same sound on the window plane based on the Huygens-Fresnel principle. Let number of elements is n and the distance between elements is d, then Eq. (4.1) becomes as Eq. (4.2)

$$\tan\phi=\frac{(n-1)d}{2L} \tag{4.2}$$

The time delay of the signal between the origin (0, 0) of array and that at the position of the element (x_i, y_i) is calculated by Eq. (4.3) and Eq. (4.4) as follows

$$\Delta\tau_d=\frac{\Delta L}{c}=\frac{\sqrt{(x_i^2+y_i^2+L^2)}-L}{c} \tag{4.3}$$

$$\approx(x_i^2+y_i^2)\frac{1}{2Lc} \tag{4.4}$$

Where, $\Delta L$is the distance between the vertical point sound source and each element, and c is the sound velocity. Therefore, time delay is applied to each element.

The Phase difference $\Delta\phi$ is calculated by Eq. (4.5) as follows

$$\Delta\phi_d=2\pi\frac{c\Delta\tau_d}{\lambda}\approx2\pi(x_i^2+y_i^2)\frac{1}{2L\lambda} \tag{4.5}$$

In this case, the sound pressure at point P(x, y, z) is calculated by Eq. (4.6) as follows

$$p(x,y,z)=\sum_{i-1}^{n}D(\theta_i)A_i\frac{e^{-2\pi i\frac{r_i+c\Delta\tau_d}{\lambda}}}{r_i} \tag{4.6}$$

According to the sound pressure coordinate system given in Fig. 4.2, r_i is the distance between position P_i of the element and the observation point P(x, y, z), (θ_i) is the angle between the z axis and the vector P_iP. The directivity and

sound pressure amplitude of each transmitting element is denoted by $D(\theta_i)$ and A_i respectively. If point P is sufficiently far from the origin in comparison to the size of the array, Eq. (4.6) can be approximated as Eq. (4.7)

$$|p(x,y,z)| = A\frac{1}{r}D(\theta)\times\left|\sum_{i-1}^{n}\exp\left\{-i\frac{2\pi}{\lambda}\left(x_i\sin\theta_x + y_i\sin\theta_y + \frac{x_i^2+y_i^2}{2L}\right)\right\}\right| \quad (4.7)$$

Here, $D(\theta)$ is the directivity of each element. The signal amplitude of each element is assumed to be equal to A.

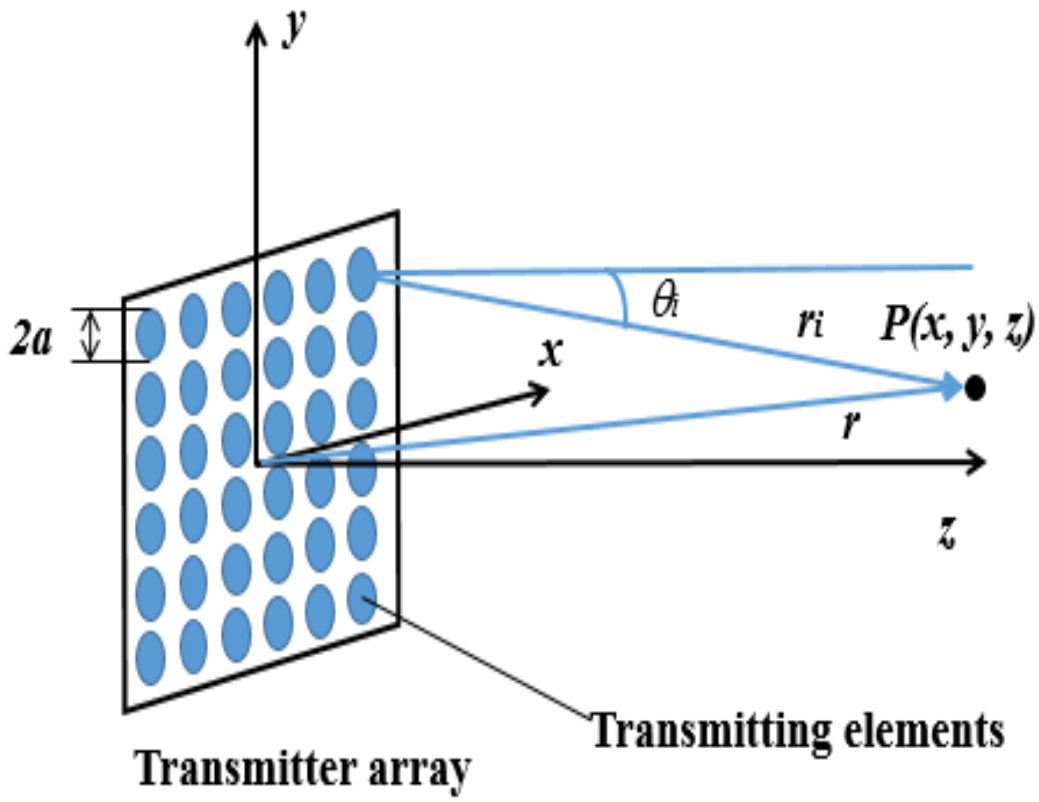

Fig. 4.2: A coordinate system of sound pressure calculations

The simulation directivities at divergences; 10°, 20°, and 30° using Eq. (4.7) are shown in Figs. 4.3 (a)-(c) respectively. The sound pressures are normalized by the peak sound pressure of one transmitter A/r. These figures are the results with $\theta_x=\theta_y = 0°$. Although, many grating lobes appear at lower divergence angles, while calculating the phase delay using Eq. (4.3), the divergence of sound becomes wider as the divergence angle ϕ increases.

The half width of the sound pressure is approximately 10° as in Fig. 4.3 (a). The divergence with wider divergence angle (ϕ) are shown in Fig. 4.3 (b) & (c). The pitch of the side lobe is calculated by Eq. (4.8) as follows [4]

$$\sin\theta_{side} = \frac{m\lambda}{(n-1)d} \tag{4.8}$$

Where, *d* is the pitch of the elements, *n* is the number of elements, and *m* is the order of the side lobes. Since elements are placed at 10 mm intervals, the number of elements is 12, and the wavelength of the ultrasonic wave is 8.6 mm, side lobes with a pitch of 4.5°, or 0.078 radians [= 8.6 mm/10 mm × (12-1)], appear at lower angles. The grating lobes appear at angle using Eq. (4.9) as follows

$$\sin\theta_{grating} = \frac{m\prime\lambda}{d} \tag{4.9}$$

Where, *m*' is the order of the grating lobes. The pitch becomes $\sin^{-1}\left(\frac{8.6\text{mm}}{10\text{mm}}\right) = 1.0 \text{ rad.} = 60 \text{ deg.}$ Therefore, one first-order grating lobe appears on each side.

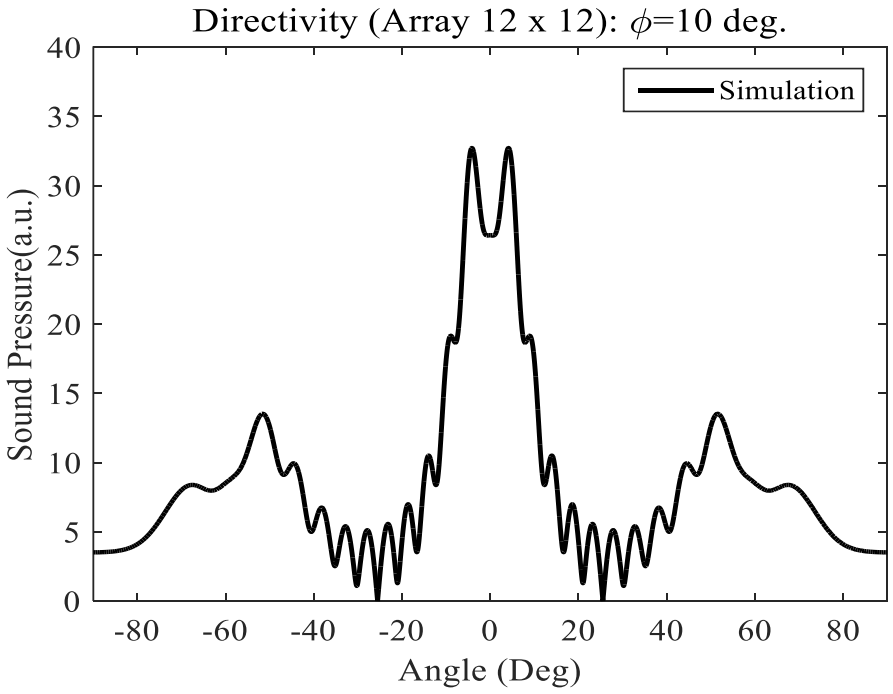

(a) ϕ=10°

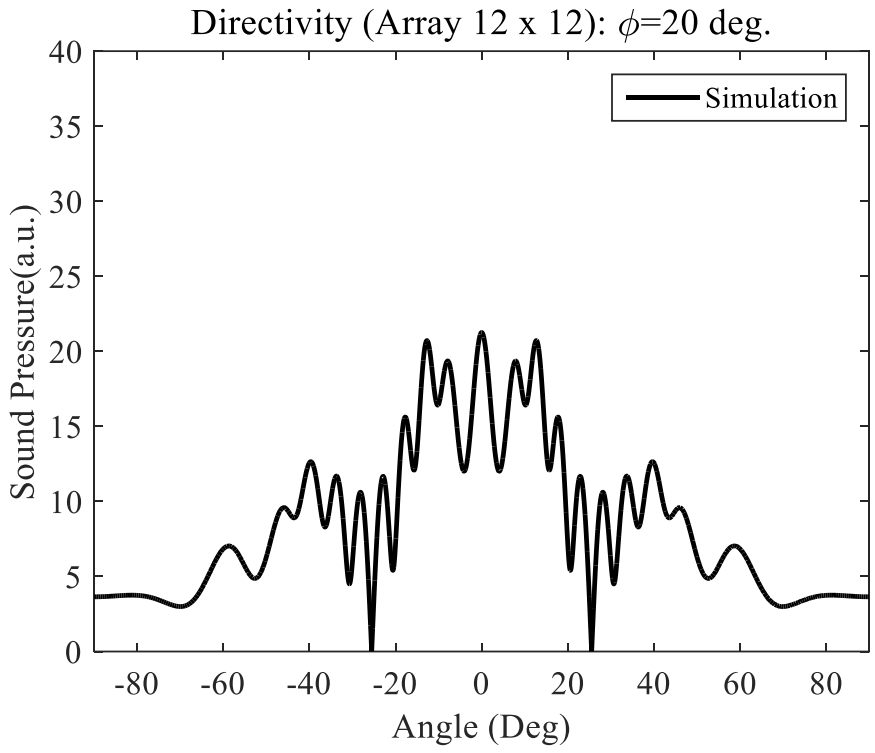

(b) ϕ=20º

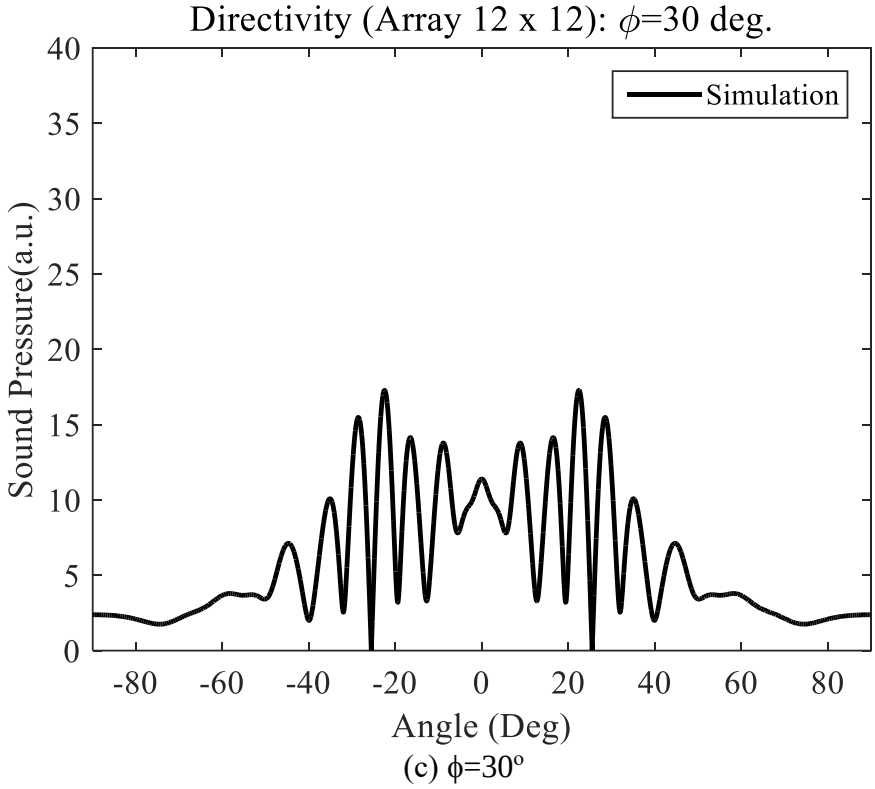

(c) ϕ=30º

Fig. 4.3: Simulation directivities at divergences of 10°, 20°, and 30°. The sound pressures are normalized by the peak sound pressure of one transmitter and θx=θy = 0°.

The sound pressure decreases with the increase in divergence angle. Fig. 4.4 shows the dependence of the mean pressure in the region of the divergence. In case, phase is not controlled, then mean value is calculated in the region within the divergence of 1°. The mean pressure is approximately inversely proportion to the divergence.

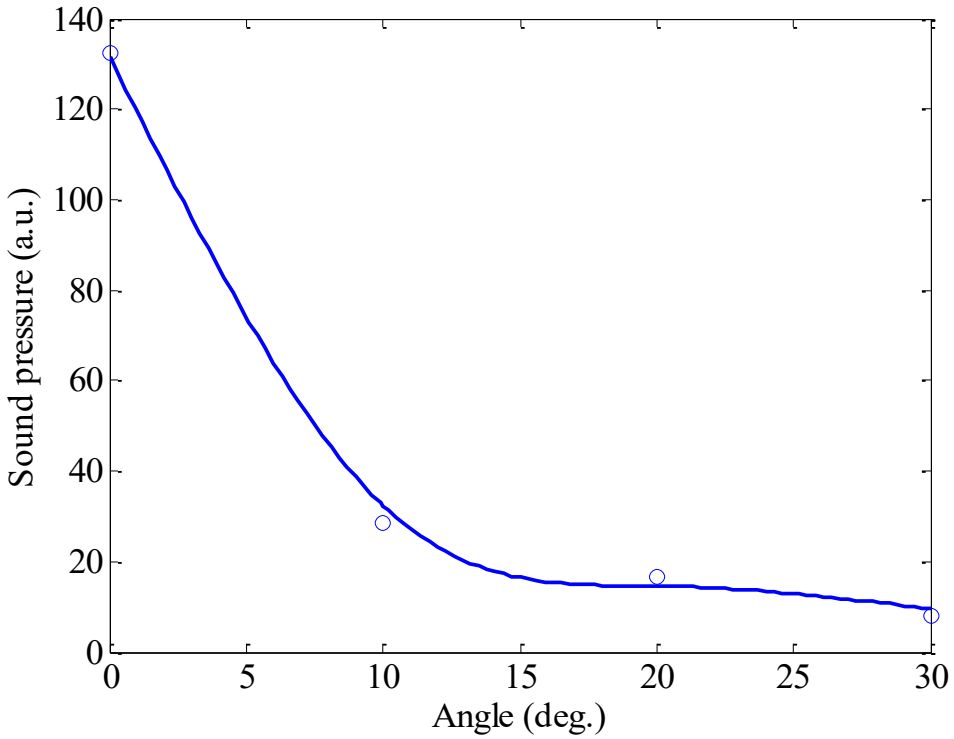

Fig. 4.4 Dependence of the mean amplitude within the divergence region. The mean pressures are normalized by the peak sound pressure of one transmitter.

Fig. 4.5 shows a two-dimensional color map of the sound pressure for the x and y directions. The divergence ϕ is 20°. The sound pressure in the square region ($\theta_x < \phi$ and $\theta_y < \phi$) is high.

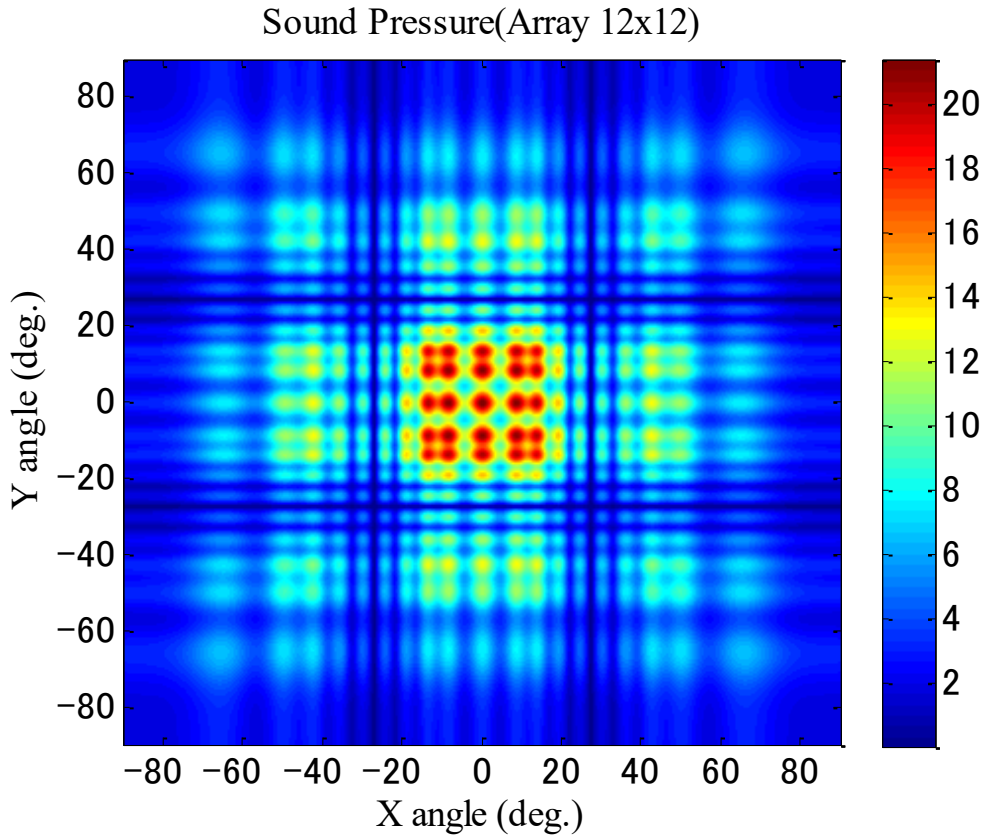

Fig. 4.5: Two-dimensional image of sound pressure. The divergence ϕ is 20°. The sound pressure is normalized by the peak sound pressure of one transmitter.

Fig. 4.6 shows the measurable range calculated using Eq. (3.11). The divergence ϕ is 20°. The ratio of sound pressure of array transmitter to the single transmitter is 16 and the absorption coefficients are 0, 0.01, 0.1, and 1 m^{-1}, respectively. The measurable range 11 m has been observed when absorption coefficient is 0.01 m^{-1}. The maximum measurable range is obtained at the minimum absorption coefficient i.e. 0 m^{-1} and measurable range of single transmitter is considered as 3 m.

Measurable range of an array transmitter without phase delay control is 28 m. Although the measurable range decreases with an increase in divergence angle. The measurable range at divergence angle 30° is still greater than that of the single transmitter.

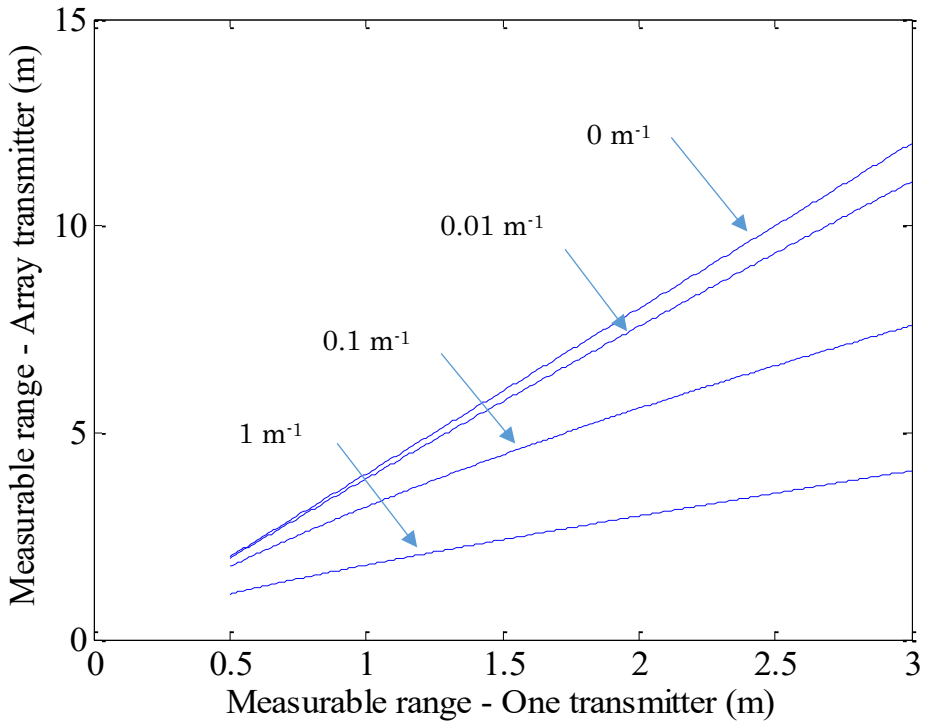

Fig. 4.6: Dependence of the measurable range of the array transmitter system as a function of the measurable range of a one-element transmitter system for absorption coefficients of 0, 0.01, 0.1 and 1 m^{-1}. The divergence ϕ is 20°.

4.3 Structure of divergence controllable transmitting system

A brief description of ultrasonic transmitting system has been given in Chapter-3. In this experiment same system has been used. The only difference is delay circuits added in the FPGA. The phase of the signal applied to each element is controlled by delay signal controllers as shown in Fig. 4.7. The phase delay of the transmitted signal, controls the divergence of the UTA by controlling the delay circuits applied on four FPGAs. Each FPGA controls the delay times of 36 elements. The sampling rate of the signal output is 1 μs. The maximum delay time of this system for each element is 512 μs. The present paper discusses primarily the behavior of this array system. The time delays have been calculated using Eq. (4.4) by the personal computer according to the input value of the divergence angle. Substituting the value of L in Eq. (4.4), then time delay is given by Eq. (4.10)

$$\Delta\tau_d \approx (x_i^2 + y_i^2)\frac{\tan\phi}{(n-1)dc} \tag{4.10}$$

The maximum time delay has relationship with the divergence control as given in Eq. (4.11) as follows

$$\Delta\tau_{d\max} = \left(\frac{b}{c}\right)\frac{1}{2Lc} = \frac{(n-1)d}{4c}\tan\phi \tag{4.11}$$

Here, b is the side length of the array (110 mm). It is calculated to be about 80° for the maximum time delay of 512 μs. The resolution of the divergence control can be calculated from the time delay of 1 μs as 0.7° in rough calculation.

Receiver structure is same as explained in Chapter-3.

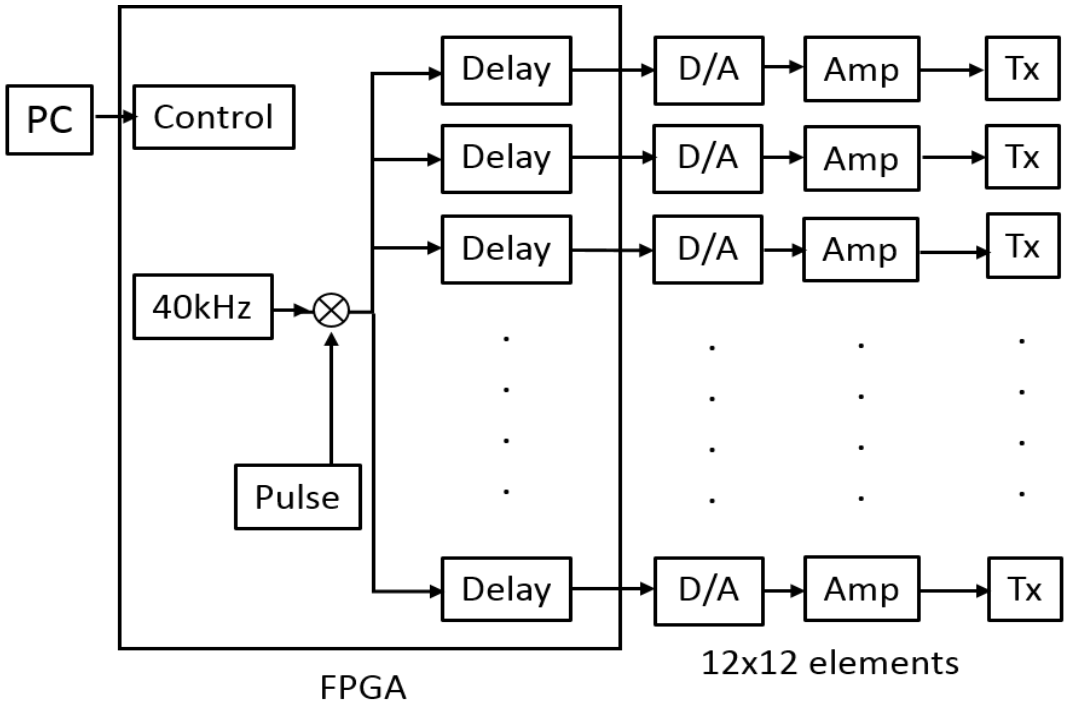

Fig. 4.7: A block diagram of the FPGA modified transmitting control system.

The ultrasonic receiving system, described in Chapter-3 is being used to receive the pulse modulated time delay signal.

4.4 Experimental results

4.4.1 SPL at different divergence

The experimental set up is same as described in Fig.2.2 (Chapter-2). The sensor is placed 5 m apart from the transmitter with their height at 1.5 m above the ground level. The sensor calibration is the same as mentioned in previous chapters. The generated 40 kHz is pulse modulated by 2 ms and pulse repetition period of 400 ms. In this experiment one additional control (spread angle or divergence angle) has been included. Now, there are three controls applied on the transmitted signal (i) pulse width (ii) pulse repetition rate (iii) spread angle. The applied divergence control is equal in x and y directions and time delay is automatically calculated by the system. Maximum peak to peak voltage is measured, rotating the UTA as mentioned in previous chapters, varying the divergence angle.

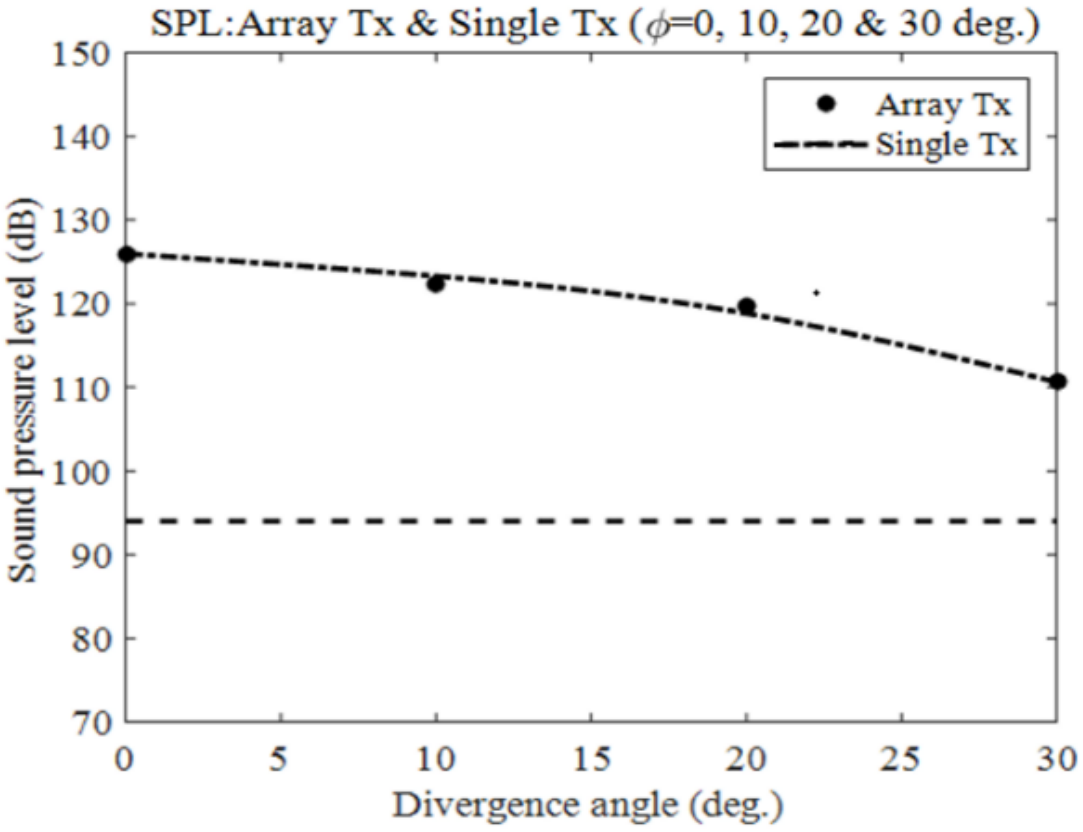

Fig. 4.8: Dependence of SPL with divergence angles.

The SPL at divergence angle ϕ = 0°, 10°, 20° and 30° are 126, 122.3, 119.8 and 110.64 dB respectively as shown in Fig.4.8 when receiver was $\theta x = \theta y$ =

0°. The black circles are the experimental results using UTA and dotted line shows that Single ultrasonic transmitter (SUT) does not have any effect on the divergence angle. Sound pressure level decreases as the divergence angle increases. However, SPL at 30° is still more than single transmitter. The SPL 94 dB has been obtained by single transmitter at 5 m.

4.4.2 Directivities at different divergence

Applying the delay time control, the experimental directivities at divergence angles; 0°, 10°, 20° and 30° are shown in Figs.4.9 (a)-(d) respectively. Solid line is the simulation result using Eq. (4.7) and black dots are the experimental results. The sound pressures are normalized by the peak sound pressure of one transmitter *A/r*. These simulation results are with $\theta x = \theta y = 0°$. Although, many side lobes appear at lower divergence angles, while calculating the phase delay using Eq. (4.5), the divergence becomes wider as the angle ϕ increases. The half width of the sound pressure is approximately 10° as in Fig. 4.9 (a). The divergence becomes wider as ϕ increases, as shown in Figs. 4.9 (b)-(d).

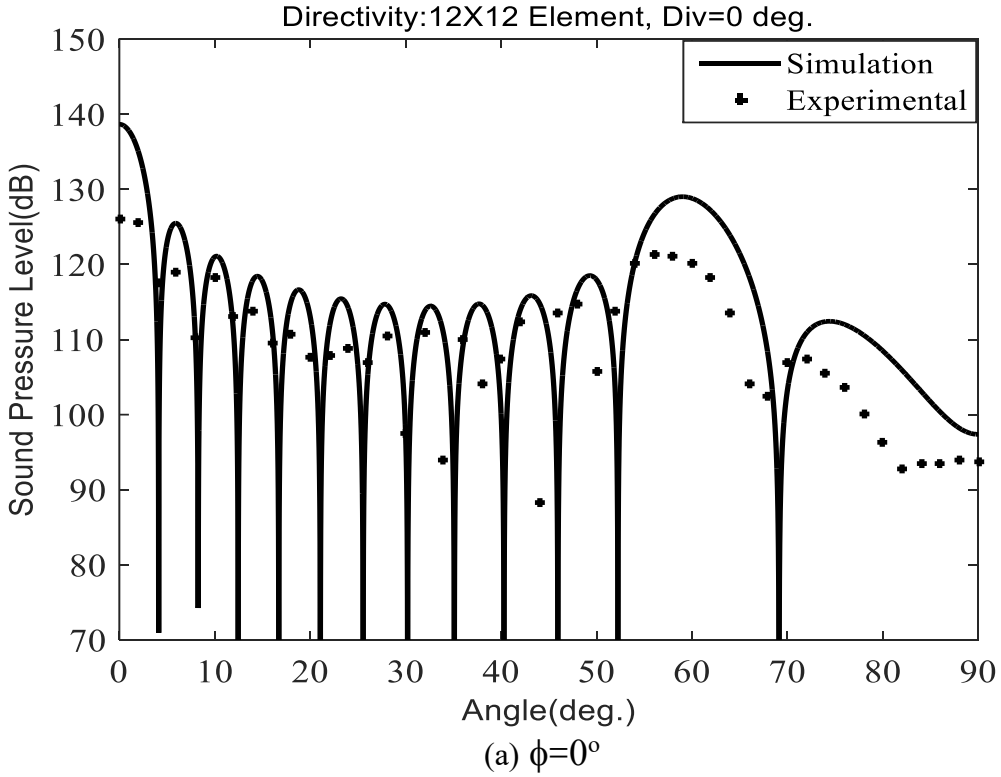

(a) ϕ=0°

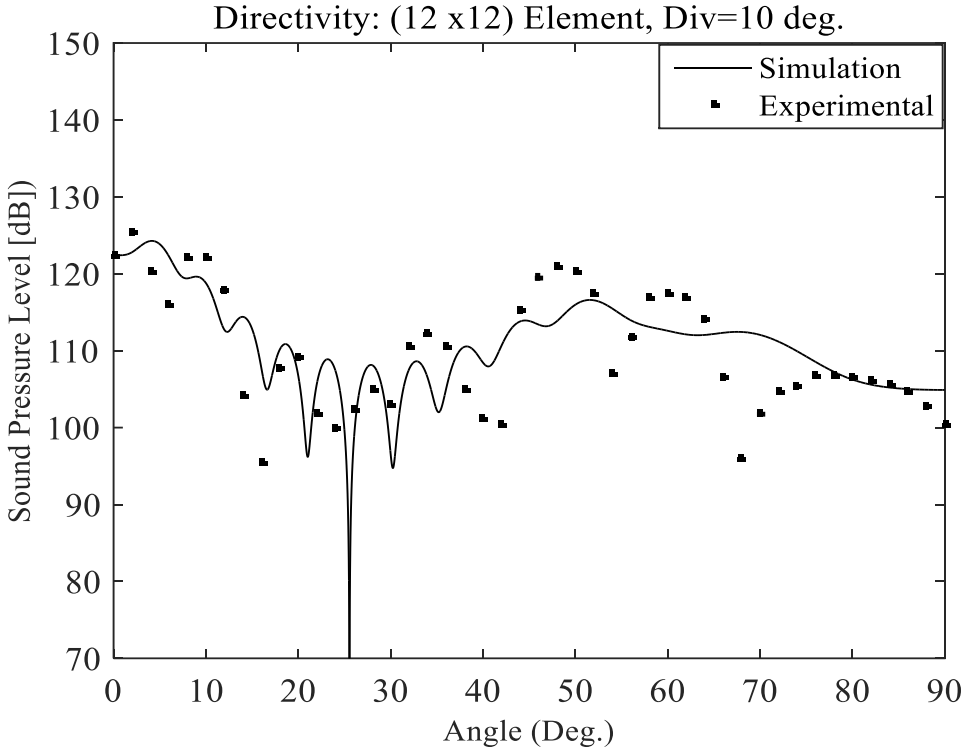

(b) $\phi=10^{o}$

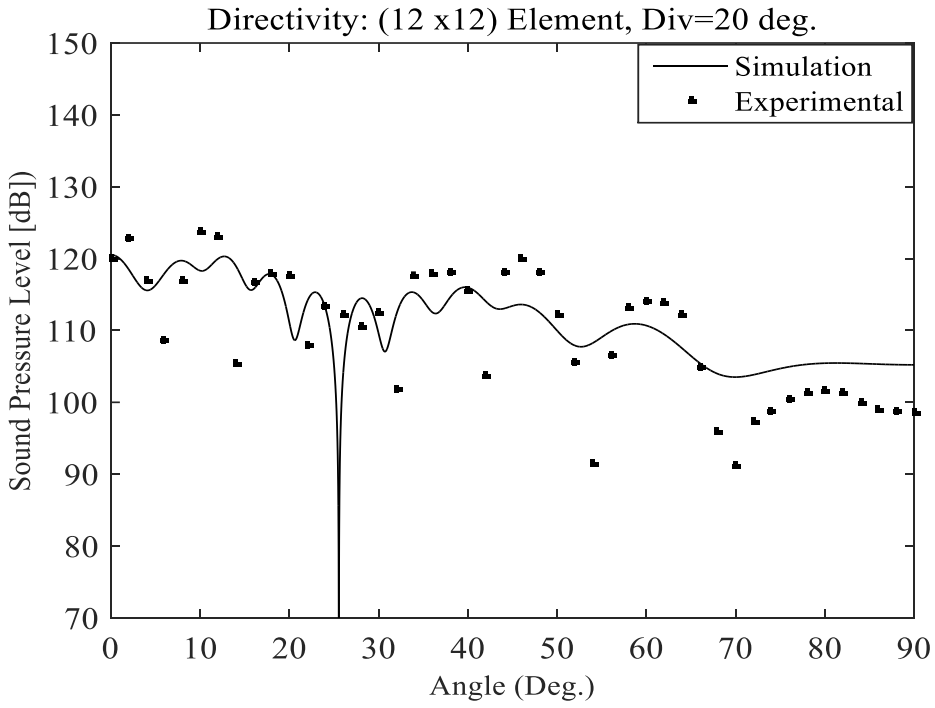

(c) $\phi=20^{o}$

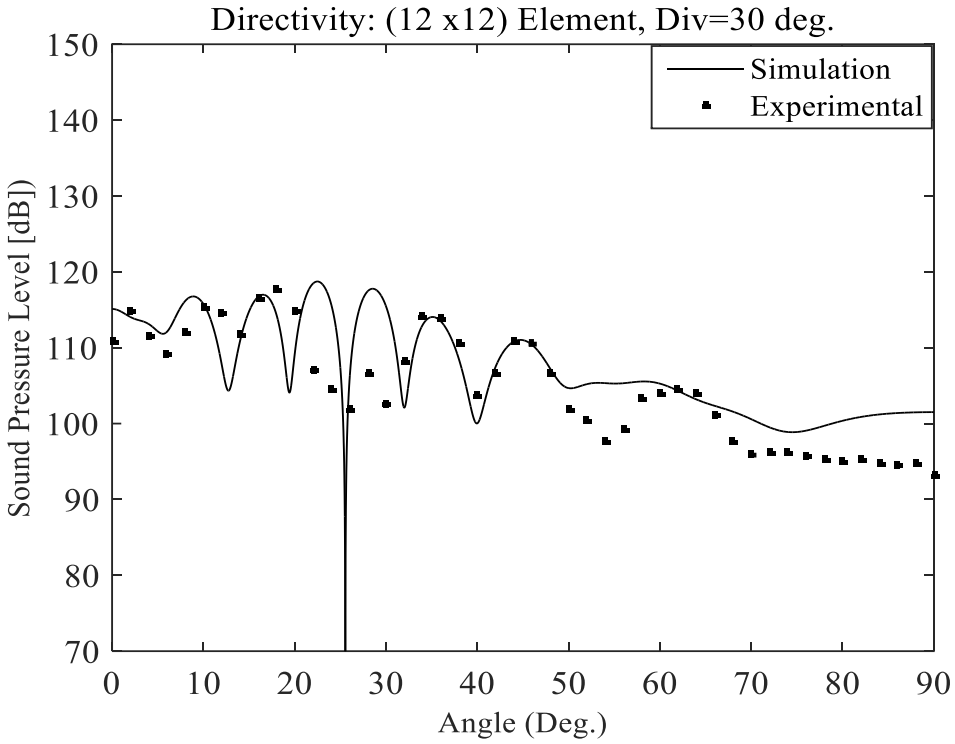

(d) ϕ=30°

Fig. 4.9: Directivities at θ = 0° and (a): ϕ = 0° (b): ϕ = 10° (c): ϕ = 20° (d): ϕ = 30°.

HWHMs on the experimental results have been obtained according to applied divergence angle in all the three cases. When, 10° divergence has been applied, the HWHM is 10°. Similarly when divergence 20° and 30° is applied, then HWHMs are 20° and 30° respectively. Experimental directivity is in good agreement with simulation directivity. Therefore the developed transmitter could successfully controlled the divergence as explained in the theory.

4.4.3 Measurable range

Figure 4.10 shows the measurable range at different divergence angles. Measurable range without divergence ϕ = 0° is 16 m ± 0.5 m, divergence ϕ = 10° & 20° is 14 m ± 0.5 m and divergence ϕ = 30° is 11 m ± 0.5 m, has been obtained using the same reflector. These measurable ranges are denoted by black circle, black triangle and circle respectively. Theoretical measurable range calculations are made with K = 40, 26, 19.5 and 6.8 according to Eq. (3.11) in Chapter-3 and marked as dashed, dotted, solid and dash-dotted lines.

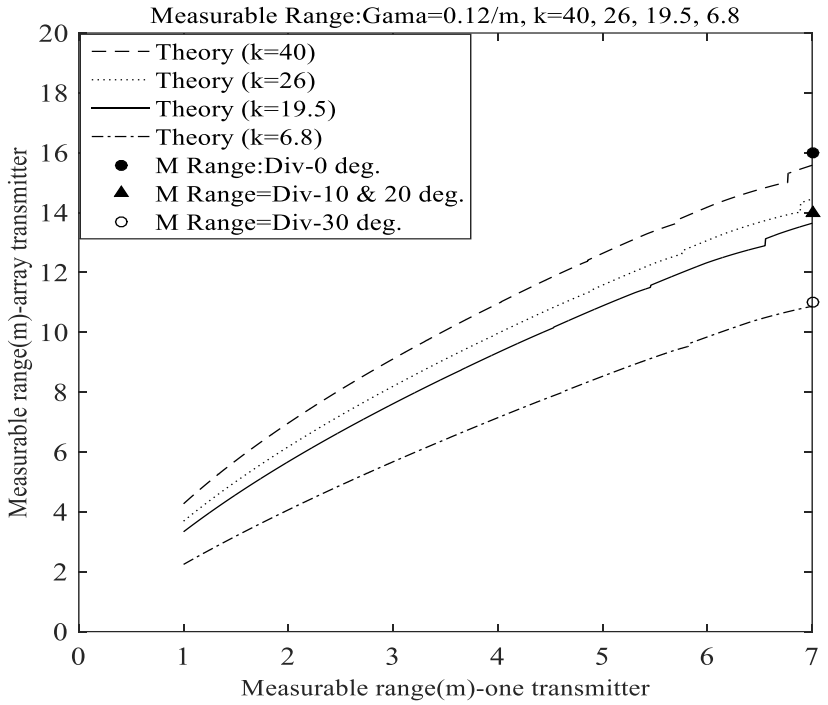

Fig. 4.10: Measurable range theoretical and experimental.

Measurable range obtained at different divergence angle is according to the theoretical calculations within measurement error of ± 0.5 m. Therefore, experimental results are in good agreement with the theory. Measurable range has been improved over single transmitter with this new divergence control system.

4.4.4 Image detection

The signal intensity and the range images are displayed in 21×21 pixels constructed by using MATLAB and Simulink. Maximum signal intensity distribution and range image data are calculated when the correlated signal reached to its maximum value. The total field of view angle of the ultrasonic receiver array in x and y directions is $105^o \times 105^o$ (full angle). A plastic board (30 cm width x 80 cm length) is used as reflector. The pixel point (11, 11) is the center. Figures 4.11 (a) - 4.14 (a) show the respective signal intensities and Figs. 4.11 (b) - 4.14 (b) are the range images when reflector was placed at 11 m in the direction $\theta x = \theta y = 0^\circ$ from the transmitter array and applied divergence are $\phi = 0^o$, 10^o, 20^o, 30^o respectively. z axis shows the distance between transmitter and reflector. The range image of the reflector is detected at (0 pixel, 0 pixel, 10.8 m), that represents the measured position

as (0º, 0º, 10.8 m) for all the four cases.

Further, reflector is placed at 11 m in the direction θ_x = 10º and 20º from transmitter array, its range image obtained at 2 pixels and 4 pixels shifted from the center position (11, 11) as (13, 11) and (15, 11) as shown in Figs.4.15 (a) and 4.16 (a). The position of the reflector placed at 11 m from the UTA in the directions θ = 10º and θ = 20º can be written as (10º, 0º, 11 m) and (20º, 0º, 11 m). The range image of the reflector is detected at (2 pixel, 0 pixel, 10.8 m) and (4 pixel, 0 pixel, 10.6 m), that represents the measured positions as (10º, 0º, 10.8 m) and (20º, 0º, 10.6 m), as shown in Figs. 4.15 (b) and 4.16 (b) respectively.

Similarly, the position of the reflector placed at 11 m in the direction θ_x= 20º and divergence ϕ = 30º is (20º, 0º, 11 m). Its range image obtained at the pixel point (15, 11) as shown in Fig. 4.17 (a). The range image of the reflector is detected at (4 pixel, 0 pixel, 10.5 m), that represent the measured position as (20º, 0º, 10.5 m) as shown in Fig. 4.17 (b). Further, range image resolution depends on the pulse width, pulse speed, distance and object size and calculated as

$$\Delta z = \left(\frac{Pulse\ \ width\ \ (s) \times Wave\ \ velocity(m/s)}{2}\right) + range\ \ error\ \ (m) = 0.55\ \ m$$

and is in agreement within experimental error of ± 0.50 m.

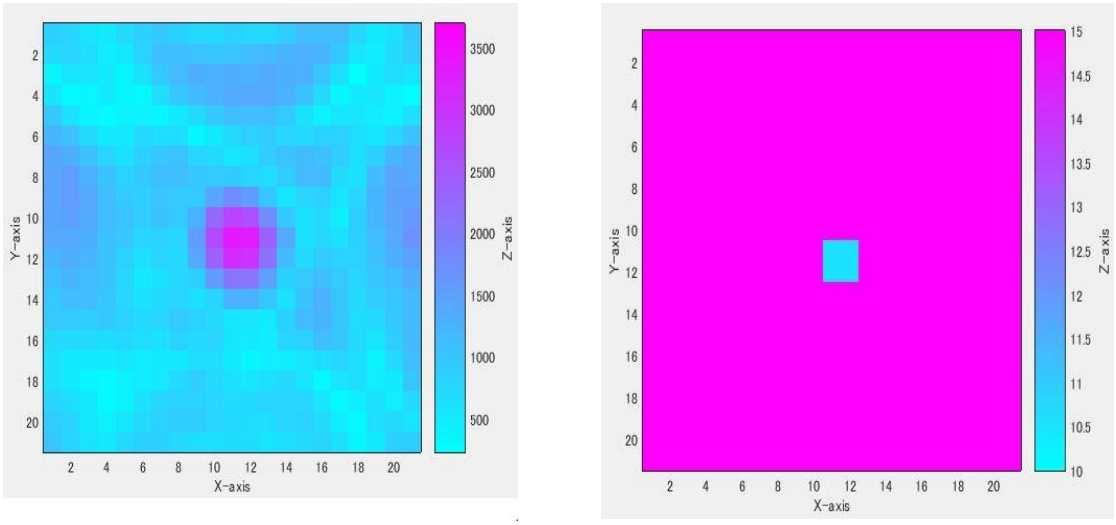

(a) Signal intensity (a.u.) on z axis. (b) Range image (m) on z axis.

Fig. 4.11: Signal intensity after delay-and-sum operations and range image: Divergence ϕ = 0º and Object: 11 m in θ = 0º direction X and Y axis are 5º/div.

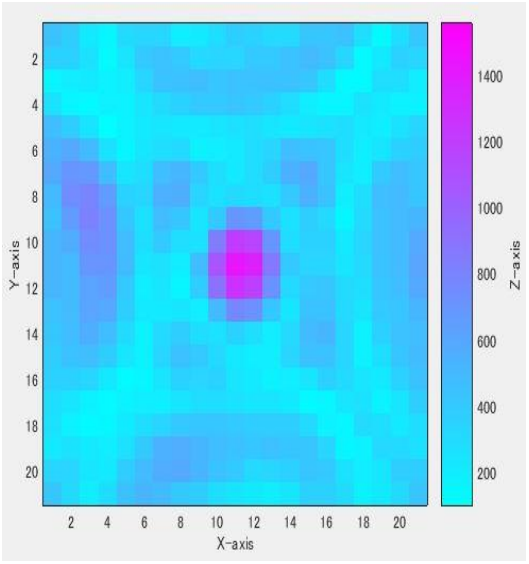

(a) Signal intensity (a.u.) on z axis.

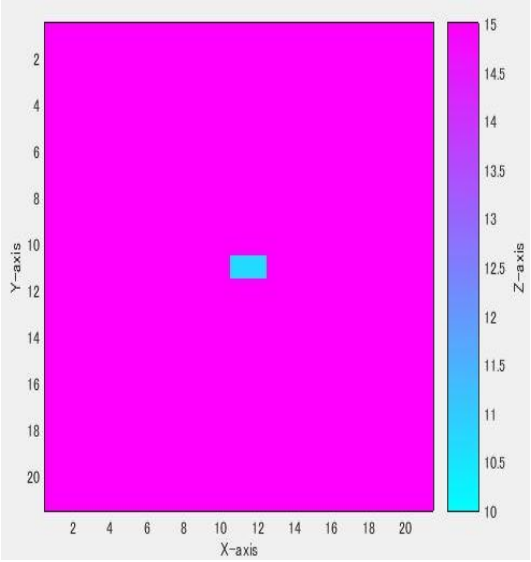

(b) Range image (m) on z axis.

Fig. 4.12: Signal intensity after delay-and-sum operations and range image: Divergence $\phi = 10^{o}$ and Object: 11 m in $\theta = 0^{o}$ direction. X and Y axis are 5°/div.

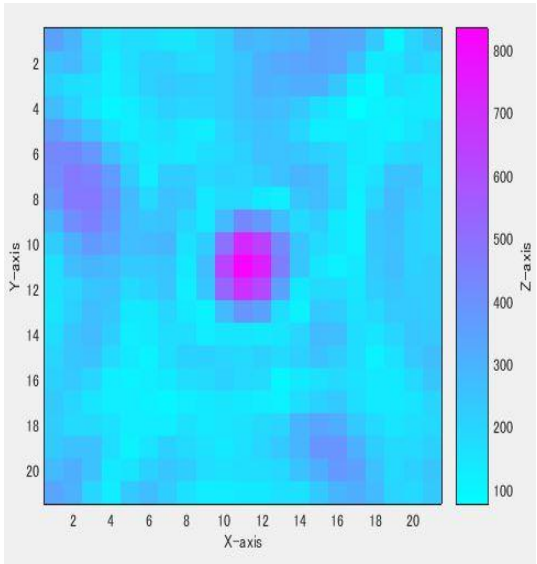

(a) Signal intensity (a.u.) on z axis.

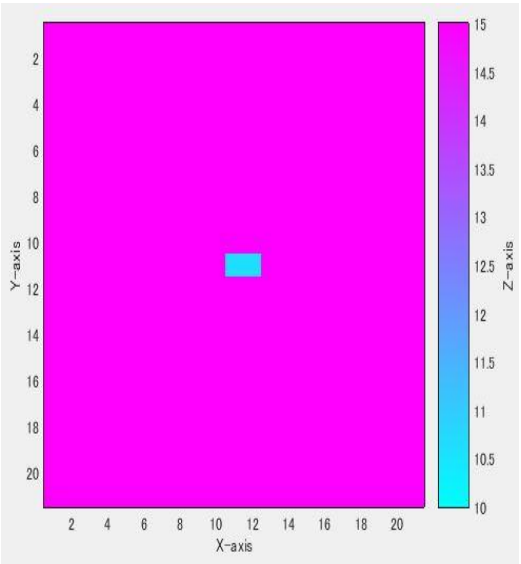

(b) Range image (m) on z axis.

Fig. 4.13: Signal intensity after delay-and-sum operations and range image: Divergence $\phi = 20^{o}$ and Object: 11 m in $\theta = 0^{o}$ direction. X and Y axis are 5°/div.

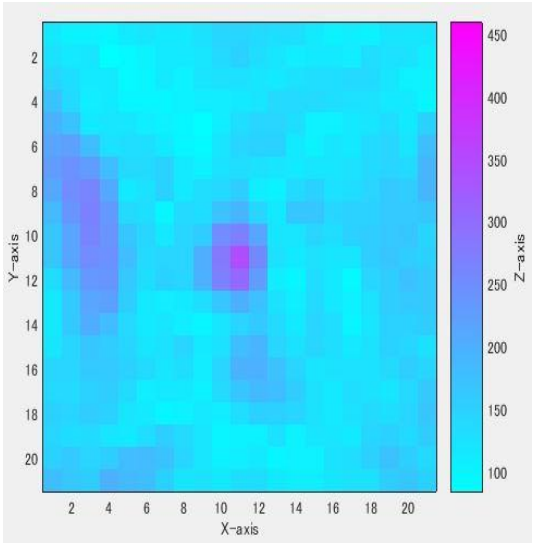

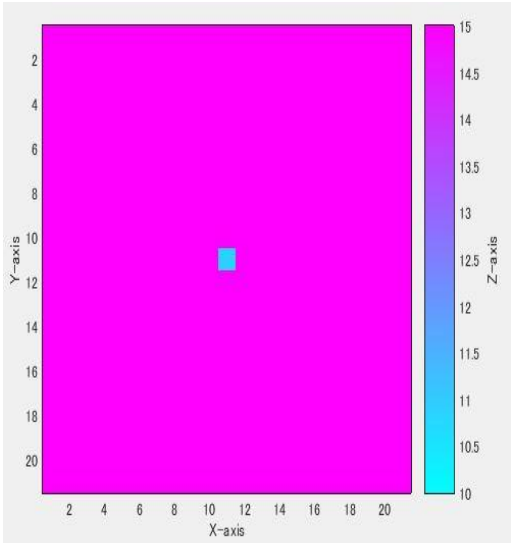

(a) Signal intensity (a.u.) on z axis. (b) Range image (m) on z axis.

Fig. 4.14: Signal intensity after delay-and-sum operations and range image: Divergence $\phi = 30^{o}$ and Object: 11 m in $\theta = 0^{o}$ direction. X and Y axis are 5^{o}/div.

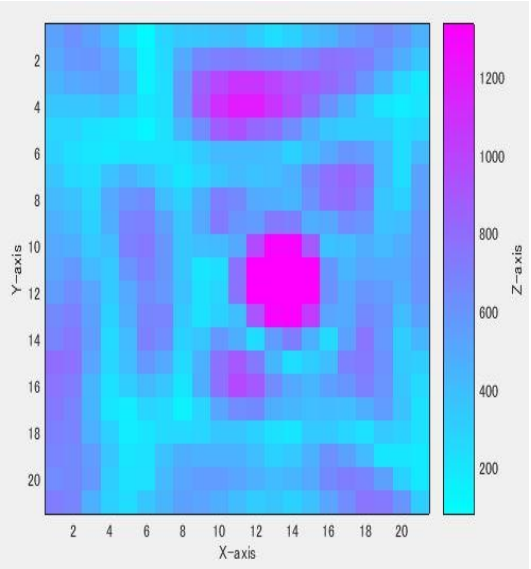

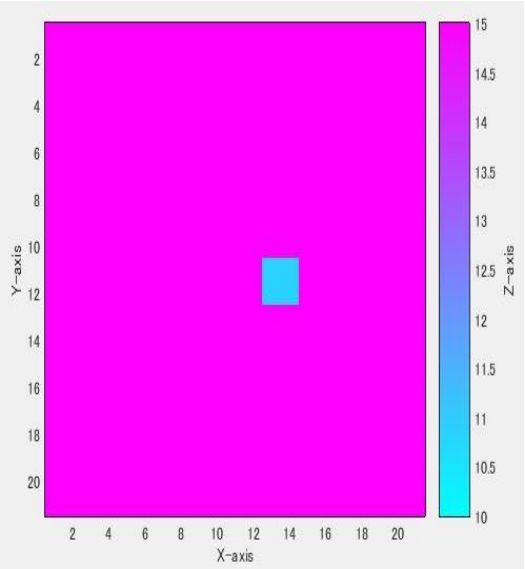

(a) Signal intensity (a.u.) on z axis. (b) Range image (m) on z axis.

Fig. 4.15: Signal intensity after delay-and-sum operations and range image: Divergence $\phi = 10^{o}$ and Object: 11 m in $\theta = 10^{o}$ direction. X and Y axis are 5^{o}/div.

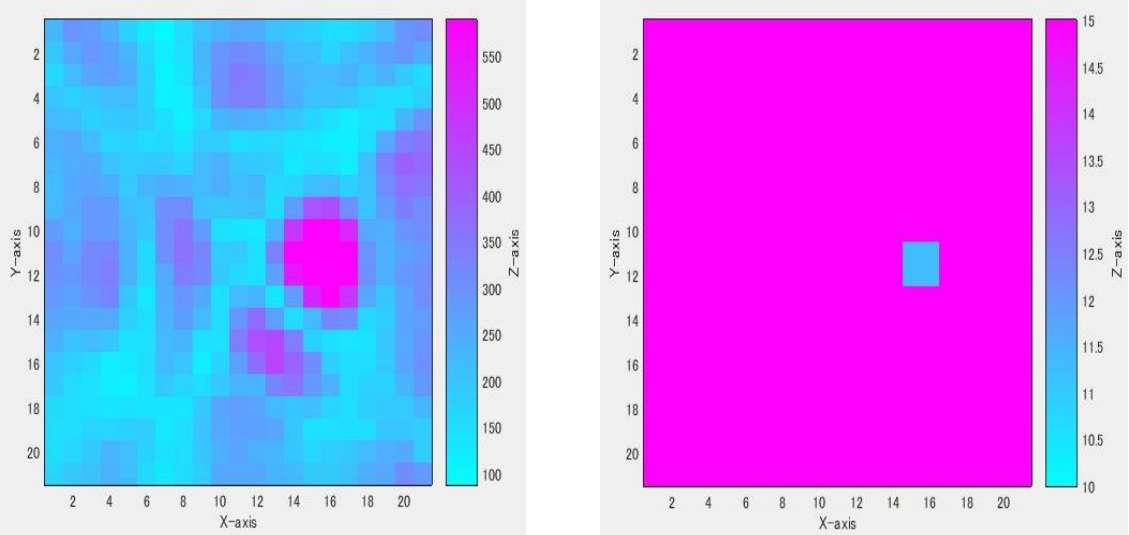

(a) Signal intensity (a.u.) on z axis. (b) Range image (m) on z axis.

Fig. 4.16: Signal intensity after delay-and-sum operations and range image: Divergence $\phi = 20^{o}$ and Object: 11 m in $\theta = 20^{o}$ direction. X and Y axis are 5^{o}/div.

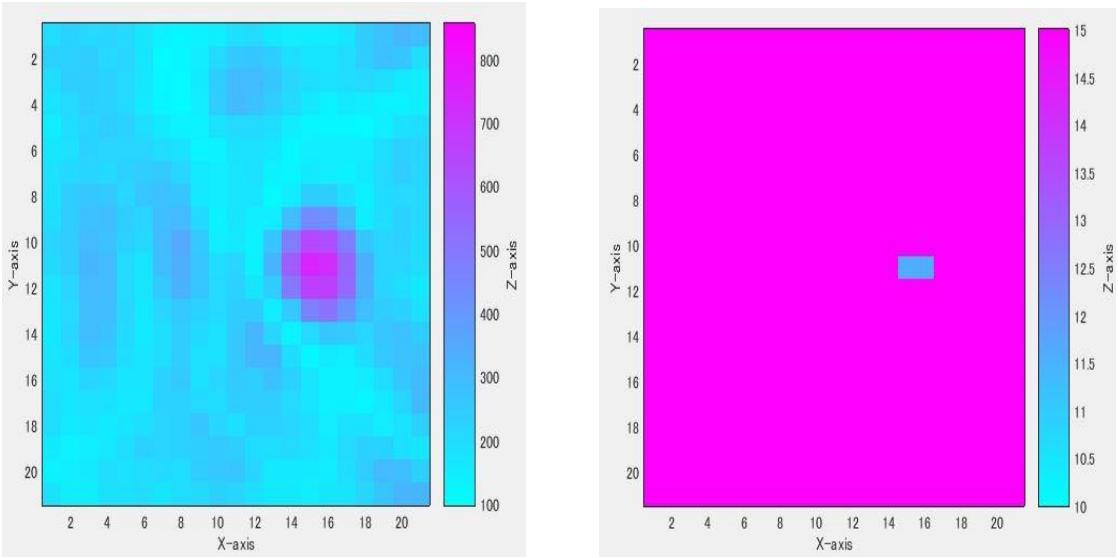

(a) Signal intensity (a.u.) on z axis. (b) Range image (m) on z axis.

Fig. 4.17: Signal intensity after delay-and-sum operations and range image: Divergence $\phi = 30^{o}$ and Object: 11 m in $\theta = 20^{o}$ direction. X and Y axis are 5^{o}/div.

Fig. 4.18 shows the signal intensities at different divergence angles. Signal intensity decreases as the divergence angle increases.

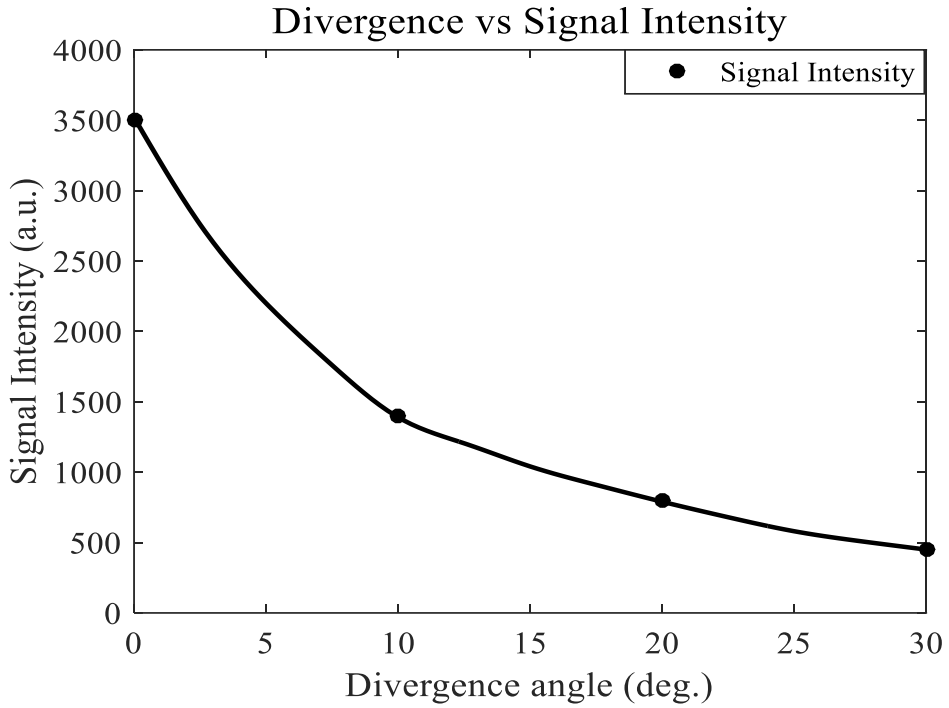

Fig. 4.18 Signal intensities after delay-and-sum operations on divergence angles

The divergence applied on the system is accurately obtained on the experimental results. Measurable range at 10° divergence is 14 m ± 0.5 m which is 2 m less than the measurable range without divergence control. However, measurable 11 m ± 0.5 m has been obtained at the divergence of 30°. This measurable range is still more than the single transmitter i.e. 7 m ± 0.5 m. Experiments are also conducted placing a hard board reflector (30 cm width x 80 cm length) at different positions and applying different divergence control angle. Each time object is clearly detected in the direction it was placed within the experimental error. It is observed that signal intensity reduces as the divergence angles increases. With the developed divergence controlled array transmitter system, divergence is successfully controlled and object is also detected accurately.

4.4.5 Object detection view angle

The measurable range using receiver array and the transmitter array with divergence control was probed using a hard board reflector; 12 cm width x 15 cm height x 4 cm depth. Figure 4.19 shows the dependence of the measurable range on the direction $\theta_x=\theta_y=0^o$. Although, measurable range becomes short with the increase in the divergence, the slope of the curves become more smooth. The view angles at the measurable range 12 m are 5°,

13°, 18° and 15° (half width) for the divergence control angle of 0°, 10°, 20° and 30°, respectively. The view angle increases until the divergence of 20°.

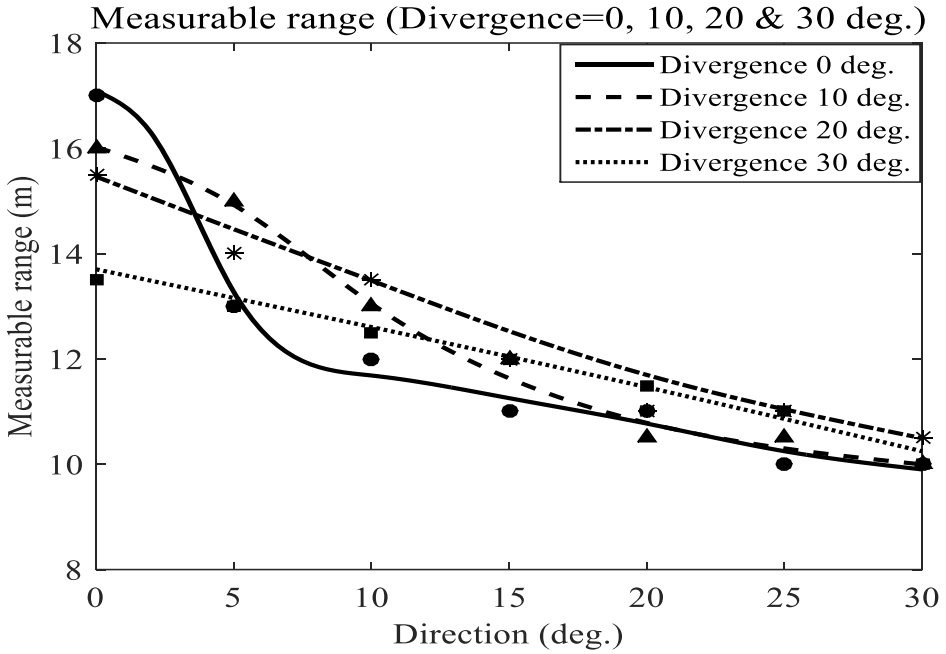

Fig.4.19: View angles at different divergences and object is in $\theta=0^{o}$ direction.

4.5 Conclusion

Divergence control of directivity was investigated theoretically by changing the phase of the signals of each element. The divergence was successfully controlled. The sound pressure was found to decrease as the divergence angle increases. A wide directional measurement field was obtained by controlling the divergence angle.

View angle has been improved to 13° and 18° with the divergence control angle of 10° and 20° respectively at the distance of 12 m. The measurable range without divergence control $\phi = 0^{o}$ is 16 m ± 0.5 m, with divergence $\phi = 10^{o}$ & 20^{o} is 14 m ± 0.5 m and with divergence $\phi = 30^{o}$ is 11 m ± 0.5 m. Experimental results are in good agreement with the theoretical results and object was detected accurately in the direction it was placed.

The measurable range can be improved maintaining high peak power in the divergence direction [15]. Therefore, we propose a new method 'An isotropic divergence controllable transmitter array system', it is expected that this new method would have long measurable range and wide view angle.

References

[1] S. Kumar, K. Ichi and H. Furuhashi, Theoretical investigation of high-power ultrasonic array transmitter for a range sensor in air, Proc. IEEE, Int. conf. on industrial technology ICIT 2013, IEEE Xplore (2013), pp.1190-1195, DOI:10.1109/ICIT.2013.

[2] S. Kumar, Q. Wei and H. Furuhashi, Characteristics of High-Power ultrasonic array transmitter in air, Proc. IEEE 2015, Int. Conf. on Recent Developments in Control, Automation and Power Engineering (RDCAPE 2015), (2015), pp. 209-213. DOI: 10.1109/RDCAPE.2015.7281397.

[3] S. Kumar and H. Furuhashi, Long-range measurement system using ultrasonic range sensor with high–power transmitter array in air, Ultrasonics 74 (2017), pp.186-195. DOI:10.1016/j.ultras.2016.10.012.

[4] S. Kumar, K. Ichi and H. Furuhashi, Theoretical investigation of divergence control of directivity of an ultrasonic transmitter array, SICE annual Conf. (2013), Abstract SuCT2.1 2013, pp.803:807.

[5] S. Kumar and H. Furuhashi, Development of a High-Power array transmitter for an ultrasonic range sensor in the air, Proc. Int. Conf. Ultrasonics 2016, (2016), P-42, pp.309-310.

[6] D.H. Turnbull and F.S. Foster, Beam Steering with Pulsed Two-Dimensional Transducer Arrays, IEEE Transactions on Ultrasonics, Ferroelectrics and Frequency control, 38 (4) (1991).

[7] B. Beardsley, M. Peterson and J.D. Achenbach, A simple scheme for self-focusing of an array, Journal of Nondestructive Evaluation: 14 (4) (1995), pp. 169-179, DOI:10.1007/BF00730887.

[8] L.E. Kinsler, A.R. Frey, A.B. Coppens and J.V. Sanders, Fundamentals of Acoustics, Fourth Edition: John Wiley & Sons, Inc., 2000.

[9] H. Inubushi, N. Takahashi, H. Zhu and K. Taniguchi, Ultrasonic 3D image sensor employing PN code and beam-forming technologies, IEICE Trans. J90 (6) (2007), pp.517-523.

[10] H. Furuhashi, Y. Uchida and M. Shimizu, Imaging sensor system using rectified delay-and-multiply operations with an ultrasonic array, Proc. IEEE, IECON 2008, IEEE Xplore (2008), pp.1891-1895.

[11] H. Furuhashi, Y. Uchida and M. Shimizu, Imaging sensor system using composite ultrasonic array, Sensors 2009, IEEE Xplore (2009), pp.1467-1472.
[12] H. Furuhashi, Y. Kuzuya, Y. Uchida and M. Shimizu, Three dimensional imaging sensor system using an ultrasonic array sensor and a camera. Sensors 2010, IEEE Xplore 2(010), pp.713-718.
[13] H. Furuhashi, Y. Kuzuya, C. Gal and M. Shimizu, Three-dimensional imaging of a human body using an array of ultrasonic sensors and a camera, Proc. IEEE, CACS 2011, Int. congress on computer application and computational science, 145 (2011), pp.325-330. DOI:10.1007/978/3-642-28308-6- (44).
[14] K. Ohtani and M. Baba, Shape recognition and position measurement of an object using an ultrasonic sensor array, www.intechopen.com.
[15] S. Kumar, K. Ichi and H. Furuhashi, Theoretical investigation of an ultrasonic array transmitter with anisotropic directivity, Proc. Int. conf. on sensor device technologies and applications SENSORDEVICES 2013 (2013), pp.131-134.

Chapter 5

Anisotropic Divergence Controllable Ultrasonic Transmitter Array for 3-D Range Imaging[1-7]

5.1 Introduction

A long range measurement system using high power ultrasonic transmitter array has been developed that can detect an objects up to 25 m. Such a long measurable range using ultrasonic sound has been obtained in open air for the first time. However, this long range imaging system has the drawback that object detection view angle is very narrow [1, 2]. To overcome this problem an improved range imaging system has been proposed and constructed. In this improved system divergence of sound is controlled [3-5]. Measurement field increases with an increase the divergence angle. Measurable range up to 16 m has been reported with this new system without divergence control. Measurable range at divergence 30^{o} is appx. 11 m that is still more than the conventional method [6, 7]. When a divergence control angle is applied, this divergence is equal in x axis and y axis. This new system also has one drawback that sound pressure level decreases as divergence angle increases, as a result, the measurable range decreases.

For the improvement of measurable range over isotropic divergence control, an anisotropic divergence control system is proposed. With this anisotropic divergence control system, divergences in x axis and y axis are independently controlled so that high peak power can be maintained in the divergence direction as a result improvement in measurable range. In particular cases it is required to measure wide horizontal and narrow vertical plane. In this chapter, we discuss the principle of the anisotropic divergence controllable transmitter array and construct the system following its principle.

First of all, the characteristics of the new transmitter array system are investigated via computer simulations and later they are confirmed experimentally.

5.2 Theory

Fig. 5.1 shows the coordinate system of anisotropic divergence control system. First of all, theory of control method is discussed.

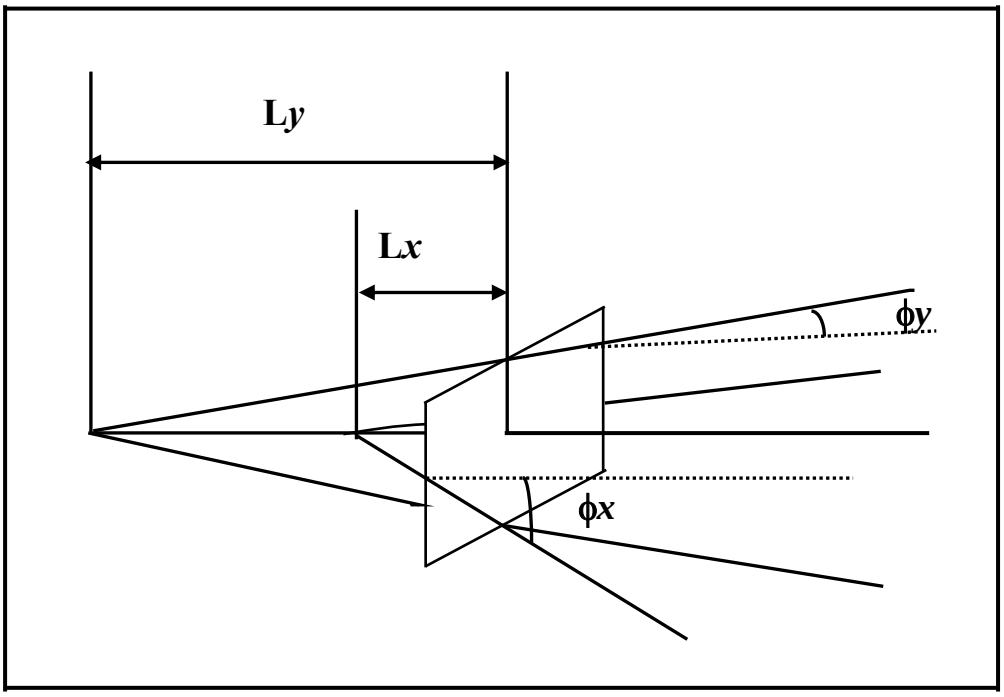

Fig.5.1: Coordinate system of anisotropic divergence control

If, D (θ_i) are the directivities of the transmitting elements. Let L_x and L_y are the distances between the center of the array and center of the divergence and calculated by Eq. (5.1) and (5.2) as follows [6, 7]

$$L_x = \frac{(n-1)d}{2\tan\phi_x} \tag{5.1}$$

$$L_y = \frac{(n-1)d}{2\tan\phi_y} \tag{5.2}$$

Here, ϕ_x and ϕ_y are the angles of the divergence in x and y directions, n is number of transmitter arrays, d is inter element space. In this case, time delay applied to each element is calculated by Eq. (5.3) as follows by modifying Eq. (4.4) in previous chapter.

$$\Delta\tau_d \approx \left(\frac{x_i^2}{L_x} + \frac{y_i^2}{L_y}\right)\frac{1}{2c} \tag{5.3}$$

Here, c is the wave velocity.

Therefore, according to the time delay applied to each element, the phase difference $\Delta\phi$ is calculated by Eq. (5.4) as follows

$$\Delta\phi_d = 2\pi\frac{c\Delta\tau_d}{\lambda} \approx \frac{2\pi}{\lambda}\left(\frac{x_i^2}{Lx} + \frac{y_i^2}{Ly}\right)\frac{1}{2} \tag{5.4}$$

Considering that there are a number of transmitting element in x, y plane at positions P_i (x_i, y_i, 0), then sound pressure at observation point P(x,y,z) is obtained by Eq. (5.5) as follows modifying Eq. (4.6) in previous Chapter,

$$|p(x,y,z)| = D(\theta_i)A\frac{1}{r}\left|\sum_{i=1}^{n} exp\left\{-i\frac{2\pi}{\lambda}\left(x_i sin\theta_x + y_i sin\theta_y + \frac{x_i^2}{2L_x} + \frac{y_i^2}{2L_y}\right)\right\}\right| \tag{5.5}$$

Here, A is the amplitude of the sound pressure of one transmitter; r is the distance between the origin (i.e. the center of the array) and the observation point P (x, y, z). The θ_x and θ_y are the angles between the vector $\overrightarrow{OP}$ & yz plane and xz plane respectively.

Simulation directivity of an UAT in which all the elements are in phase using Eq. (5.5) is shown in Fig.5.2 (a) and its signal intensity image is shown in

Fig. 5.2 (b) respectively. The radius of the element is 4.3 mm, wavelength is 8.6 mm, wave velocity is 345 m/s, frequency is 40 kHz.

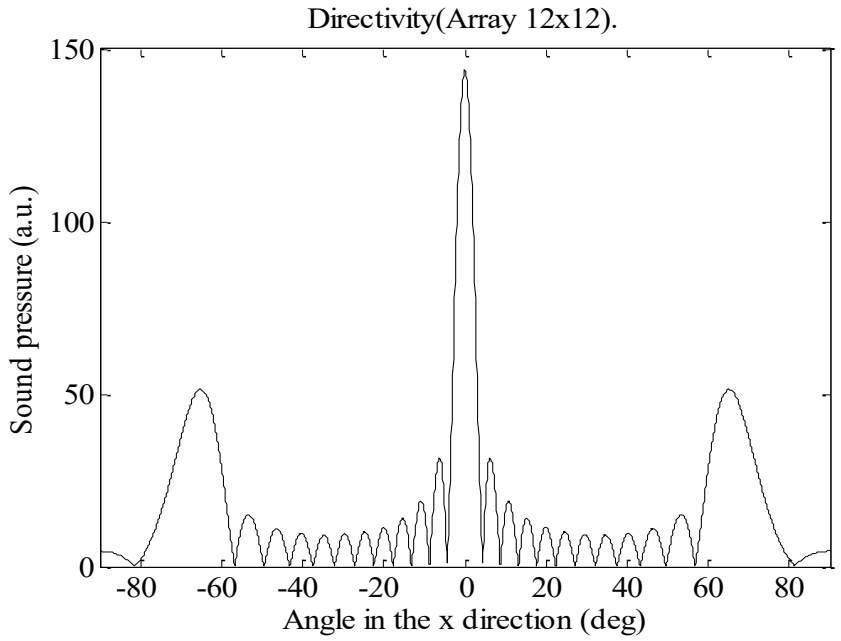

(a)

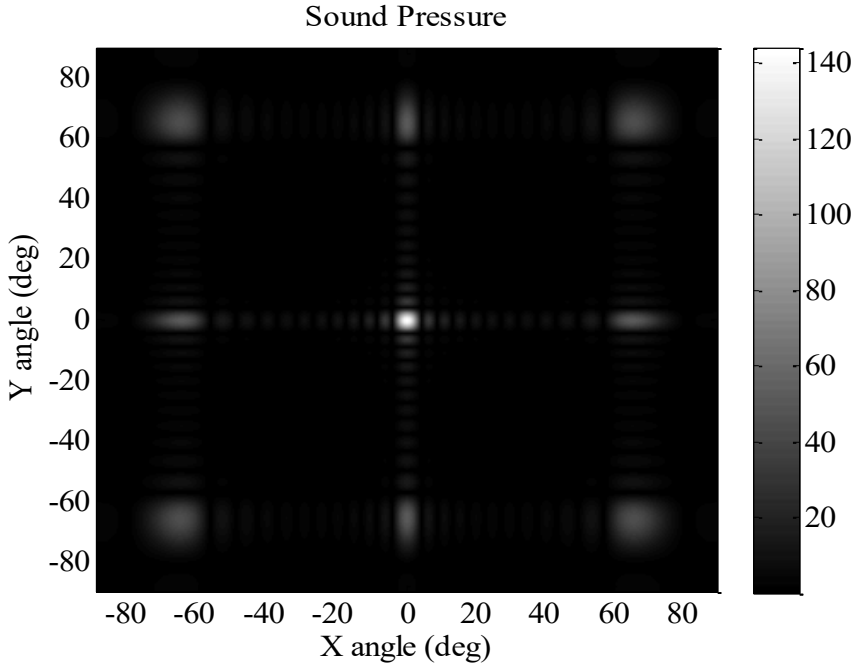

(b)

Fig. 5.2 (a): Simulation directivity of UTA (elements in phase); (b): Signal intensity.

The elements are placed (12 x12) matrix with the inter element space 10 mm. The sound pressure is normalized by A/r considering sound pressure (a.u.) of single transmitter is 1. The sound pressure (a.u.) 144 times higher than that of single element has been obtained by the UTA and has the directivity of $\pm 2^{o}$. This directivity is too narrow for many applications [1-7].

Figure 5.3 shows the directivity of UTA in which the divergence angle of the transmitted signal is controlled, using Eq. (5.5). The angle of the divergence is 20^{o} in both x and y directions and sound pressure is normalized by A/r. The length L is calculated to be 151 mm. The time delay is calculated using Eq. (4.4) of previous chapter and is 0 to 58 μs. The peak sound pressure with isotropic divergence $\phi = 20^{o}$ is 22 times higher than that of a single transmitter element, and it is 7 times lower than that of an array transmitter when elements are in phase.

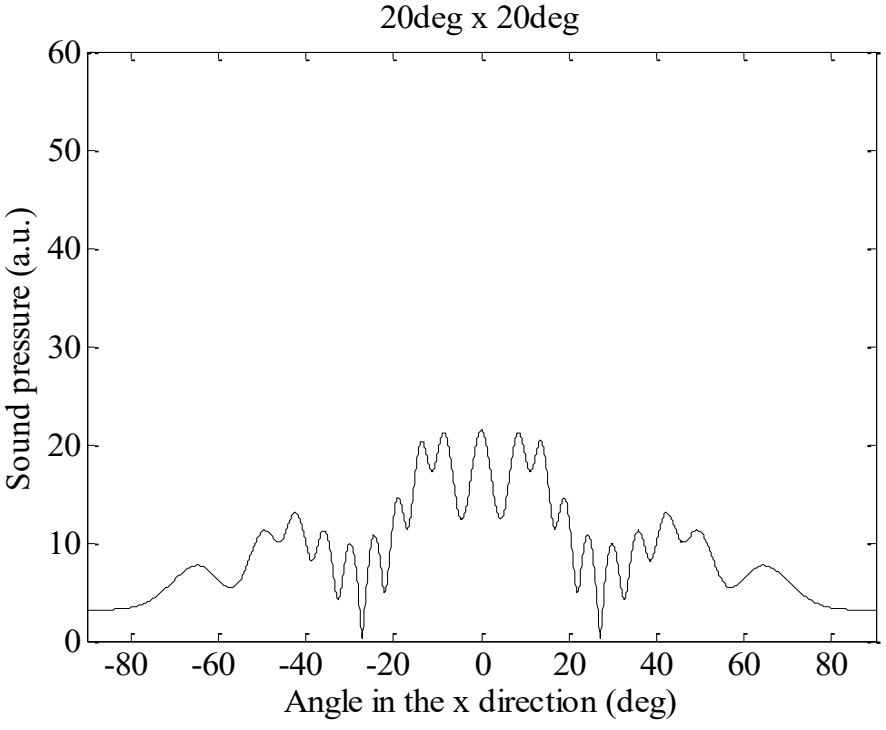

(a)

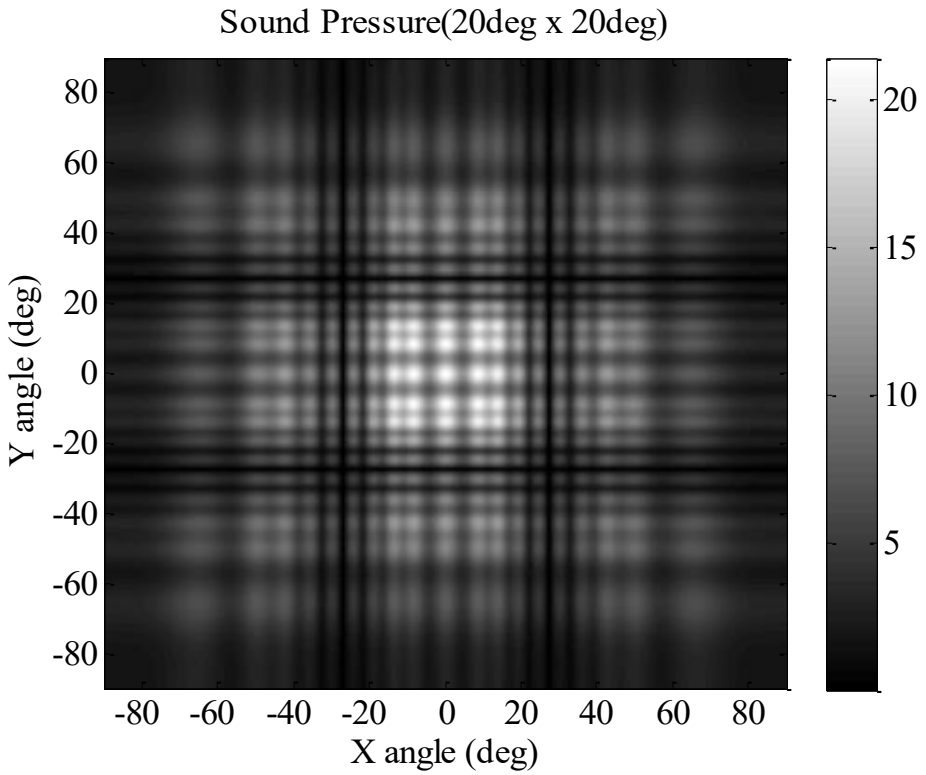

(b)

Fig. 5.3: (a) Directivity of UTA ($\phi_x = \phi_y = 20^o$); (b): Signal intensity image.

Fig. 5.4 shows the directivities of an array transmitter for which the anisotropic directivity is calculated by Eq. (5.5). The angle of horizontal divergence and vertical divergence are 20^o and 5^o (in *x* and *y* directions) respectively. Figure 5.4 (a) shows the simulation directivity in x direction, (b) simulation directivity in y direction, and (c) signal intensity image. The UTA has the peak pressure about 48 times higher than that of single transmitter with anisotropic divergence control. Peak pressure with anisotropic divergence is 2.2 times higher than that of isotropic divergence control angle. The simulated result of the divergence is controlled successfully and it is about 20^o x 5^o (half width).

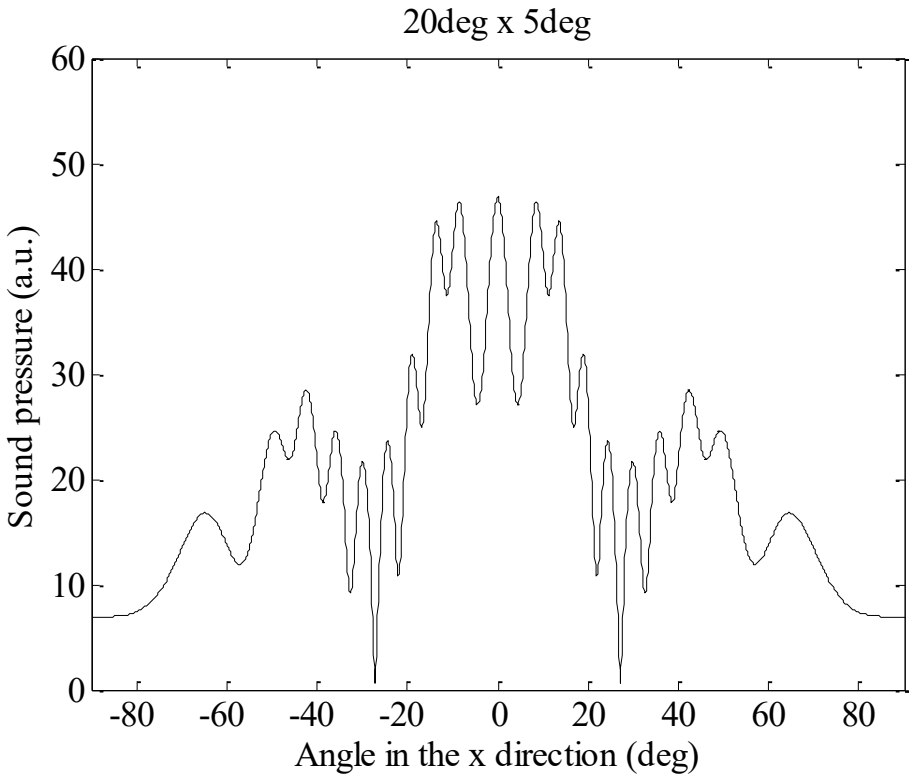

(a) (ϕ_x=20°; ϕ_y= 5°) in x direction.

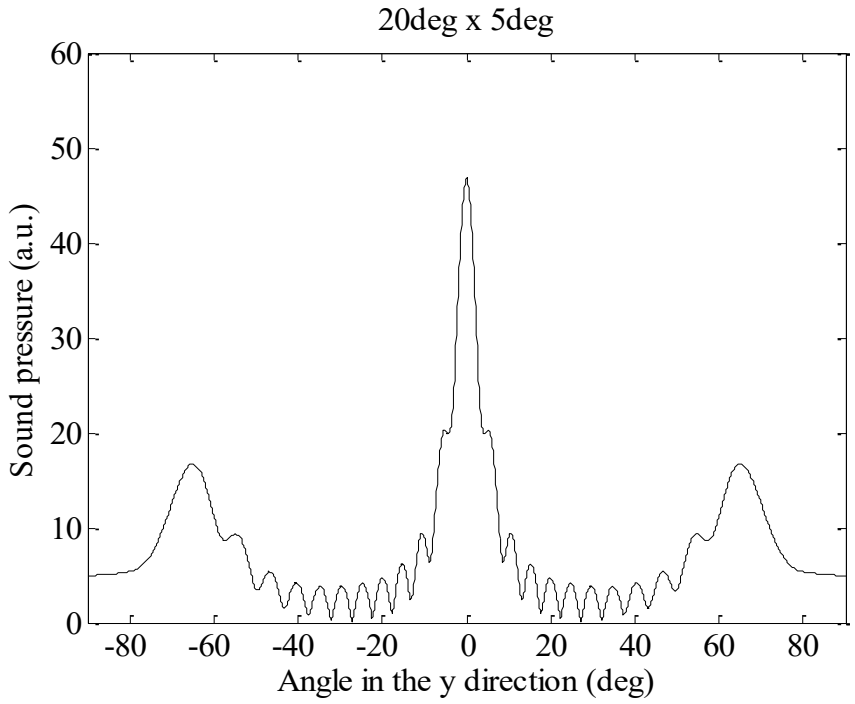

(b) (ϕ_x=20°; ϕ_y= 5°) in y direction.

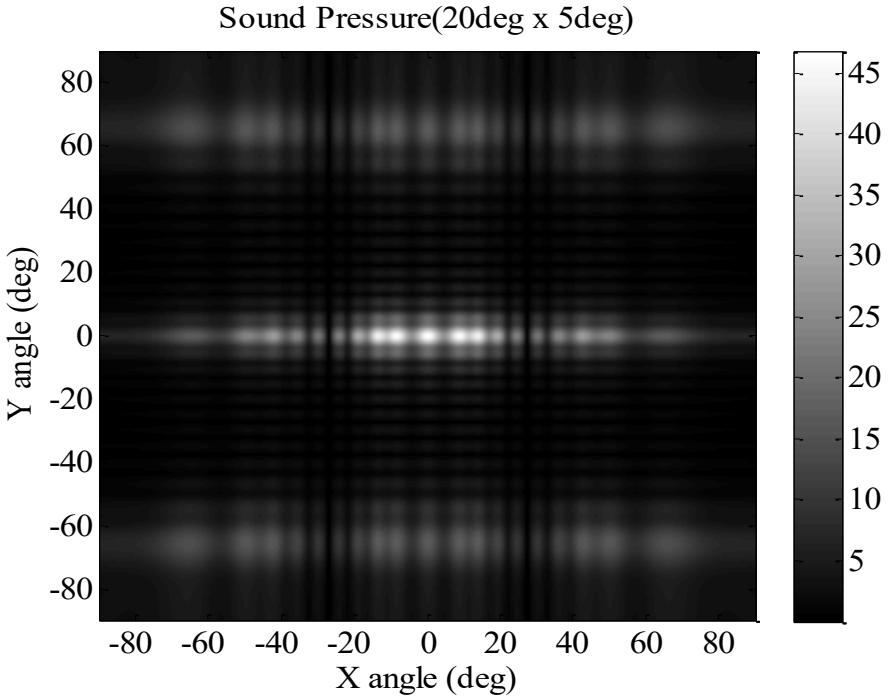

(c) (ϕ_x=20°; ϕ_y= 5°) signal intensity image

Fig. 5.4 (a) Directivity in x axis. (b) Directivity in y axis (c) Signal intensity image.

Fig. 5.5 shows the dependence of the sound pressure on the angle of the divergence in the *y* direction. The angle of the divergence in the *x* direction is changed.

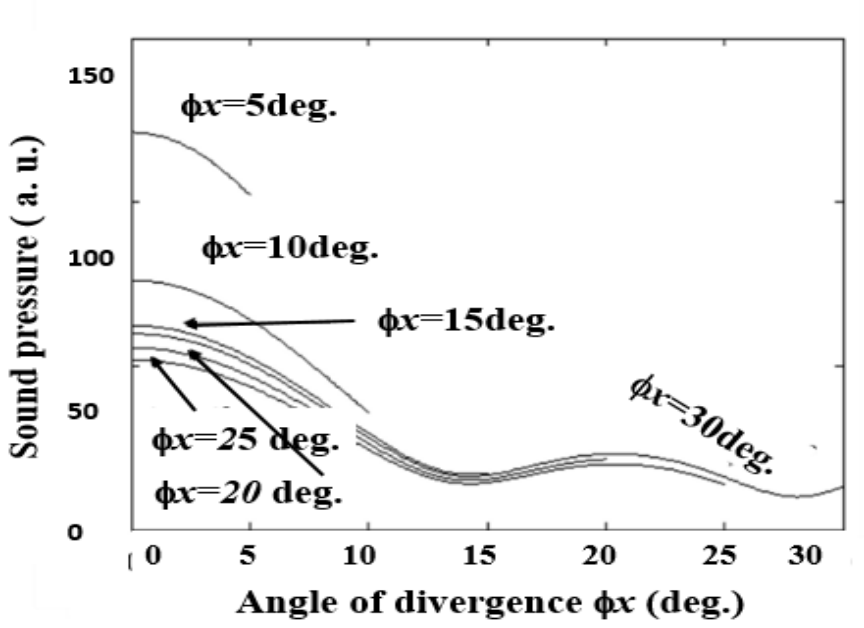

Fig. 5.5: Dependence of sound pressure on the angles of the divergence in x direction.

The sound pressure decreases with an increase in the angle of divergence in x direction. The sound pressure level decreases in large quantity up to 10^{o} and after that very small change is found maintaining high peak power in the divergence direction.

5.3 Structure of the divergence controllable transmitting system

The system configuration is the same as described in Chapter-4. The block diagram is shown in Fig.5.6 again. The difference in this system is the delay time calculations, which are calculated by the personal computer from the two input divergence angle (i) horizontal (ii) vertical. Putting the values of L_x and L_y in delay time Eq. (5.3) that can be rewritten as Eq. (5.3A) [6-10]

$$\Delta\tau_d \approx \left(\frac{x_i^2}{L_x} + \frac{y_i^2}{L_y}\right)\frac{1}{2c} \tag{5.3}$$

$$\Delta\tau_d \approx \frac{1}{(n-1)dc}\left(x_i^2 \times tan\emptyset_x + y_i^2 \times tan\emptyset_y\right) \tag{5.3A}$$

Working principle of ultrasonic receiving system is the same as described in Chapter-4.

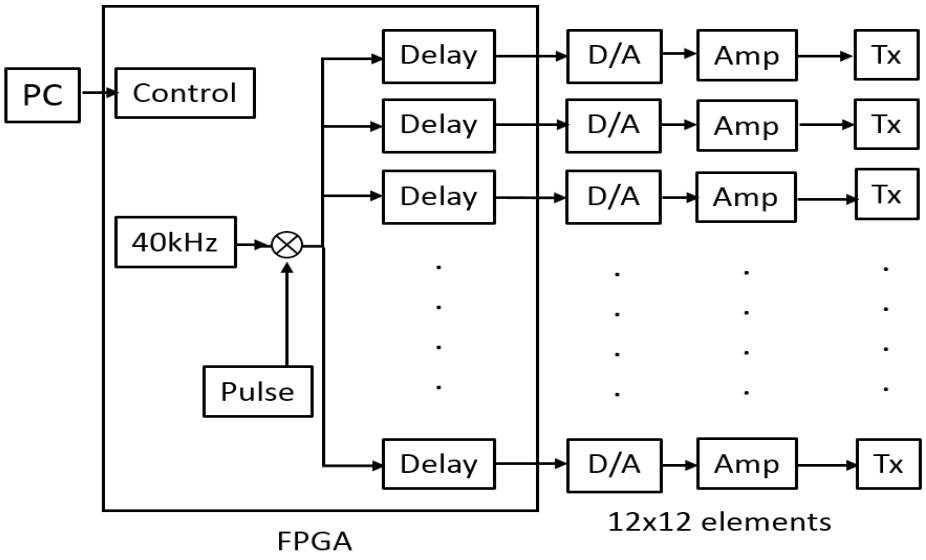

Fig. 5.6: A block diagram of modified UTA

5.4 Experimental results

5.4.1 SPL of array transmitter with anisotropic divergence

The transmitted signal is received by a sensor as depicted in Fig.2.2 of Chapter-2. The sensor is placed 5 m apart from the transmitter with their height at 1.5 m above the ground level. The additional two divergence control angle (horizontal and vertical) were included in the control system. The calibration of sensor and peak to peak voltage measurement method by rotating the UTA are the same as mentioned in previous chapters.

Fig. 5.7 shows the dependences of the sound pressure level on the divergence ϕ_x for the transmitter array with isotropic and anisotropic divergence control. The sound pressure levels for an array transmitter without divergence control and for a single transmitter are also shown. Sound pressure levels with isotropic divergence i.e. $\phi_x = \phi_y$; are shown by the circles.

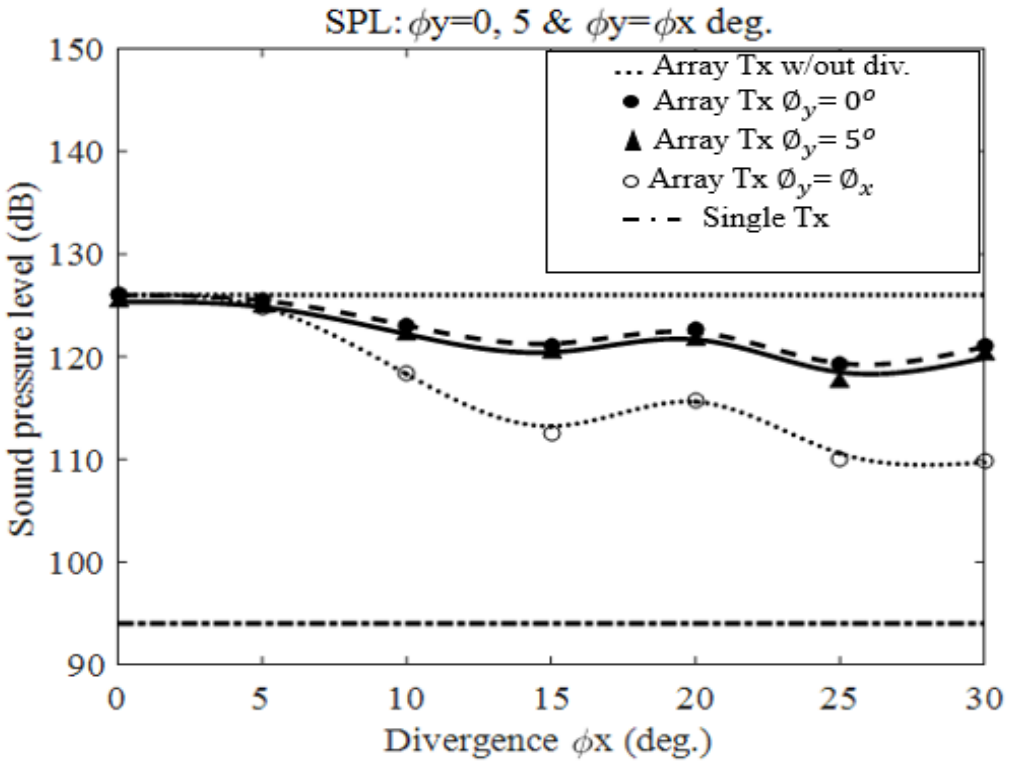

Fig.5.7: Dependence of SPL on isotropic and anisotropic divergence angles.

Sound pressure levels of single transmitter and array transmitter without divergence control are shown by straight dash-dotted line and narrow dotted

line respectively. Sound pressure levels with vertical divergence ϕ_y=0° are shown by the black circles, and ϕ_y = 5° are shown by the black triangles. Sound pressure level at ϕ_y = 5° and ϕ_y = 0° differ slightly, but decreases significantly with the isotropic divergence. Therefore, high peak sound pressure can be maintained with the anisotropic divergence control. Sound pressure levels with ϕ_x = 0°, 5°, 10° and 15°; ϕ_y = 5° are obtained 125.3 dB, 124.8 dB, 119.9 dB and 115 dB respectively. The rate of decrease of SPL is higher in isotropic divergence than anisotropic divergence.

5.4.2 Directivities with anisotropic divergence

Figs. 5.8 (a)-(c) show the directivities of the array transmitter when divergence ϕ_x = 5°, 10° and 15°; ϕ_y = 5° respectively. The black dots are the experimental results and smooth line shows the simulation results. Applying the horizontal and vertical divergence on the system, experimental results are obtained accordingly through half width at half maximum (HWHM). The experimental results are in good agreement with the simulation results.

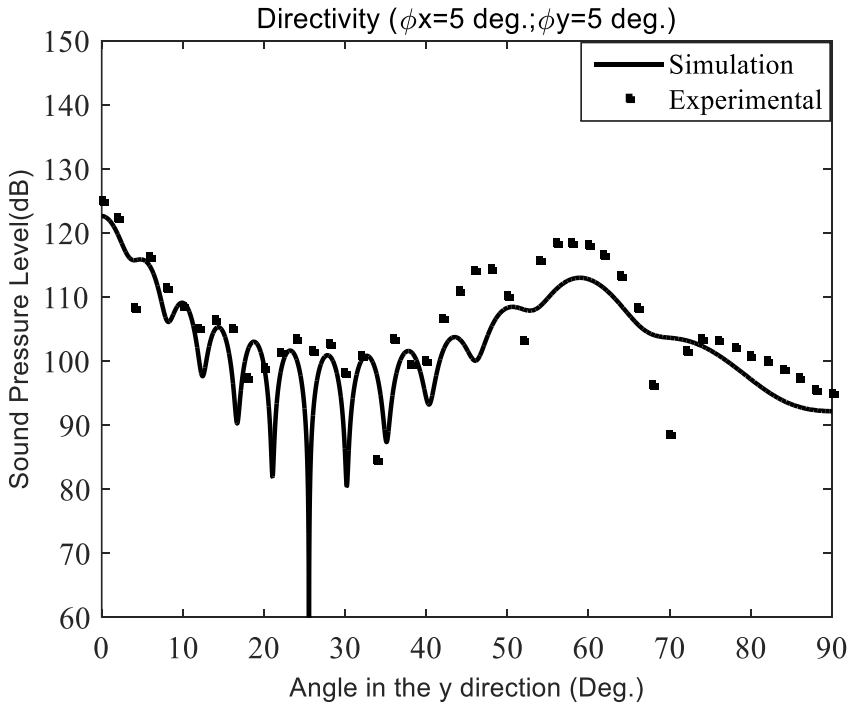

(a) (ϕ_x=5°; ϕ_y=5°)

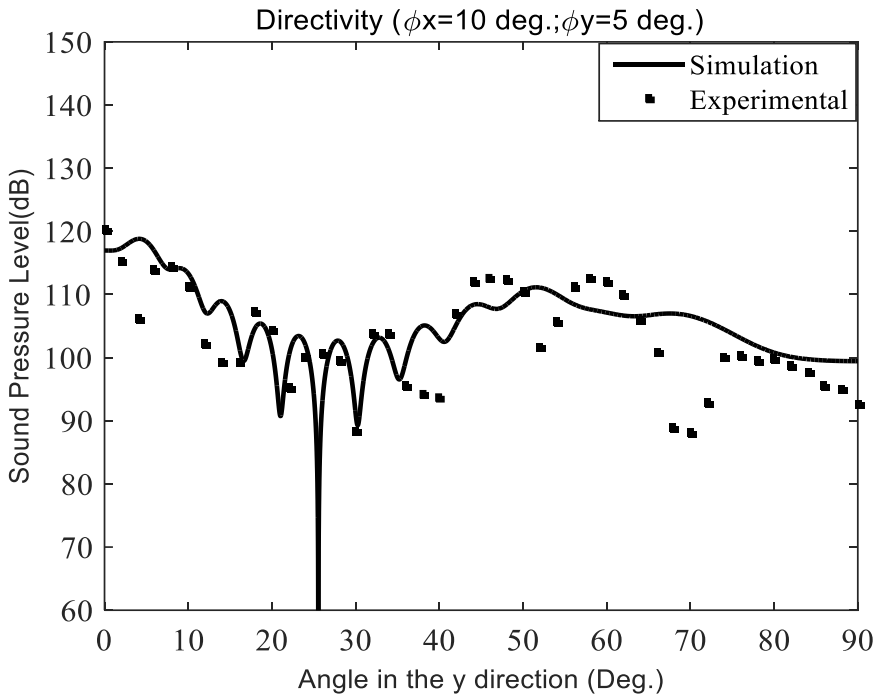

(b) (ϕ_x=10°; ϕ_y=5°)

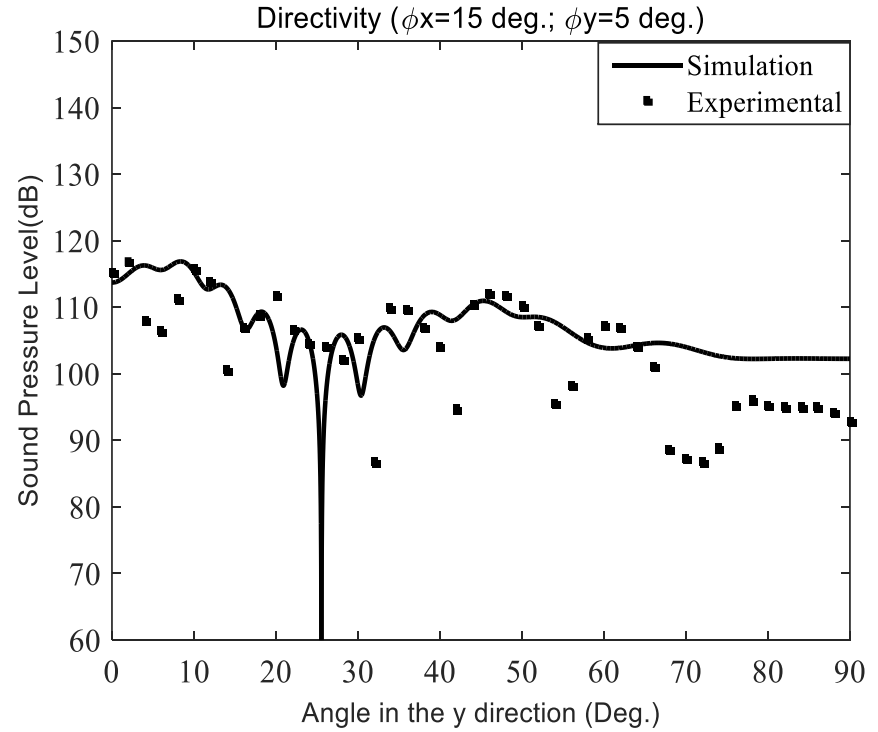

(c) (ϕ_x=15°; ϕ_y=5°)

Fig. 5.8: Directivities at different horizontal and fixed vertical divergence angles.

5.4.3 Measurable range using anisotropic divergence

Experimental set-up and measurement method of measurable range is the same as explained in Chapter-4. Fig. 5.9 shows the measurable range at different divergence angles using same reflector (30 cm width x 80 cm length). The ratio of sound pressure K is calculated using Eq. (3.11) of Chapter-3. Here, K is the ratio of sound pressure transmitted by the array transmitter to that of single transmitter and calculated as 34.7, 19.7 and 11.2 when $\phi_x = 5^o$, 10^o &15^o and $\phi_y = 5^o$, respectively.

Theoretical measurable ranges for different K are denoted by dashed, dash-dotted and smooth black line, respectively at $\gamma = 0.12/\text{m}$ according to Eq. (3.10). Measurable range without divergence control is 17 m ± 0.5 m. Measurable ranges for isotropic divergence angles $\phi_x = \phi_y = 10^o$ and anisotropic divergence angle $\phi_x = 10^o$ and $\phi_y = 5^o$ are 14 m ± 0.5 m and 16 m ± 0.5 m [16-19]. Measurable range of the anisotropic divergence control is less than the without divergence, but higher than isotropic divergence. Measurable range has been improved over 2 m ± 0.5 m over isotropic divergence.

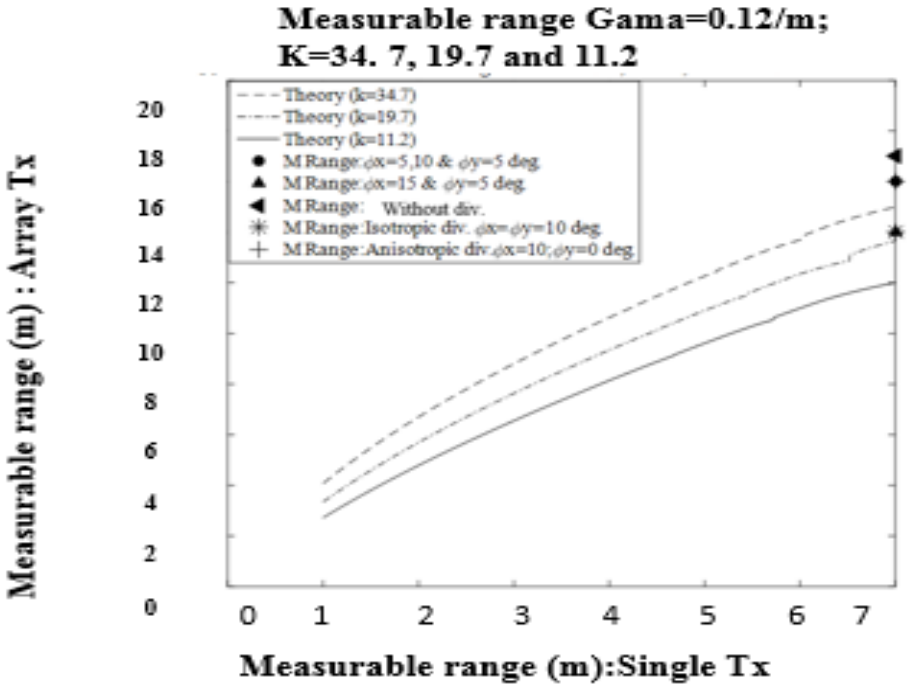

Fig. 5.9: Measurable range at isotropic and anisotropic divergence control angles.

The theoretical measurable range for K=34.7, 19.7 and 11.2 are shown as dotted, dash-dotted and smooth line, respectively. The experimental results are in good agreement with the simulation results [6, 7].

5.4.4 Detection of range image

Fig. 5.10 shows the dependence of the signal intensities after delay-and-sum operations of the URA on the fix divergence angle $\phi_y = 0^o$ and varying the divergence angle ϕ_x from 0^o – 30^o at the step of 5^o are shown by circles. Similarly, signal intensities on the fix divergence angle $\phi_y = 5^o$ and varying the divergence angle ϕ_x from 0^o – 30^o at the step of 5^o are shown by triangles. Signal intensity reduces at $\phi_y = 5^o$ in comparison to $\phi_y = 0^o$.

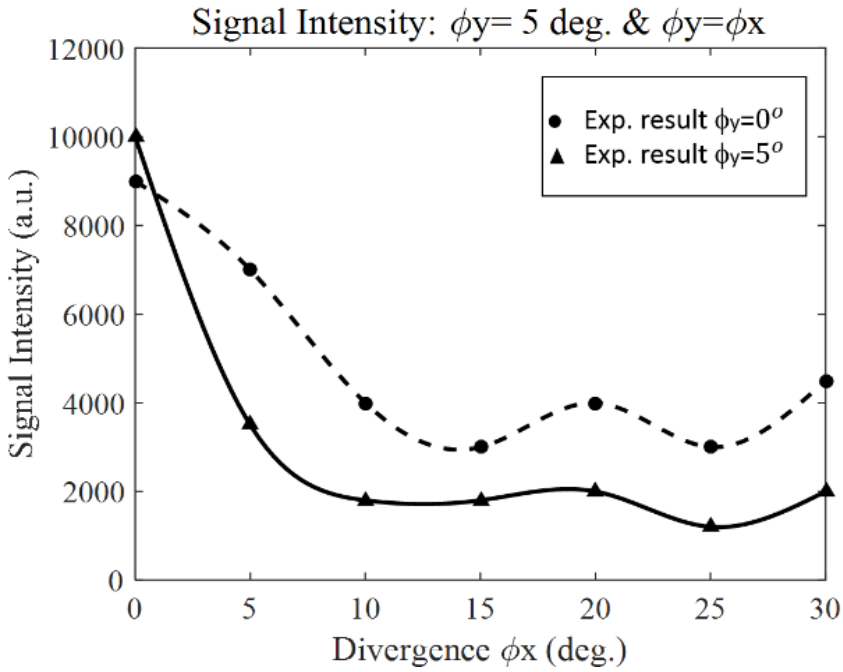

Fig. 5.10: Signal intensities at different divergences.

When reflector is placed at 12 m in the direction $\theta_x = -10^o$ and anisotropic divergence ($\phi_x = 10^o$ & $\phi_y = 5^o$) is applied on the system. The position of the reflector is written as (-10^o, 0^o, 12 m). The range image of the reflector is detected at (2 pixel, 0 pixel, 11.7 m) as shown in Fig. 5.11 (a) and it represents the measured positon as (-10^o, 0^o, 11.7 m) as shown in Fig 5.11 (b). Similarly, when reflector is placed at 12 m in the direction $\theta_x = -10^o$ and anisotropic divergence ($\phi_x = 20^o$ & $\phi_y = 5^o$) and ($\phi_x = 30^o$ & $\phi_y = 5^o$) are applied

on the system. The positions of the reflector can be written as (-10°, 0°, 12 m) for both the cases and respective images are detected at (2 pixel, 0 pixel, 11.7 m) and (2 pixel, 0 pixel, 11.5 m) as shown in Figs. 5.12 (a) and 5.13 (a). The respective measured positions are represented as (-10°, 0°, 11.7 m) and (-10°, 0°, 11.5 m) and shown in Figs.5.12 (b) and 5.13 (b), respectively.

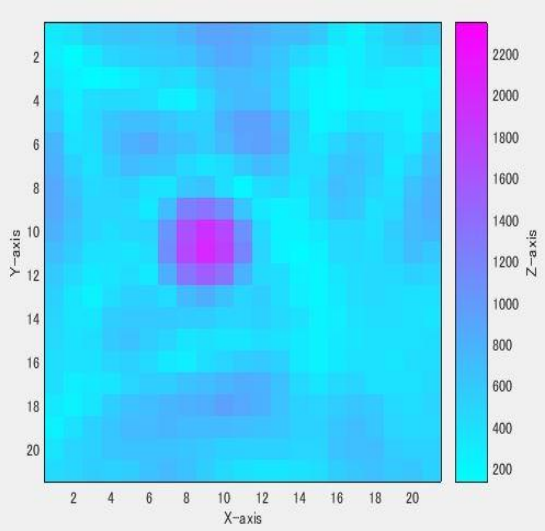

(a) Signal intensity (a.u.) on z axis.

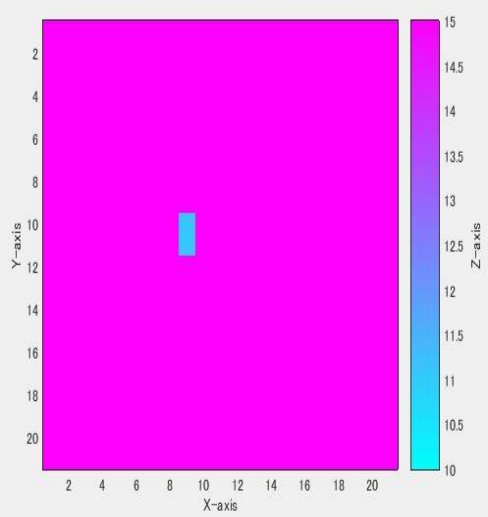

(b) Range image (m) on z axis.

Fig. 5.11: Signal intensity after delay-and-sum operations and range image: Divergence $\phi_x = 10^o$; $\phi_y = 5^o$ and Object at 12 m in $\theta = -10^o$ direction. X and Y axis are 5°/div.

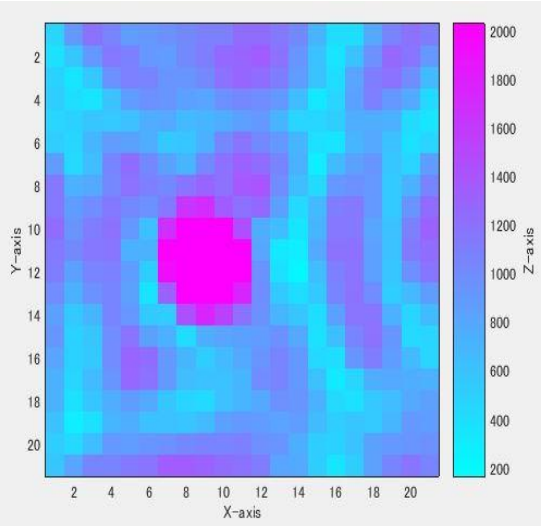

(a) Signal intensity (a.u.) on z axis.

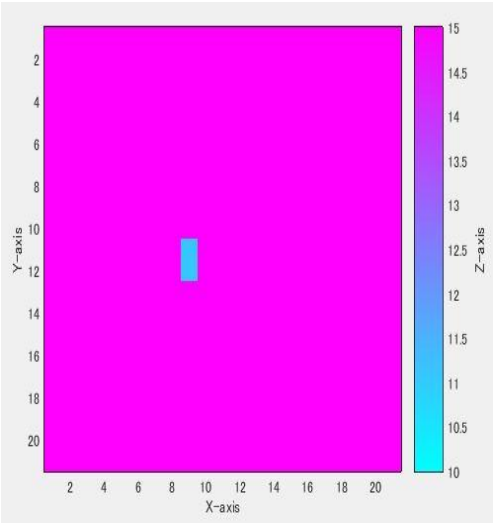

(b) Range image (m) on z axis.

Fig. 5.12: Signal intensity after delay-and-sum operations and range image: Divergence $\phi_x = 20^o$; $\phi_y = 5^o$ and Object at 12 m in $\theta = -10^o$ direction. X and Y axis are 5°/div.

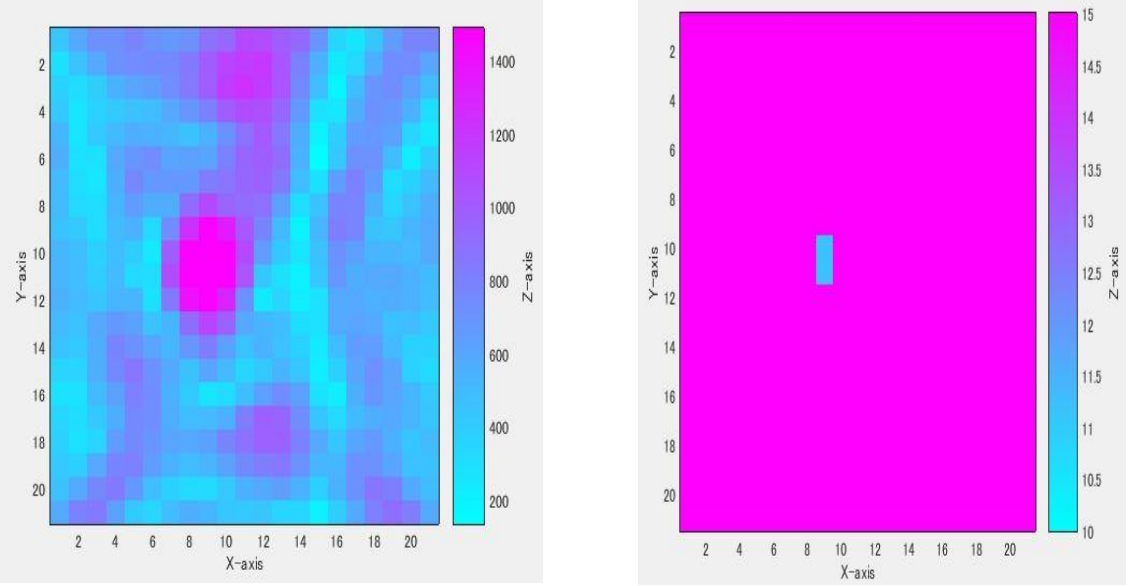

(a) Signal intensity (a.u.) on z axis. (b) Range image (m) on z axis.

Fig. 5.13: Signal intensity after delay-and-sum operations and range image: Divergence $\phi_x = 30^o$; $\phi_y = 5^o$ and Object at 12 m in $\theta = -10^o$ direction. X and Y axis are 5°/div.

The distribution of the maximum signal intensity in the range image data was calculated when the correlated signal reached to its maximum value. The signal intensity and the range images are displayed in 21 × 21 pixels constructed using MATLAB and Simulink. The total field of view angle of the array transmitter in x and y directions is 105° × 105°. The position of the object can be written as (-10°, 0°, 12 m) for each case and range images were detected at the pixel point (9, 11). The range images are obtained at (2 pixel, 0 pixel 11.7 m), (2 pixel, 0 pixel, 11.7 m), and (2 pixel, 0 pixel, 11.5 m) for the three cases and object is detected (-10°, 0°, 11.7 m), (-10°, 0°, 11.7 m), and (-10°, 0°, 11.5 m), respectively. Further, pixel measurement error in considered (1×1) pixel for the variation in the view angle of 5°. An object range image resolution depends on the pulse width, wave velocity, distance and size of the object. It becomes as

$$\Delta z = \left(\frac{Pulse\ \ width\ \ (s) \times Wave\ \ velocity(m/s)}{2}\right) + range\ \ error\ \ (m)$$

$$= \frac{.002 \times 345}{2} + 0.20 \ = 0.55 \ \ m$$

for a pulse width 2 ms, ultrasonic wave speed 345 m/s and object range error 0.20 m and is in agreement within experimental error of ± 0.50 m.

With anisotropic divergence control measurable range has been improved over isotropic divergence control. Controlling the vertical divergence and varying the horizontal divergence high peak pressure can be maintained in the divergence direction. Object was also detected applying the new control system and accurate location is measured. Experimental directivities are in good agreement with the theoretical calculations.

5.5 Conclusion

Anisotropic long-range three-dimensional measurement system has been developed and divergences are successfully controlled by controlling the delay time. Measurable range of the system with anisotropic divergence control has been improved over the isotropic divergence control more than 2 m ± 0.5 m. Measurable range without divergence control is 17 m ± 0.5 m but the view angle is very narrow, most wide view angle is obtained on isotropic divergence control angle 20^{o} and further improvement in the view angle is observed with the anisotropic divergence controlled angle system. This anisotropic divergence controllable transmitter array system for three-dimensional imaging system that comprising an UTA and URA, clearly detects the object in the direction it was placed and high peak sound pressure is maintained in the divergence direction. As the result, improvement in measurable range and view angle is obtained. Our experimental results are in agreement with the theoretical calculations and good control on anisotropic divergence angle has been obtained. Experiments were conducted applying the different divergence angles and varying the position of the reflector. The developed system accurately detected the object within experimental error of ± 0.50 m. System worked satisfactorily in the object detection.

References

[1] S. Kumar, K. Ichi and H. Furuhashi, Theoretical investigation of high-power ultrasonic array transmitter for a range sensor in air, Proc. IEEE, Int. conf. on industrial technology ICIT 2013, IEEE Xplore (2013), pp.1190-1195, DOI:10.1109/ICIT.2013.

[2] S. Kumar, Q. Wei and H. Furuhashi, Characteristics of High-Power ultrasonic array transmitter in air, Proc. IEEE 2015, Int. Conf. on Recent Developments in Control, Automation and Power Engineering (RDCAPE 2015), (2015), pp. 209-213. DOI: 10.1109/RDCAPE.2015.7281397.

[3] S. Kumar and H. Furuhashi, Long-range measurement system using ultrasonic range sensor with high–power transmitter array in air, Ultrasonics 74 (2017), pp.186-195. DOI:10.1016/j.ultras.2016.10.012.

[4] S. Kumar, K. Ichi and H. Furuhashi, Theoretical investigation of divergence control of directivity of an ultrasonic transmitter array, SICE annual Conf. (2013), Abstract SuCT2.1 2013, pp.803:807.

[5] S. Kumar and H. Furuhashi, Development of a High-Power array transmitter for an ultrasonic range sensor in the air, Proc. Int. Conf. Ultrasonics 2016, (2016), P-42, pp.309-310.

[6] S. Kumar, K. Ichi and H. Furuhashi, Theoretical investigation of an ultrasonic array transmitter with anisotropic directivity, Proc. Int. conf. on sensor device technologies and applications SENSORDEVICES 2013 (2013), pp.131-134.

[7] S. Kumar and H. Furuhashi, Development of ultrasonic array transmission system with anisotropic divergence control for 3-D measurement of objects in air, J. Pure Appl. Ultrason. 38 (2016), pp.1-11.

[8] D. Ensminger and L. J. Bond, Ultrasonics: Fundamentals, Technologies and Application: Third edition.

[9] R. Hickling and S.P. Marin, The use of ultrasonics for gauging and proximity sensing in air, J.Acoust.soc.Am. 79(4) (1986), pp.1151-1160, DOI:10.1121/1.393387.

[10] D.H. Turnbull and F.S. Foster, Beam Steering with Pulsed Two-Dimensional Transducer Arrays, IEEE Transactions on Ultrasonics, Ferroelectrics and Frequency control, 38 (4) (1991).

Chapter 6

Summary

This thesis concerns the development of long range three-dimensional imaging system in open air. Ultrasonic sound has large absorption while propagate in air, therefore object detection is possible for a few meters only restricting the long range measurement. For long range measurement a high-power ultrasonic transmitter array has been proposed and developed.

In Chapter - 1, historical progress of the 3-D imaging system and comparison with other conventional techniques such as stereo camera, laser scanning and pattern projections has been discussed. Further, merits and demerits of the range imaging system also discussed in detail.

In Chapter - 2, characteristics of the developed ultrasonic transmitter array are investigated theoretically and confirmed experimentally. Directivity of the transmitter consisting of different pattern transmitting element's such as (1×1), (2×2), (5×5), (10×10), (12×12) and (20×20) were also investigated. According to the theoretical calculations sound pressure level increase linearly as number of transmitting elements increases, but experimentally this relationship is not found. Pulse modulated directivity also investigated and sound pressure level does not vary much with the 2 ms, 1 ms and 0.5 ms pulses, however small variation was observed and it was due the frequency response of each element. Transmitting power has been improved 40 times higher than that single transmitter with this (12 x 12) array pattern ultrasonic transmitter.

In Chapter - 3, ultrasonic transmitting and receiving systems have been developed for the echo detection. Receiver is calibrated with transmitted ultrasonic frequency (40 kHz). Measurable range is considered until reflected signal is clearly detected from the background noise. Measurable range using; single transmitter with single receiver, single transmitter with array receiver, array transmitter with single receiver and array transmitter with array receiver has been measured. Maximum signal intensity

distributions is considered when correlated signal reaches to its maximum value. This object detection method has been designed by MATLAB and Simulink, applying the delay-and-sum operation on the received signal. The Measurement range up to 25 m has been obtained using array transmitter and array receiver locating an object.

In Chapter - 4 divergence controlled system has been developed with an idea that if sound divergence could be controlled then measurement field can be improved. First, we discussed the theory via computer simulation and then constructed the divergence controllable system. According to the theoretical calculation, it is observed that increasing the divergence angle measurement field increases. Experiments were conducted on the developed system. The result obtained were in good agreement with the theory. The divergence is successfully controlled with this system. Object detection view angle also improved from 5^{o} (without divergence) to $>18^{o}$ at the divergence angle 20^{o}. Object is also successfully detected in the direction it was placed.

In Chapter - 5, we focused on the improvement of the measurable range in the divergence control system. Because as divergence angle increases, measurable range reduces in the previous system. Then, with the idea, if peak pressure is maintained in the divergence direction then further measurable range can be improved. Therefore, anisotropic divergence control system is proposed in which horizontal and vertical divergence can be controlled independently. After conducted the theoretical calculations, experiments are conducted and measurable range has been improved 2 m over previous (isotropic) system. Therefore, anisotropic divergence control system is far better than isotropic control system. This system also detect the object accurately and maintain high peak pressure in the divergence direction.

In Chapter - 6, the summary of this thesis is given. The system, we developed is capable to detect an object at different locations and also useful in adverse atmospheric conditions such as rain, fog, smoke, darkness etc. Further, scope for the future work is also given.

Scope of the Future Work

Ultrasonic sound when propagate in air has two main drawbacks, i.e. absorbed by the medium and spread widely. These two factors restrict the measurable up to a few meters, however ultrasonic sound has high directionality. We have developed an ultrasonic imaging sensor system. With the developed system three-dimensional shape and position of an object is measured. Many experiments have been conducted and our results are very satisfactory except measurable range. In the present paper we focus on the improvement of the measurable range. A qualitative marginal improvement in the measurable has been obtained using the Spread Spectrum Pulse compress Technique, but we are striving for quantitative improvement. A particular array of transmitting elements due to beam formation may be used to perform different types of work, with this motive a high power ultrasonic transmitter array has been constructed that consists of (12×12) arrays of transmitting elements. The effectiveness of the developed technique is greatly depends on the capability to focus the ultrasound. In general, a transducer whose focal length is fixed is inflexible in the direction of ultrasonic radiation. Using more number of transmitting elements and applying time delay, flexibility in the direction is obtained that can generate a focal spot in the acoustic beam at specified beam angle.

Applying the same principle we have developed a high power ultrasonic transmission system. This transmission system is applied on a range sensor using the modulated pulse. The behaviour of the system is investigated theoretically and experimentally. Experimental results have been compared with the simulation results and experimental result show the similar characteristics as in the simulation results. Our experimental results show that using the high power ultrasonic array transmission system measurable range has been improved > 25 m.

Directivity and sound pressure are also investigated by changing the signal delay for each element. Directivity is successfully controlled by controlling the divergence. Therefore the area of directional measurement is controlled by controlling the directivity of the transmitter.

It is observed that sound pressure level of the array transmitter decreases with the isotropic divergence control as we increase the angle of divergence. In many cases horizontal measurement is required instead of vertical. Therefore anisotropic divergence control is investigated in which decrease of sound pressure is limited and high power is maintained.

In future, experiments will be conducted to confirm the isotropic directivity and as well as anisotropic directivity with the short pulse modulation. This technology is very important in the future so that it can be used as an eye of the robot. Robotics has the fastest rate of growth in engineering recently. To save the human labor, to work in hazardous condition, for fast and accurate measurement robots are the perfect technology. If a product is developed that can measure 3D position and shape of an object using ultrasound and it can advance the research further. The other reason is that this technology is useful in adverse atmospheric conditions such as rain, fog, dark etc. making it more versatile.

List of research papers

Published in Journals/International Conference/Symposium/Domestic Conference by the author related to this dissertation

論文題目	公表の方法及び時期	著者
1. 学位請求に関する論文等 (1) 学術論文(査読あり) 1. Anisotropic divergence controlled ultrasonic transmitter array for three-dimensional range imaging.	J.Pure Appl. Ultrason., Vol.38, No.3, pp. 49-57 (2016).	Sahdev Kumar and Hideo Furuhashi
2. Long-range measurement system using ultrasonic range sensor with high-power transmitter array in air	Ultrasonics, Vol.74, pp.186-195 (2017). DOI: 10.1016 /j.ultras.2016.10.012	Sahdev Kumar and Hideo Furuhashi
(2) 国際会議 (査読あり) 1. Theoretical Investigation of the Near Field Sound Wave for an Ultrasonic Array Transmitter	4th Int. Conf. on Environmental Science and Information Application Technology 2012 (ESIAT 2012), 1-2 Dec. 2012. Indonesia. Advances in Biomedical Engineering, Vol.14 pp. 422-427 (2012).	Sahdev Kumar, Kentaro Ichi, and Hideo Furuhashi
2. Theoretical Investigation of High-Power Ultrasonic Array Transmitter for a Range Sensor in Air	IEEE Int. Conf. on Industrial Technology 2013 (ICIT 2013). 25-28 Feb. 2013. South Africa, IEEE Xplore, pp. 1190-1195. DOI: 10.1109/ICIT.2013.6505842	Sahdev Kumar, Kentaro Ichi, and Hideo Furuhashi

3. Theoretical Investigation of Divergence Control of Directivity of an Ultrasonic Transmitter Array	SICE Annual Conference 2013, 14-17, Sep. 2013. Nagoya, Japan, AbstractSuCT2.1, Conference Proceedings, pp. 803-807 (2013).	Sahdev Kumar, Kentaro Ichi, and Hideo Furuhashi
4. Theoretical Investigation of an Ultrasonic Array Transmitter with Anisotropic Directivity	The Fourth Int. Conf. on Sensor Device Technologies and Applications (SENSORDEVICE2013). 25-31 Sep. 2013. Spain. Sensor Devices 2013, pp. 131-134 (2013).	Sahdev Kumar, Quanwei and Hideo Furuhashi
5. Characteristics of High Power Ultrasonic Array Transmitter in Air	Int. Conf. on Recent Developments in Control, Automation and Power Engineering 2015 (RDCAPE), 12-13, Mar. 2015. India. IEEE Xplore, pp. 209-213 (2015). DOI: 10.1109 /RDCAPE.2015.7281397	Sahdev Kumar, Quanwei and Hideo Furuhashi
6. Improvement in the directivity of an array transmitter for an ultrasonic depth sensor operating in air by random phase shift of transmitting elements	IEEE Sensors 2016, 30 Oct- 2 Nov. 2016. USA. A-20-397 (2016).	Sahdev Kumar and Hideo Furuhashi
(3) 国際会議（査読なし） 1. Development of a High Power Array Transmitter for an Ultrasonic Range Sensor in the Air	2nd Int. Conf. on ultrasonic-based applications: from analysis to synthesis (ULTRASONICS-2016), 6-8, June 2016. Portugal. Conference Proceedings, pp. 312-313 (2016).	Sahdev Kumar and Hideo Furuhashi

論文題目	公表の方法及び時期	著者
2. その他の論文等 (1) 国際会議（査読あり） 1. Signal Processing of a 3D Ultrasonic Imaging Sensor that uses the Spread Spectrum Pulse Compression Technique	Int. Conf. on Future Information Technology and Management Science & Engineering 2012 (FITMSE 2012), 12-13 Apr. 2012, Hong Kong. Lecture Notes in Information Technology, Vol.14, pp. 145-150, (2012).	Hideo Furuhashi, Sahdev Kumar, and Masatoshi Shimizu
2. Imaging of a wave reflected by an object using an acoustic lens in air	IMEKO XXI World Congress, 30 Aug-4 Sep. Czech Repubulic. in USB 5 pages. (2015).	Sai Hou, Buren Mandula, Wei Quan, Sahdev Kumar, and Hideo Furuhashi
3. Characteristics of parametric speakers using a PWM amplifier	44th Inter-Noise Congress & Exposition on Noise Control Engineering, 9-12, Aug. 2015. (USA, Proceedings. Vol. 250. No. 4, pp. 2406-2413 (2015).	Wei Quan, Cheng Geer, Sahdev Kumar, and Hideo Furuhashi
4. Characteristics of parametric speakers using a PDM amplifier	44th Inter-Noise Congress & Exposition on Noise Control Engineering, 9-12, Aug. 2015. USA, Proceedings. Vol. 250. No. 4, pp. 2414-2421 (2015).	Wei Quan, Cheng Geer, Sahdev Kumar, and Hideo Furuhashi
(2) 国際会議(査読なし） 1. Development of a High Power Parametric Speaker	2nd Int. Conf. on ultrasonic-based applications: from analysis to synthesis (ULTRASONICS-2016), 6-8, June 2016. Portugal. Conference Proceedings, pp. 105-106 (2016).	Hideo Furuhashi, and Sahdev Kumar

(3) 国内口頭発表（査読なし)		
1. 複数コードを用いたスペクトル拡散方式超音波距離計測	第 54 回自動制御連合講演会（於豊橋技科大学), 平成 23 年 11 月	阿古達木, クマール サハデウ, 古橋秀夫，清水雅年
2. 空中超音波 3 次元計測のための高出力パルス音源の開発	平成 24 年度 電気関係学会東海支部連合大会（於豊橋技科大学）平成 24 年 9 月	市健太郎, クマール サハデウ、古橋秀夫
3. 音響レンズを用いた超音波レンジセンサの研究	平成 25 年度電気関係学会東海支部連合大会（於静岡大学） 平成 25 年 9 月	斉放, クマール　サハデウ, 古橋秀夫
4. アレイ方式高出力超音波パルス発生器の動作特性	平成25年度第17回照明学会東海支部若手セミナーシンポジウム(於名城大学) 平成 26 年 3 月	全威、クマール　サハデウ, 古橋秀夫
5. 空中超音波アレイ送信機の FPGA による位相制御	平成 26 年度電気関係学会東海支部連合大会（於中京大学） 平成 26 年 8 月	布仁満都垃，全威, Kumar Sahdev, 古橋秀夫
(4) その他（査読なし）		
1. パラメトリックスピーカーにおける生成音の位相シミュレーション	総合技術研究所研究報告､第 18 号　（印刷中）	クマール　サハデウ, 古橋秀夫

ACKNOWLWDGEMENT

The author indeed feels extreme pleasure to express his sincere thanks and gratitude to his research supervisor Professor Hideo Furuhashi, Department of Electronics and Electrical Engineering, Aichi Institute of Technology, Japan, for his kind hospitality, guidance, supervision and encouragement throughout the course of this dissertation work, which was absolutely new to me when I joined my Doctor of Engineering/Philosophy program. Professor Furuhashi taught me starting from the fundamentals of science, maths and engineering related to this useful ultrasonic technology to bring me to the level where I am today to enable me to complete my dissertation in its present form. Professor Furuhashi not only enabled me through his compatible guidance to do difficult experiments for directivity and range imaging related to this research work but also encouraged me to have the golden opportunities to present the theoretical and experimental research investigations and our novel findings in the national, the international conferences, the symposiums and the international journals of high reputations. I am highly grateful for his encouragement, love and affection throughout this work which would not have been possible without his generous attitude to train me to become an experimentalist researcher in this advanced engineering and technology field of ultrasonic which has several applications in our day-to-day life. It also gives me extreme pleasure to thank the faculties of electronics and electrical engineering department for their continuous encouragement, assistance and guidance.

My heartiest sincere most special thanks are due to respected Professor Masakazu Mori, Professor Norio Tsuda, Professor Teruyuki Kozuka and Professor Yoshiyuki Uchida, who always stood ready to help me whenever I approached him for electric circuit related discussions and guidance. The author also wish to convey his deep sense of gratitude to Professor Mori for giving me opportunities to have teaching assistant experience for 3 and half years which not only helped me to meet my financial needs in the expensive Japanese life but also helped and guided me through learning and teaching

process with engineering students. Providing me the opportunity of teaching assistance under his own kind supervision, undoubtedly will be very useful for my career in research and teaching activities. This gave me an opportunity to interact with bright young students of engineering department to help them in their experiments and the laboratory report activities. My sincere gratitude is also due to Professor Miss Hayashi and all other university staffs in the international student affair office, student affair office, library and departmental office, for their direct or indirect timely help, always. The author is whole heartedly thankful to Professor Masakazu Mori, Professor Norio Tsuda, Professor Teruyuki Kozuka and Professor Yoshiyuki Uchida for their valuable comments and suggestions in thesis writing.

I sincerely appreciate and gratefully acknowledge the financial assistance from prestigious Rotary Yoneyama Memorial Foundation Scholarship and Ichihara International Scholarship Foundation, Japan, which helped me to devote my more time to do my difficult experimental research studies and without which it might not have been possible to complete this work in stipulated time.

I am very much thankful to all the students and my colleagues in Furuhashi Laboratory and Mr. Takeshi Yoshimatsu from Tsuda Laboratory who their direct or indirect help during my stay in electrical engineering department for not only successful completion of my present research work but also to learn the beautiful Japanese language. I would like to thank my Indian colleagues Dr. Prem Pal (IIT Hyderabad), Dr. Vijay Srinivasan and Dr. Kumar (both Post doctorate in AIT) for their valuable suggestions during my research work. They have contributed a lot through constructive discussions and valuable suggestions time to time. I especially appreciate the help of my respected elder brother Dr. Brahm Pal Singh and my respected sister-in-law (Bhabhi) Dr. Kumud Brahm Singh for their constant encouragement and support at every step from my first day of coming to Japan and spending their precious time from their busy schedule to become the bridge to make me understand this new research field and their suggestions to learn typical Japanese culture.

My special thanks are due to my wife Mrs. Pushpa Singh and Lovely

daughter Miss Aishwarya Singh for their support, understanding and encouragement ever since I joined the Aichi Institute of Technology, Japan. I am also thankful to my nieces Miss Madhurya, Miss Priya and Miss Shubhakshi who always make me to feel at home in Japan.

Last but not least, I dedicate this dissertation to my beloved parents Shri Birbal Singh and Shanti Devi and eldest brother Shri Dharam Pal Singh Head Master ji who enabled me through their love to achieve this highest milestone in One's educational career but could not share the joy with me and my other family members to receive my 'Doctor of Engineering' degree.